CALIFORNIA INSTITUTE OF TECHNOLOGY

EARTHQUAKE ENGINEERING RESEARCH LABORATORY

# MODELING AND ANALYSIS OF HYSTERETIC STRUCTURAL BEHAVIOR

By

Ravi Shanker Thyagarajan

Report No. EERL 89-03

Pasadena, California

1989

# MODELING AND ANALYSIS OF HYSTERETIC STRUCTURAL BEHAVIOR

Thesis by

Ravi Shanker Thyagarajan

In Partial Fulfillment of the Requirements

for the Degree of

Doctor of Philosophy

California Institute of Technology

Pasadena, California

1990

(Submitted October 2, 1989)

# ACKNOWLEDGEMENTS

# ABSTRACT

For damaging response, the force-displacement relationship of a structure is highly nonlinear and history-dependent. For satisfactory analysis of such behavior, it is important to be able to characterize and to model the phenomenon of hysteresis accurately. A number of models have been proposed for response studies of hysteretic structures, some of which are examined in detail in this thesis. There are two popular classes of models used in the analysis of curvilinear hysteretic systems. The first is of the distributed element or assemblage type, which models the physical behavior of the system by using well-known building blocks. The second class of models is of the differential equation type, which is based on the introduction of an extra variable to describe the history dependence of the system.

Owing to their mathematical simplicity, the latter models have been used extensively for various applications in structural dynamics, most notably in the estimation of the response statistics of hysteretic systems subjected to stochastic excitation. But the fundamental characteristics of these models are still not clearly understood. A response analysis of systems using both the Distributed Element model and the differential equation model when subjected to a variety of quasi-static and dynamic loading conditions leads to the following conclusion: Caution must be exercised when employing the models belonging to the second class in structural response studies as they can produce misleading results.

The Massing's hypothesis, originally proposed for steady-state loading, can be extended to general transient loading as well, leading to considerable simplification in the the analysis of the Distributed Element models. A simple, nonparametric identification technique is also outlined, by means of which an optimal model representation involving one additional state variable is determined for hysteretic systems.

# TABLE OF CONTENTS

# LIST OF TABLES AND FIGURES

# CHAPTER 1
# INTRODUCTION

Most structures respond inelastically when subjected to strong seismic excitations. Not only is the restoring force behavior of such structures highly nonlinear, it also depends on the previous history of the response. This history-dependence phenomenon is referred to as *Hysteresis*, the study of which has attracted considerable attention from researchers in earthquake engineering.

Previous research on the earthquake records of severely shaken buildings by Iemura and Jennings [19], Beck [8] and McVerry [32] has clearly indicated that the response behavior of the structures is markedly nonlinear, the conclusion of all the researchers being that the use of linear models is sufficient to reproduce the actual behavior of the structures only up to the onset of damage.

Several mathematical models have been proposed to describe the hysteretic behavior of structures excited beyond the elastic range [10,13,14,20,24,47,49,54], some of which are examined in detail in this thesis. These range from the simple elastoplastic model to the very sophisticated Takeda's model. The reason for the surfeit of models is that no single model has proven entirely satisfactory for the analysis of hysteretic systems for one reason or another. For instance, the elastoplastic model is often felt to be too simple to yield good approximations of actual systems when tested against experimental data, while the Takeda's model is so complex that there are numerous cumbersome rules to be followed, depending on the loading regime.

Since earthquakes are usually modeled by a stochastic excitation, the theory of random vibration is often employed in conjunction with the theory of equivalent linearization in order to obtain approximate response statistics of nonlinear systems

subjected to earthquake excitation. Initially, such a technique was successfully used for nonhysteretic nonlinear systems. Recently, it has been extended to some piecewise-linear hysteretic systems [3,36,47] with the help of representations provided by Asano and Iwan [3], and Suzuki and Minai [47], which have helped cast the systems in a purely history-independent framework involving an expanded set of state variables. Unfortunately, there are only a few physically motivated hysteretic systems for which such representations are available, basically being restricted to systems with a piecewise linear hysteretic characteristic.

Most experimentally observed hysteresis loops [39] suggest that the transition from the linear or elastic range into the yielding range of the deformation is not abrupt as modeled by piecewise-linear models, but rather is quite smooth. There are two classes of models that exhibit curved or rounded hysteresis loops, which are described in further detail in the following two paragraphs.

The first class of models is physically motivated. A very large number of elastoplastic elements are combined in a certain way so as to provide curvilinear hysteretic behavior. One such model for hysteresis has been used by Iwan [20] to determine the steady-state dynamic response of a softening system subjected to trigonometric excitation and also to compare steady-state results predicted by the model with experimental results from an actual structure, namely, a single-story structure having structural steel columns. The ability of these models to adequately represent the nonlinear behavior of an actual steel structure is also demonstrated in [24]. Thus, these models can not only be constructed from simple, well-understood physical building blocks, but they are also quite well suited for the hysteretic modeling of actual steel structures.

In the second class of models, a finite number of additional state variables (usually one or two) are introduced in the mathematical formulation to describe hysteretic behavior, with each new state variable itself satisfying a first-order, single-valued, nonlinear ordinary

differential equation. Typical examples of such models are (i) the model originally proposed by Bouc and later generalized by Wen [54], (ii) Casciyati's model [10], (iii) Özdemir's model [35], etc. Even though such models have been used for various applications in structural dynamics, it is in the response analysis of hysteretic systems by the method of equivalent linearization that they have been most widely applied. The models belonging to this class have also been referred to in this thesis as *endochronic* models because of the similarity in the quasi-static response behavior of these and of the endochronic models [7,50] employed in plasticity.

A question that has never been answered clearly so far is how appropriate the models in the second class are in the characterization of physical systems, being mathematically and not physically motivated. Certain nonphysical behavior of these models has been examined earlier, although briefly [24,36]. One of the main goals of this thesis is to answer this question by subjecting an endochronic model, namely, the Wen-Bouc model, and the corresponding physical Distributed Element hysteretic model, to a variety of quasi-static and dynamic tests and by comparing their respective responses.

The contents of this thesis have been distributed among six relatively independent chapters. Chapter 1 is the introduction. Chapter 2 is a description of various mathematical models for hysteresis, including piecewise-linear as well as curvilinear hysteretic models. Special emphasis has been placed on two topics: the first, a category of models defined in the chapter as the *differential equation* category of hysteretic models; the second, the extension of the Massing's hypothesis, originally proposed for steady-state loading, to general transient loading as well.

A nonparametric identification technique is proposed in Chapter 3, by means of which an optimal endochronic model representation with one additional state variable is determined for hysteretic systems. This method is employed to identify three hysteretic

systems; the predicted optimal models are then evaluated in their ability to represent the original systems adequately.

In Chapter 4, an endochronic model, namely, the Wen-Bouc model, and the corresponding Distributed Element model are subjected to various quasi-static loading sequences in displacement as well as in force. Comparison of the resulting responses of the two models clearly demonstrates the qualitative differences in their physical behavior.

Chapter 5 undertakes a systematic investigation to determine the adequacy of the endochronic models to represent real physical systems when subjected to dynamic excitations, such as earthquakes. For this purpose, the Wen-Bouc model and the corresponding Distributed Element model are each subjected to a variety of dynamic excitations, including deterministic functions, recorded earthquakes, stochastic excitation and simulated earthquakes, and a quantitative comparison is made in a few typical response quantities.

Some general conclusions and a few suggestions for future research are presented in Chapter 6.

# CHAPTER 2
# MATHEMATICAL MODELING OF HYSTERETIC BEHAVIOR

## 2.1 Introduction

The modeling of the restoring force behavior of systems subjected to strong shaking has been a research area of much interest. Inelastic response behavior is highly nonlinear and depends not only on the instantaneous value of the deformation, but also on its past history.

There are two conflicting criteria in the selection of mathematical models to describe hysteresis. The analysis of hysteretic systems is difficult enough when the excitation is a deterministic function; it becomes much more complex in the case of a stochastic excitation. For this reason, the mathematical models describing hysteresis have to be as simple as possible. However, they must be descriptive enough to represent the features of real hysteretic systems adequately.

Bilinear and elastoplastic hysteretic models have been studied extensively, mainly because of their simplicity. One of the significant drawbacks of these models is that they have a sharp yield transition. Most experimentally observed hysteresis loops [39] exhibit a smooth transition from the linear range into the yielding range of deformation. The other observed phenomenon is that an assemblage composed of individual components with a sharp yield transition, tends itself to exhibit smooth force-deflection behavior.

In this chapter, various nonlinear hysteretic models are discussed, covering systems with sharp as well as smooth yield transitions. Models belonging to the Distributed Element class which yield rounded hysteresis loops are seen to satisfy an extended version of the Massing's hypothesis; this results in considerable simplification in the evaluation of the restoring force of such models.

It will be seen that some of the models described in this chapter fall into a category of models with a similar mathematical representation. In this representation, the equations of motion describing the complete dynamical system can be expressed purely as a coupled set of first-order, ordinary differential equations in a finite number of state variables. These differential equations involve single-valued functions, depending only on the instantaneous values of the state variables. This results in a <u>history-independent</u> mathematical representation for the system involving an expanded number of state variables. Hysteretic models that can be expressed in this fashion will be referred to as the DEQ (Differential EQuation) type of hysteretic models. The advantage of the DEQ representation for hysteretic models with regard to their analytical treatment will be explained in a later section of this chapter.

## 2.2 Piecewise-linear hysteretic (PLH) models:

## 2.2.1 Introduction:

As the name suggests, the hysteretic characteristic of this class of models is composed of segments, within each of which the relationship between the restoring force and displacement is linear. These models therefore have sharp yield transitions. The most well-known examples of PLH models are the Elastoplastic, Bilinear and the Polylinear hysteretic models.

If $k$ is the initial stiffness of a nonlinear system with a post-yielding stiffness $\alpha k$, then the restoring force of the system may be expressed as:

$$f = \alpha k u + (1 - \alpha)kz \tag{2.1}$$

where $u$ is the displacement of the system and $z$ is the normalized hysteretic force component that depends on the history of $u$.

Asano and Iwan [3] provided an expression for $\dot{z}$, the rate of change of $z$ with respect to time, for a basic bilinear building block. Suzuki and Minai [47,48] offered similar

representations for $\dot{z}$ for various other PLH models. In both cases, the motivation for proposing the expressions was to cast the systems into the DEQ category of models in order that direct statistical linearization might be performed. This section describes a few PLH models.

## 2.2.2 Elastoplastic and Bilinear models:

The elastoplastic hysteretic characteristic shown in Fig. 2.1a can be thought of as arising from the action of two different types of elements: a linear spring element of stiffness $k$ and a Coulomb slip element that slips at a force level of $ku_y$. The configuration of these two elements is as shown in Fig. 2.1b. Since this system has a zero post-yielding stiffness, the value of $\alpha$ in Eqn. (2.1) is zero.

Let $z$ be the relative displacement of the linear spring element, and let $u$ be displacement of the system. From the physical behavior of the slip element attached to the linear spring, the following may be written for $\dot{z}$:

$$\dot{z} = \dot{u}\,[1 - H(\dot{u})H(z - u_y) - H(-\dot{u})H(-z - u_y)] \qquad (2.2.1)$$

where $H(u)$ is the Heaviside's unit step function given by

$$H(u) = \begin{cases} 1 & \text{for } u \geq 0 \\ 0 & \text{for } u < 0 \end{cases} \qquad (2.2.2)$$

Eqn. (2.2) expresses the fact that the relative velocity of the slip element must be zero when $-u_y < z < u_y$ and equal to $\dot{u}$ when either (i) $z=u_y$ with $\dot{u}>0$, or (ii) $z=-u_y$ with $\dot{u}<0$.

The bilinear hysteretic model has a nonzero $\alpha$ and can be constructed from an elastoplastic system by the addition of a linear spring of stiffness $\alpha k$ in parallel to the spring-damper combination. The restoring force of such a system is given by Eqn. (2.1) in conjunction with Eqn. (2.2).

It can be seen that these models can be cast into the DEQ category by the inclusion of the additional state variable $z$ to the conventional state variables $u$ and $\dot{u}$ to describe the

governing equations of motion. For example, the equations of motion of a bilinear single-degree-of-freedom oscillator subjected to an external force $F(t)$ can be written as

$$\dot{\mathbf{x}} = \mathbf{h}(\mathbf{x}) \tag{2.3.1}$$

where the elements of the vector $\mathbf{x}$ are

$$x_1 = u, \quad x_2 = \dot{u}, \quad x_3 = z \tag{2.3.2}$$

and the vector $\mathbf{h}$ is given by

$$\mathbf{h}(\mathbf{x}) = \left\{ \begin{array}{c} x_2 \\ \dfrac{1}{m}[F(t) - \alpha k x_1 - (1 - \alpha)k x_3] \\ x_2[1 - H(x_2)H(x_3 - u_y) - H(-x_2)H(-x_3 - u_y)] \end{array} \right\} \tag{2.3.3}$$

### 2.2.3: Polylinear hysteretic model:

To achieve a polylinear hysteretic characteristic with an initial stiffness $k$ and an post-yielding stiffness $\alpha k$, $\bar{N}$ blocks, each consisting of a linear spring-slip combination, are connected in parallel with a linear spring element as shown in Fig. 2.2. If $z_i$ is the relative displacement of the $i^{th}$ spring element, then the normalized hysteretic component of the restoring force for the polylinear model can be expressed as

$$z = \frac{1}{(1 - \alpha)k} \sum_{i=1}^{\bar{N}} k_i z_i \tag{2.4.1}$$

where

$$\dot{z}_i = \dot{u}\,[1 - H(\dot{u})H(z_i - u_{yi}) - H(-\dot{u})H(-z_i - u_{yi})] \quad \text{for } i = 1, 2, ..., \bar{N} \tag{2.4.2}$$

and

$$\sum_{i=1}^{\bar{N}} k_i = (1 - \alpha)k \tag{2.4.3}$$

$k_i$ is the spring stiffness of the $i^{th}$ block and $k_i u_{yi}$ is the maximum force corresponding to the force level of the slip element in the $i^{th}$ block.

In this case, $\bar{N}$ additional state variables, $(z_1, z_2, ..., z_{\bar{N}})$, are necessary in addition to $u$ and $\dot{u}$ in order that this system be expressed in the DEQ representation.

## 2.2.4 The Clough-Johnston hysteretic model:

Clough and Johnston [14] presented the stiffness-degrading hysteretic model shown in Fig. 2.3a, which is an idealization of the hysteretic behavior of reinforced concrete structures. In this model, all unloading paths have the initial system stiffness, while the stiffness of loading paths is controlled by the previous yield point in the loading direction. For instance, the stiffness of the loading path 9-10 shown in Fig. 2.3a is such that the path "shoots" for the point 2, the previous yield point in the positive $u$ direction. Since the yield strength for concrete is more in compression than in tension, $ku_{yt} < ku_{yc}$.

The behavior of $z$, the normalized hysteretic component of the restoring force for the Clough's model is as shown in Fig. 2.3b. It can be seen that $(U^+ + u_{yc})$ and $(U^- + u_{yt})$ are the absolute values of the maximum and minimum displacement. $U^+$ and $U^-$ are introduced therefore to keep track of the values of the current positive and negative peak deformation, respectively.

As before, Eqn. (2.1) is an expression for the total restoring force of the system, $f$. Here, $\dot{z}$ satisfies

$$\dot{z} = \dot{u}H(z)[A^+H(\dot{u})\{1 - H(z - u_{yc})\} + H(-\dot{u})]$$
$$+ \dot{u}H(-z)[A^-H(-\dot{u})\{1 - H(-z - u_{yt})\} + H(\dot{u})] \qquad (2.5.1)$$

where

$$A^+ = \frac{(u_{yc} - z)}{(U^+ + u_{yc} - u)} \quad , \quad A^- = \frac{(u_{yt} + z)}{(U^- + u_{yt} + u)} \qquad (2.5.2)$$

with

$$\dot{U}^+ = \dot{u}H(\dot{u})H(z - u_{yc}) \qquad (2.5.3)$$

$$\dot{U}^- = -\dot{u}H(-\dot{u})H(-z - u_{yt}) \qquad (2.5.4)$$

Eqns. (2.5) contain all the information about the stiffnesses of the loading and unloading paths of the Clough's hysteretic model. It is evident that three state variables ($z$, $U^+$ and $U^-$) are needed in addition to the usual $u$ and $\dot{u}$ in order to express the Clough's model in the DEQ representation.

### 2.2.5 Other piecewise-linear hysteretic models:

Similar expressions for $\dot{z}$ are also available [48] for other PLH models such as the origin-oriented model, the peak-oriented model, the double bilinear model, the slip model, etc. The consequence of the availability of these expressions is that these models can be included in the DEQ category of hysteretic models.

## 2.3 Curvilinear hysteretic models:

### 2.3.1 Massing's model:

In a study of the material response behavior of brass rods [28], Massing proposed the following hysteretic model for steady-state response of the system in terms of its initial loading behavior. Let the initial load-deflection curve be given by

$$z = \phi(u) \tag{2.6.1}$$

where $\phi$ is an odd function of $u$. That is,

$$\phi(-u) = -\phi(u) \tag{2.6.2}$$

Then, for steady-state response behavior (or for cycling between fixed displacement limits) as shown in Fig. 2.4, Massing proposed the following relations. For the branch curve ABC, $z$ is given by

$$\frac{Z_0 - z}{2} = \phi\left(\frac{U_0 - u}{2}\right) \tag{2.7.1}$$

and for branch CDA, $z$ is given by

$$\frac{z + Z_0}{2} = \phi\left(\frac{u + U_0}{2}\right)^{\cdot} \tag{2.7.2}$$

where $(U_0, Z_0)$ and $(-U_0, -Z_0)$ are the coordinates of the two load reversal points A and C, respectively. Thus there is a functional similarity between the unloading and loading branches, and the initial load-deflection behavior. Eqns. (2.7.1) and (2.7.2) may be combined to yield

$$\frac{z - Z_L}{2} = \phi\left(\frac{u - U_L}{2}\right) \tag{2.7.3}$$

where $(U_L, Z_L)$ are the coordinates of the last load reversal. That is, $(U_L, Z_L)$ is $(U_0, Z_0)$ for ABC and $(-U_0, -Z_0)$ for CDA.

It can be seen that Eqns. (2.7) describe a closed loop whose load reversal points lie on the initial loading curve. Also, if $\phi$ is a smooth function of $u$, then it is apparent that this model yields rounded hysteresis loops with a smooth yield transition.

Massing reports that the predictions by the above hypothesis agreed very well with the experimentally obtained results for the unloading and compressive loading curve ABC.

## 2.3.2 The parallel-series (P-S) Distributed Element (DEL) model:

By assuming that a general hysteretic system consists of a very large number of ideal elastoplastic elements having different yield levels, Iwan [20] constructed the model shown in Fig. 2.5 consisting of a set of $\bar{N}$ Jenkin's elements connected in parallel. Each such element consists of a linear spring with stiffness $k/\bar{N}$ in series with a slip element of ultimate strength $f_i^*/\bar{N}$.

The system has a polylinear hysteretic characteristic of the type described in Sec. 2.2.3. For example, for initial loading in the positive $u$ direction (path OA in Fig. 2.4), the restoring force $kz$ is given by:

$$kz = \sum_{i=1}^{n} \frac{f_i^*}{\bar{N}} + \frac{ku(\bar{N}-n)}{\bar{N}} \qquad (2.8)$$

where $n$ is the total number of elements that have yielded; that is, the number of elements for which $f_i^* < ku$. Eqn. (2.8) expresses a linear relationship between $z$ and $u$. As n tends to $\bar{N}$, the slope of the linear segment tends to zero.

By making the number of elements $\bar{N}$ very large, Eqn. (2.8) may be written in its equivalent form

$$z = \frac{1}{k} \int_o^{ku} f^* \varphi(f^*) df^* + u \int_{ku}^{\infty} \varphi(f^*) df^* \qquad (2.9)$$

$$\equiv \phi(u) \quad \text{for } u \geq 0 \qquad (2.10.1)$$

where $\varphi(f^*)$ represents the proportion of the elements of the system with strength $f^*$, and satisfies

$$\int_0^{\infty} \varphi(f^*) df^* = 1 \qquad (2.10.2)$$

Since the initial loading curve is symmetric about the origin, let an odd extension be made for the function $\phi$ for $u<0$. That is,

$$\phi(u) = -\phi(-u) \quad \text{for } u < 0 \qquad (2.10.3)$$

Then $\phi(u)$ as defined is an expression for the initial loading behavior of the system for loading in both the positive and negative $u$ directions. If the second term vanishes in Eqn. (2.9) as $u \to \infty$, the ultimate or yield force of the system, $f_y$, is given by

$$\int_0^{\infty} f^* \varphi(f^*) df^* = f_y \qquad (2.11)$$

If $y(f^*)$ is the displacement of the linear spring element which is connected to the slip element with ultimate strength $f^*$, then for the initial loading curve OA shown in Fig. 2.4,

$$y(f^*) = \begin{cases} f^*/k & \text{for } 0 \leq f^* \leq ku \\ u & \text{for } ku \leq f^* < \infty \end{cases} \qquad (2.12)$$

In general, given $y(f^*)$, the normalized restoring force $z$ can be uniquely determined by

$$z = \int_0^\infty y(f^*)\varphi(f^*)df^* \qquad (2.13)$$

For a piecewise continuous distribution function $\varphi(f^*)$ and for a finite $f_y$, rounded hysteresis loops are shown to result [20].

One of the major advantages of this model is that it can be used not only for steady-state but also for transient dynamic response by simply keeping track of the number of the elements in each of the yielded and unyielded states at any given instant. For example, consider the sequence of loading shown in Fig. 2.6. For path 01, the expression for $y(f^*)$ is given by Eqn. (2.12), which when used with Eqn. (2.13) yields the normalized restoring force $z$. The behavior of $y(f^*)$ for path 01 is shown in Fig. 2.7a.

Let there be a load reversal at 1 as shown in Fig. 2.6. Along path 12, the total restoring force results from three groups of elements: those elements that were in a positive yield state after initial loading and have now changed to a negative yield state; those elements that were in a positive yield state after initial loading but have not yet changed to a negative yield state; and those elements that were unyielded on initial loading and are still unyielded. Along path 12, the function $y(f^*)$ for the system is given by

$$y(f^*) = \begin{cases} -\dfrac{f^*}{k} & \text{for } 0 \leq f^* \leq \dfrac{k(U_1-u)}{2} \\[2mm] u - \dfrac{(kU_1 - f^*)}{k} & \text{for } \dfrac{k(U_1-u)}{2} \leq f^* \leq kU_1 \\[2mm] u & \text{for } kU_1 \leq f^* < \infty \end{cases} \qquad (2.14)$$

which is true for $-U_1 \leq u \leq U_1$, where $U_1$ is the displacement corresponding to the load reversal at 1. Eqn. (2.14) in conjunction with Eqn. (2.13) yields the normalized restoring force $z$. $y(f^*)$ given by Eqn. (2.14) is shown in Fig. 2.7b.

In a similar fashion, keeping track of the elements in various yielded and unyielded states, expressions for $y(f^*)$ can be obtained for each of the paths 23,34,45,56 and 67.

The behavior of the function along these paths is shown in Figs. 2.7c-g, respectively. The task of obtaining $y(f^*)$ in this manner is quite cumbersome. Also, once $y(f^*)$ is found, the determination of $z$, using Eqn (2.13), is quite laborious, involving evaluation of several integrals, especially when the number of nested loops gets large. However, a considerable simplification can be achieved in the following manner.

Let the load reversal points also be referred to as *turning points*. Let a positive turning point be defined as one, where the loading changes from a value of $\dot{u}$ greater than 0 to a value of $\dot{u}$ less than 0. Similarly, let a negative turning point be one, where the loading changes from a value of $\dot{u}$ less than 0 to a value of $\dot{u}$ greater 0. The turning points 1, 3 and 5 in Fig. 2.6 are positive turning points and 2, 4 and 6 are negative points. It is evident that the turning points occur as alternate positive and negative turning points.

A key observation can be made from Fig. 2.7. Every time a positive turning point is introduced, the $y$-$f^*$ relationship undergoes the following change. The first linear segment, which was in a positive yield state before the introduction of the turning point, splits into two linear segments, the first one being the collection of elements that are in a negative yield state and the second one being the collection of elements that are not yet in a negative yield state. Similarly, when a negative turning point is introduced, the first negative yield segment splits into a positive yield segment and one that is not yet in a positive yield state.

The slope of the restoring force-displacement relationship, $dz/du$, is the normalized stiffness of the system (that is, the stiffness divided by the initial stiffness) at any instant. The system stiffness has contributions from all elements that are in an unyielded state at that instant. From the $y$-$f^*$ behavior in each of Figs. 2.7 a-g, it can be seen that the only elements in a yielded state are those in the first linear segment of the plots. Generalizing this observed behavior to a situation with $N$ nested turning points, $U_1, U_2, U_3, \ldots, U_N$, the following may be written:

$$\frac{dz}{du} = \int_{kS_v(u-U_N)/2}^{\overline{\phantom{-}}} \varphi(f^*)df^* \qquad (2.15.1)$$

valid for the last nested loop, that is, for $u$ between $U_N$ and $U_{N-1}$. $S_v$ is $sgn(\dot{u})$, the signum function. That is,

$$sgn(\dot{u}) = \begin{cases} +1 & \text{if } \dot{u} \geq 0 \\ -1 & \text{if } \dot{u} < 0 \end{cases} \qquad (2.15.2)$$

Thus $S_v$ is +1 or -1 according to whether $U_N$ is a negative or a positive turning point.

Integration of Eqn. (2.15.1), after some algebra, yields

$$\frac{S_v(z-Z_N)}{2} = \int_0^{kS_v(u-U_N)/2} \frac{f^*}{k} \varphi(f^*)df^* + \frac{S_v(u-U_N)}{2} \int_{kS_v(u-U_N)/2}^{\infty} \varphi(f^*)df^* \qquad (2.16)$$

where $Z_N$ is the normalized restoring force corresponding to the $N^{th}$ turning point. From Eqn.(2.16) and the definition of $\phi$ in Eqn. (2.10), the following equation is obtained for $z$ in terms of the coordinates of the $N^{th}$ turning point, $(U_N, Z_N)$:

$$\frac{z-Z_N}{2} = \phi\left(\frac{u-U_N}{2}\right) \qquad (2.17)$$

which is true for $u$ between $U_N$ and $U_{N-1}$, $N>1$. For $N=1$, Eqn. (2.17) holds with $U_0=-U_1$. For $N=0$, $z=\phi(u)$.

The relationship in Eqn. (2.17) can be seen to be very similar to the Massing's hypothesis for steady-state response. Basically, Eqn. (2.17) says that the restoring force-displacement relationships for all paths are geometrically similar to the initial loading curve, and this observation provides an impetus for the definition of an extended version of Massing's hypothesis to hold for the modeling of transient response behavior as well.

The loading sequence shown in Fig. 2.6 is considered now, with a few changes in order that it may be easier to understand the variation of $y(f^*)$ with the history of $u$. Consider the situation of path 23 being continued past 3 without a load reversal at 3. The $y(f^*)$ behavior is given by Fig. 2.7c, and $(U_2, Z_2)$ is used in Eqn. (2.17) to obtain $z$. Substituting $u=U_1$ in the end points of the piecewise linear segments of Fig. 2.7c yields

Fig. 2.7a for $u=U_1$. Thus the extension of path 23 passes through 1. For any further loading in the positive $u$ direction, $y(f^*)$ behavior is as in Fig. 2.7a. For purposes of determination of $z$ from this instant on, it as if the loop 1231 never happened at all.

Consider a different situation wherein path 56 is continued in decreasing $u$ direction past $U_6$. The $y(f^*)$ behavior is given by Fig. 2.7f, and $(U_5, Z_5)$ is used in Eqn. (2.17) to obtain $z$ until the path reaches 4, after which Fig. 2.7d controls the behavior of $y(f^*)$; for purposes of determination of $z$ from this instant on, the fact that the loop 4564 occurred is of absolutely no consequence. If $u$ continues to decrease past $U_4$, Fig. 2.7d controls $y(f^*)$, and $(U_3, Z_3)$ is used in Eqn. (2.17) until the path reaches 2, when Fig. 2.7b comes into effect. On the other hand, if there is a load reversal at some point between $U_2$ and $U_4$, the $y(f^*)$ is governed by Fig. 2.7e, and the values of $u$ and $z$ corresponding to that load reversal are used in Eqn. (2.17) in the determination of $z$ until the path reaches 3, and so on.

It must be mentioned here that the result of Eqn. (2.17) was derived for the case where the largest excursion is to the positive $u$ direction (that is, $U_1 > 0$). In exactly the same manner, the result can be shown to be true also for the case where the largest excursion is to the negative $u$ direction ($U_1 < 0$).

## 2.3.3 The Extended Massing's hypothesis:

From the similarity between the relations expressed by Eqns. (2.7) and (2.17), it is possible to extend the Massing's hypothesis originally proposed for steady-state response to transient dynamic response as well. In his work on the determination of optimal nonlinear models by applying system identification techniques to inelastic pseudo-dynamic test data, Jayakumar [24] originally proposed this extension of the Massing's hypothesis by stipulating the following two rules for the system behavior during complete and incomplete loops:

• Rule 1: Incomplete loops

The equation of any hysteretic response curve, irrespective of steady-state or transient response, can be obtained simply by applying the original Massing rule to the virgin loading curve using the latest point of loading reversal.

• Rule 2: Completed loops

The ultimate fate of an interior curve under continued loading or unloading can be determined as follows: Once an interior curve crosses a curve from a previous load cycle, the load-deformation curve then follows that of the previous cycle.

By showing that these two rules could be used to predict the behavior of the parallel-series Distributed Element model for paths 12 and 23 of Fig. 2.6, he concluded that the two rules could be used to completely describe the transient hysteretic behavior of the said model [24]. The following representation for the same rules is felt to be in a form more amenable to numerical implementation.

Let $z = \phi(u)$ be an expression for the initial loading behavior of a system where $\phi$ is an odd function of $u$. Let the derivative of the function $\phi$ be $\psi$, i.e., $\psi(u) \equiv \phi'(u)$, and let $\mathbf{U} = \{U_1, U_2, U_3, \ldots, U_N\}^T$ be the array of $N$ nested turning points, which is continually updated in a manner described below. As before, $U_i$ and $Z_i$ are the displacement and normalized restoring force corresponding to the $i^{th}$ load reversal ($i=1,2,\ldots,N$). Thus, $U_N$ is the displacement corresponding to the last load reversal up to the instant under consideration. Let the next load reversal be at a displacement of $U_0$. If there are no load reversals after $U_N$, then the following hypothesis holds with $U_0 \rightarrow \infty S_V$, i.e., $+\infty$ or $-\infty$ according to whether $\dot{u}>0$ or $\dot{u}<0$. As $u$ moves from $U_N$ to $U_0$, the following rules express the manner in which (i) the normalized restoring force, $z$, is determined and (ii) the array $\mathbf{U}$ is updated:

(1) If $N=0$:

$$z = \phi(u) \qquad (2.18.1)$$

In differential form,

$$\frac{dz}{du} = \psi(u) \qquad (2.18.2)$$

(2) If $N \neq 0$:

let $S_1 = sgn(U_1)$.

(a) If $S_V S_1 = 1$:

and if $U_1 S_1 \leq u S_1$, new $N=0$, $\qquad (2.19.1)$

or if $U_{2j+1} S_1 \leq u S_1 < U_{2j-1} S_1$, $j = 1,2,....,\left(\frac{N}{2}-1\right)$, new $N=2j$. $\qquad (2.19.2)$

If $S_V S_1 = -1$:

and if $u S_1 \leq -U_1 S_1$, new $N=0$, $\qquad (2.20.1)$

or if $-U_1 S_1 < u S_1 \leq U_2 S_1$, new $N=1$, $\qquad (2.20.2)$

or if $U_{2j} S_1 < u S_1 \leq U_{2j+2} S_1$, $j = 1,2,....,\left(\frac{N-3}{2}\right)$, new $N=2j+1$. $\qquad (2.20.3)$

(b) If new updated $N=0$, $z$ is given by Eqn. (2.18).

If new updated $N \neq 0$, $\dfrac{z-z_N}{2} = \phi\left(\dfrac{u-u_N}{2}\right)$ $\qquad (2.21.1)$

In differential form,

$$\frac{dz}{du} = \psi\left(\frac{u-u_N}{2}\right) \qquad (2.21.2)$$

(3) If $u=U_0$, $N$ is increased by 1 and the size of array U is increased by the addition of $U_0$

to the end of the array.

Rules (2)(a) and (3) perform a continuous updating of the array so as to yield the

right branch of the hysteretic curve. Rules (1) and (2)(b) yield the normalized restoring

force $z$ corresponding to the displacement $u$. Even though all the branches of the restoring force diagram obey the same relationship given by Eqn. (2.21) (for $N \neq 0$), since the array is being updated continually depending on the history of $u$, the values of $U_N$ and $Z_N$ that are used in the equation are different, thus yielding the appropriate hysteretic branch.

One point of interest here is in the nondependence of the differential formulation on the quantity $Z_N$ as evidenced in Eqn. (2.18.2) and Eqn. (2.21.2). Use of the differential formulation does not involve memorizing the array of the values of $z$ corresponding to the nested turning points. However, an integration needs to be done to obtain $z$. In dynamical systems, the equations of motion frequently involve writing expressions for the derivatives of the state variables. The differential formulation of the Extended Massing's hypothesis is very convenient for the purpose.

## 2.3.4 Other DEL models satisfying the Extended Massing's hypothesis:
## 2.3.4.1 Two other parallel-series models:

Two other P-S DEL models can be constructed by (i) varying the stiffness of each linear spring in the individual elements while keeping the slip force level constant for the slip damper in all the elements, and (ii) varying both the stiffness and slip level in the elements.

In the first model, the physical configuration of the springs and dampers remains the same as in Fig. 2.5. However, in this case, all the slip elements have the same maximum allowable force $f_y$, but the springs have stiffnesses $k^*$ varying continuously. If $\varphi(k^*)$ represents the distribution function of the proportion of the system with stiffness $k^*$, then

$$\int_0^\infty \varphi(k^*)dk^* = 1 \tag{2.22.1}$$

Let $k$ be the initial stiffness of the system. That is,

$$k = \int_0^\infty k^* \varphi(k^*)dk^* \tag{2.22.2}$$

For initial loading in the positive direction ($\dot{u}>0$), there are two groups of elements that contribute to the normalized restoring force $z$: one in an unyielded state as yet, and another in a state of positive yield. Adding their respective contributions, the following can be written:

$$z = \frac{1}{k}\int_0^{f_y/u} k^* u\, \varphi(k^*)dk^* + \frac{1}{k}\int_{f_y/u}^{\infty} f_y\, \varphi(k^*)dk^* \qquad (2.23.1)$$

$$\equiv \phi(u) \quad \text{for } u \geq 0 \qquad (2.23.2)$$

Again, an odd extension is made for the function $\phi$ for values of $u$ less than zero. As $u \to \infty$, it can be seen that $z \to f_y/k$, the normalized yield strength or ultimate strength of the system. In a manner similar to that in Sec. 2.3.2, it can be shown that this model satisfies the Extended Massing's hypothesis for $\phi$ as defined in Eqn. (2.23.2).

The second P-S model which is considered is the one in which a very large number of elements are connected in parallel such that each element consists of a linear spring of stiffness $k^*$ in series with a slip element of maximum allowable force $f^*$, where both $k^*$ and $f^*$ may range continuously from 0 to $\infty$.

Let $\varphi(f^*,k^*)$ be the distribution function of the proportion of elements with properties $f^*$ and $k^*$ such that

$$\int_0^{\infty}\int_0^{\infty} \varphi(f^*,k^*)df^*dk^* = 1 \qquad (2.24.1)$$

and

$$\int_0^{\infty}\int_0^{\infty} k^*\varphi(f^*,k^*)df^*dk^* = k \qquad (2.24.2)$$

where $k$ is the initial stiffness of the system.

Upon initial loading in the positive direction ($\dot{u}>0$), two groups of elements, one in a state of positive yield and the other in an unyielded state as yet, contribute to $z$ such that

$$z = \frac{1}{k}\int_0^{\infty}\left\{\int_0^{k^*u} f^*\varphi(f^*,k^*)df^* + \int_{k^*u}^{\infty} k^* u\,\varphi(f^*,k^*)df^*\right\}dk^* \qquad (2.25.1)$$

$$\equiv \phi(u) \quad \text{for } u \geq 0 \qquad (2.25.2)$$

where, again, an odd extension is made for $\phi$. As $u \to \infty$, if the second term in Eqn. (2.25.1) vanishes, $z \to f_y / k$, where $f_y$ is the ultimate strength of the system given by

$$f_y = \int_0^\infty \int_o^\infty f^* \varphi(f^*, k^*) df^* dk^* \qquad (2.26)$$

For each value of $k^*$, this system is exactly the same as the one treated in Sec. 2.3.2, and the analysis of this system can thus be carried out in a strictly analogous fashion to show that this model also satisfies the Extended Massing's hypothesis with $\phi$ as defined in Eqn. (2.25.2).

## 2.3.4.2 The series-parallel (S-P) model:

In this model, the basic building blocks are connected in series to form the system as shown in Fig. 2.8a. Each basic block consists of a spring of stiffness $\bar{N}k$ in parallel to a slip element with a maximum allowable force of $f^*$. The basic block thus has a restoring force characteristic as shown in Fig. 2.8b. Let $\bar{N}$ be made very large with $\varphi(f^*)$, representing the distribution function of the the proportion of the elements with maximum allowable force $f^*$ such that

$$\int_0^\infty \varphi(f^*) df^* = 1 \qquad (2.27)$$

In the configuration of this system, the normalized force $z$ is the same in each of the building blocks, but each block has a different displacement $y(f^*)$, with both the individual components of the block having this displacement. The total displacement of the system, $u$, is given by

$$u = \int_0^\infty y(f^*) \varphi(f^*) df^* \qquad (2.28)$$

Upon initial loading in the positive direction ($\dot{u} > 0$), there are two groups of elements that contribute to the response of the system. One group, with $f^*/k > z$, does not have any movement in the slip elements, and the corresponding spring elements are hence "inactive," meaning that they do not contribute to the system displacement. The other group with

$f^*/k<z$ has slipping elements and "active" springs, meaning that the springs have relative displacements and contribute to the system displacement. Hence,

$$u = \int_0^{kz} \left( z - \frac{f^*}{k} \right) \varphi(f^*) df^* \qquad (2.29.1)$$

$$\equiv \tilde{\phi}(z) \quad \text{for } z \geq 0 \qquad (2.29.2)$$

Let an odd extension of $\tilde{\phi}$ be made for $z<0$. The initial loading curve here expresses $u$ as a function of $z$. Let the inverse function of $\tilde{\phi}$ be $\phi$. That is, the initial loading curve may also be expressed as:

$$z = \phi(u) \qquad (2.29.3)$$

The restoring force characteristic of the S-P model has two significant differences from the P-S model. By differentiating Eqn. (2.29.1), it may be shown that $dz/du \rightarrow \infty$ as $u \rightarrow 0$, and $\rightarrow k$ as $u \rightarrow \infty$. That is, this system has an infinite initial stiffness and an asymptotic stiffness $k$ at large deformations. It does not have an ultimate force level as did the P-S model in Sec. 2.3.2.

By observing the $y(f^*)$ behavior of a few nested loops as was done for the case of the P-S model in Fig. 2.7, it can be shown that the active elements of the system contributing to the system compliance (where the compliance is the inverse of the stiffness) satisfy the following inequality:

$$f^* \leq \frac{kS_v(z - Z_N)}{2} \qquad (2.30.1)$$

Since the springs in the active elements are connected in series, the compliances of the elements add to give the total system compliance, $du/dz$. Hence,

$$\frac{du}{dz} = \int_0^{S_v k(z-Z_N)/2} \varphi(f^*) df^* \qquad (2.30.2)$$

is true for the last nested loop. Integration of Eqn. (2.30.2), after some algebra, and making use of the odd property of $\tilde{\phi}$ yields

$$\frac{u - U_N}{2} = \tilde{\phi}\left(\frac{z - Z_N}{2}\right) \qquad (2.31)$$

Using the inverse function of $\tilde{\phi}$, namely, $\phi$, the following may be written

$$\frac{z - Z_N}{2} = \phi\left(\frac{u - U_N}{2}\right) \qquad (2.32)$$

which is true for the last nested loop.

It is thus seen that the S-P system also satisfies the relations of the Extended Massing's hypothesis.

### 2.3.4.3 Stiffness- and strength-degrading model:

The physical configuration of this model is of the P-S type considered in Sec. 2.3.2. The only difference is in the behavior of the slip element in each building block. In the model considered here, the slip element "breaks," once it has slipped a certain specified displacement. For subsequent loading, the system cannot recover the stiffness and strength of this building block. This results in a stiffness- and strength- degrading model. Cifuentes [13] used such a model for the identification of reinforced concrete structures. A typical restoring force diagram of this model for a structure has been reproduced from his work [13] in Fig. 2.9. The deterioration in both system stiffness and strength as the deformation increases is evident from the figure.

Assume that the elastoplastic unit of stiffness $k$ and ultimate strength $f^*$ breaks when the relative displacement of the slip element reaches an absolute value equal to $\lambda$ times the yield displacement $f^*/k$, $\lambda$ ($>0$) being the same for all the elastoplastic units. The behavior of such an elastoplastic unit may be used for the modeling of the failure of concrete because of spalling in the compressive loading direction and because of cracking in the tensile loading direction.

Let $a$ be the largest absolute value of the displacement until the instant under consideration. Then those elements that have broken thus far satisfy the inequality

$$f^* \le \frac{ka}{\lambda + 1} \tag{2.33}$$

To account for the removal of the broken elements, the updated $\tilde{\varphi}(f^*)$ is defined as follows:

$$\tilde{\varphi}(f^*) = \begin{cases} 0 & \text{for } 0 \le f^* \le \dfrac{ka}{\lambda + 1} \\ \varphi(f^*) & \text{for } f^* > \dfrac{ka}{\lambda + 1} \end{cases} \tag{2.34}$$

where $\varphi(f^*)$ is the distribution function of the proportion of the system with strength $f^*$ ($0 \le f^* < \infty$) in the virgin state of the system.

Let $\tilde{\phi}(u)$ be defined as

$$\tilde{\phi}(u) \equiv \frac{1}{k} \int_0^{ku} f^* \tilde{\varphi}(f^*) df^* + u \int_{ku}^{\infty} \tilde{\varphi}(f^*) df^* \quad \text{for } u > 0 \tag{2.35.1}$$

$$\tilde{\phi}(u) = -\tilde{\phi}(-u) \quad \text{for } u < 0 \tag{2.35.2}$$

For all nested loops of $u$ within $[-a,a]$, the system essentially behaves as the P-S model discussed in Sec. 2.3.2 with a distribution function $\tilde{\varphi}(f^*)$ as in Eqn. (2.34). Thus, this model satisfies the Extended Massing's hypothesis, and $z$ may be obtained from

$$\frac{z - Z_N}{2} = \tilde{\phi}\left(\frac{u - U_N}{2}\right) \tag{2.36}$$

for $N \ne 0$. If $N=0$, $z$ is given by $\tilde{\phi}(u)$.

There is one qualifying remark that must be made here about the function $\phi$. The function $\phi$ in Eqn. (2.17) does not vary with the history of $u$. The corresponding function $\tilde{\phi}$ for this model used in Eqn. (2.36) changes, depending on the history of $u$ (actually, on $a$, the largest absolute value of the displacement). There is thus an implicit memory-dependence which is described by Eqns. (2.34) and (2.35).

Once $u$ passes $\pm a$, the parameter $a$ assumes the value of the new maximum of $|u|$, $\tilde{\varphi}$ changes as per Eqn. (2.34), $\tilde{\phi}$ changes as per Eqn. (2.35) and the normalized restoring force $z$ is given by Eqn. (2.36).

A remark that may be made here regards a difference in the two memory parameters U and $a$. U is an array of nested turning points that can be completely "forgotten" (that is, disregarded) once the system displacement passes either $\pm U_1$. The fact that the nested loops occurred has no future significance in the determination of $z$. In contrast, $a$ represents an effect that cannot be recovered since once the elements are broken, they cannot contribute to the system response behavior any more. $a$ is a cumulative damage parameter, and cannot be "forgotten." This property of $a$ ensures that the system has a permanent degradation of system properties.

## 2.3.5 Curvilinear models with one or two hidden state variables:
## 2.3.5.1 The endochronic models:

Endochronic theories of material behavior were introduced and employed by Valanis [50] to develop a constitutive law for metals which characterizes strain-hardening, unloading behavior, cross-hardening (for example, the effect of pretwist on axial behavior), the alteration of hysteresis loops with continued cyclic straining and sensitivity to strain rate. Bazant and Bhat further developed the theory to describe the liquefaction of sand, and the failure of concrete [7].

Fundamentally, the endochronic models do not make use of a yield condition as do most classical theories of plasticity, but instead use a quantity referred to as the intrinsic time. This quantity is introduced into the constitutive laws of viscoelasticity in place of the real time. By starting with a one-dimensional Maxwell model, Bazant and Bhat [7] constructed the following version of a simple endochronic model:

$$d\sigma = Ed\varepsilon - \frac{1}{Z}\sigma|d\varepsilon| \qquad (2.37.1)$$

where $\sigma$ is the stress, $\varepsilon$ is the strain, $E$ is the Young's modulus and $Z$ is the relaxation time of the material. Equivalently,

$$\dot{\sigma} = E\dot{\varepsilon} - \frac{1}{Z}\sigma|\dot{\varepsilon}| \qquad (2.37.2)$$

where, as usual, the dot superscript refers to the derivative with respect to time.

The model in Eqn. (2.37) is rate-independent, and the stress approaches the limit $ZE$ asymptotically for large strains. It can be seen that Eqn. (2.37) is a complete description of the material behavior. There are no yield conditions, hardening rules, etc. However, having a representation as simple as this does have its price. The behavior of such models can be quite nonphysical. More will be said about this in Chapter 4.

## 2.3.5.2 The Wen-Bouc model and the Casciyati models:

A differential equation model for hysteresis originally proposed by Bouc was later generalized by Wen [53,54]. The model is widely used in structural dynamics, especially in the stochastic response analysis of hysteretic systems. Essentially, the model requires that the normalized hysteretic restoring force satisfy the first-order, nonlinear differential equation

$$\dot{z} = \frac{1}{\eta}[A\dot{u} - v(\beta|\dot{u}||z|^{n-1}z - \gamma\dot{u}|z|^{n})] \qquad (2.38)$$

where the parameters $A$, $\beta$, $\gamma$, $\eta$, $v$ and $n$ govern the amplitude, shape of the hysteresis loop and the smoothness of transition into the inelastic range. The total restoring force of the system, $f$, is again given by Eqn. (2.1). The ability of this model to depict curvilinear hysteretic behavior has been shown for the case $n=1$ in [54]. In the same paper, Wen extended the above model to include stiffness- and/or strength-degradation of the restoring

force. A hysteretic energy dissipation, which is a measure of the cumulative effect of the severe response and repeated oscillations, is defined as follows:

$$E(t) = (1 - \alpha)k \int_0^t z(\tau)\dot{u}(\tau)d\tau \qquad (2.39)$$

where $k$ and $\alpha$ are, as usual, the initial stiffness and the post-yielding stiffness ratio of the system. Stiffness- and strength-degradation can be jointly introduced by prescribing $A$ as a degrading function of $E(t)$. That is,

$$A(t) = A_0 - \delta_A E(t) \qquad (2.40.1)$$

where $\delta_A$ is the deterioration rate and $A_0$ is the value of $A$ at the commencement of loading. Similarly, strength-degradation can be introduced by

$$\nu(t) = \nu_0 + \delta_\nu E(t) \qquad (2.40.2)$$

and stiffness-degradation by

$$\eta(t) = \eta_0 + \delta_\eta E(t) \qquad (2.40.3)$$

where $\delta_\nu$ and $\delta_\eta$ control the degradation rates, and $\nu_0$ and $\eta_0$ are the initial values of $\nu$ and $\eta$, respectively, at the commencement of loading.

In the case $n=1$, $\eta = \nu = 1$, $A=E$, $\beta = 1/Z$, $\gamma = 0$, it can be seen that the $z$-$u$ relationship as per Eqn. (2.38) is exactly the same as the $\sigma$-$\varepsilon$ relationship expressed by Eqn. (2.37.2) for the simple endochronic model. The similarity in the initial loading behavior of these models was noted first by Jayakumar [24]. Thus, even though the endochronic model and the Wen-Bouc model were motivated by different reasons and for application to different fields of research, their behavior is very similar. For this reason, it is felt that it will not be inappropriate to refer to the group of models included in this section as the endochronic group of models.

The family of endochronic models exhibit certain unrealistic characteristics that are quite inconsistent with observed physical behavior. These will be enumerated in detail in Chapter 4. In an effort to minimize one such unrealistic feature of the Wen-Bouc model,

namely, the possible nonclosure of hysteresis loops, Casciyati [10] proposed the following amendment for the case $n=1$:

$$\dot{z} = A\dot{u} - \beta|\dot{u}|z + \gamma\dot{u}|z| + \delta|\dot{u}|sgn(z) \qquad (2.41)$$

where $\delta$ is a parameter intended to control loop closure.

As a final remark, it may be mentioned that the endochronic models can be easily cast in the DEQ category described in Sec. 2.1. For nondegrading systems, this is achieved by the addition of the hidden state variable, $z$, to the conventional state variables $u$ and $\dot{u}$ to describe the system response. For degrading models, the inclusion of $z$ as well as $E(t)$ can be done to formulate the system in a purely history-independent fashion involving an expanded number of state variables.

## 2.4 The DEQ category of hysteretic models:

Random vibration studies of linear systems have been used very successfully to determine various statistical measures of the response of single- and multi-degree-of-freedom systems subjected to random excitation. Unfortunately, to date there are no systematic analytical methods to obtain closed-form solutions to the stochastic response of a general nonlinear dynamical system. The scarcity of exact solutions has necessitated the analytical development of approximate solution techniques.

One of the most promising of such approximate analysis techniques is the method of equivalent linearization. In the case of random excitation, this method approximates the original set of nonlinear stochastic differential equations with a more tractable linear set which are easily analyzed. The general results of Iwan [22], Atalik and Utku [4], Caughey [12], Spanos and Iwan [45] provide a sound foundation for this method. As of now, this method is capable of satisfactorily handling nonlinear systems that can be described by a set of finite number of single-valued, possibly nonlinear, ordinary differential equations. The keyword is "single-valued," meaning that the equations cannot be history-dependent.

Caughey [11] used the additional Krylov-Bogoliubov (K-B) approximation to examine the random response of a bilinear hysteretic system subjected to white noise excitation. However, it has been shown that this method does not produce wholly satisfactory results when the response is wide band (as in the case of elastoplastic or nearly elastoplastic systems).

If, in some manner, the history dependence of the system could be "removed" by the addition of one or more state variables, rendering the expanded system description history-independent, then the theory of equivalent linearization could be used in the analysis of hysteretic systems as well. It is precisely with this point in mind that several of the models described in this chapter have been proposed. The hysteretic behavior of these systems is controlled by the behavior of the instantaneous values of the newly included state variables, which are "internal" or "hidden" in the system. This is not to say that all physical hysteretic systems can be formulated in such a representation; the Distributed Element models with a continuous hysteretic characteristic have not yet been shown to have such a representation. But for systems that do, for example, the piecewise-linear hysteretic models, the endochronic models, etc., the method has been used to calculate the stochastic response of the systems when subjected to random excitations [3,48,53]. Being able to perform the approximate analysis of hysteretic systems in this fashion has been the driving force behind the quest of the DEQ representation for the systems.

## 2.5 A history-independent representation for a Distributed Element model:

It may be mentioned here that it is possible to derive a history-independent representation even for the Distributed Element models; for instance, the equations of motion of a single-degree-of-freedom system whose restoring force behavior is described by the parallel-series model (Sec. 2.3.2) can be written as

$$m\ddot{u} + k\int_0^\infty y(f^*,t)\,\varphi(f^*)\,df^* = F(t) \qquad (2.42.1)$$

$$\frac{\partial}{\partial t}y(f^*,t) = \dot{u}\left[1 - H(\ddot{u})H(y - \frac{f^*}{k}) - H(-\ddot{u})H(-y - \frac{f^*}{k})\right] \qquad (2.42.2)$$

where $m$ is the mass, $k$ is the initial stiffness, $H$ is the Heaviside's unit step function and $F(t)$ is the external force. $u$, $y$, $\varphi$ and $f^*$ have the same meaning as in Sec. 2.3.2. These equations are obtained by starting with Eqn. (2.4) for the polylinear hysteretic model and letting $N$ become very large.

The integro-differential nature of Eqn. (2.42) calls to mind the following quote from Picard [38] in 1907, who also gave *hereditary mechanics* its name:

" In all this study (of classical mechanics), the laws which express our ideas of motion have ben condensed into differential equations, that is to say, relations between variables and their derivatives. We must not forget that we have, in fact, formulated a principle of *nonheredity*, when we suppose that the future of a system depends at a given moment only on its actual state, or in a more general manner, if we regard the forces as depending also on velocities, that the future depends on the actual state and the infinitely neighboring state which precedes. This is a restrictive hypothesis and one which, in appearance at least, is contradicted by the facts. Examples are numerous where the future of a system seems to depend upon former states. Here we have *heredity*. In some complex cases, one sees that it is necessary, perhaps, to abandon differential equations and consider functional equations in which there appear integrals taken from a distant time to the present, integrals that will be, in fact, this hereditary part."

Even though Eqn. (2.42) is a history-independent representation for the system in $u$, $\dot{u}$ and $y$, this representation does not admit the inclusion of the model in the DEQ category, because the additional state variable $y$ is not a scalar but a continuous function of an independent variable $f^*$, and also, a partial differential equation rather than an ordinary one

is involved. Currently, there are no techniques that can help perform a direct linearization of this system of equations. An extension of the theory of equivalent linearization to include representations such as this would prove very beneficial in the analysis of curvilinear hysteretic systems.

(a)



(b)
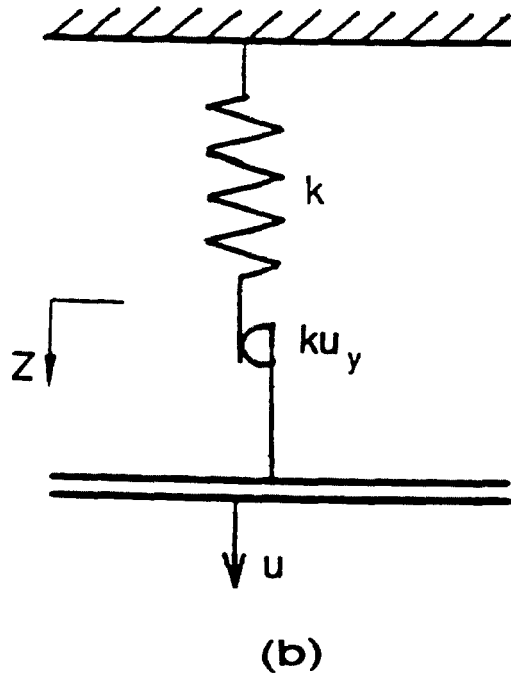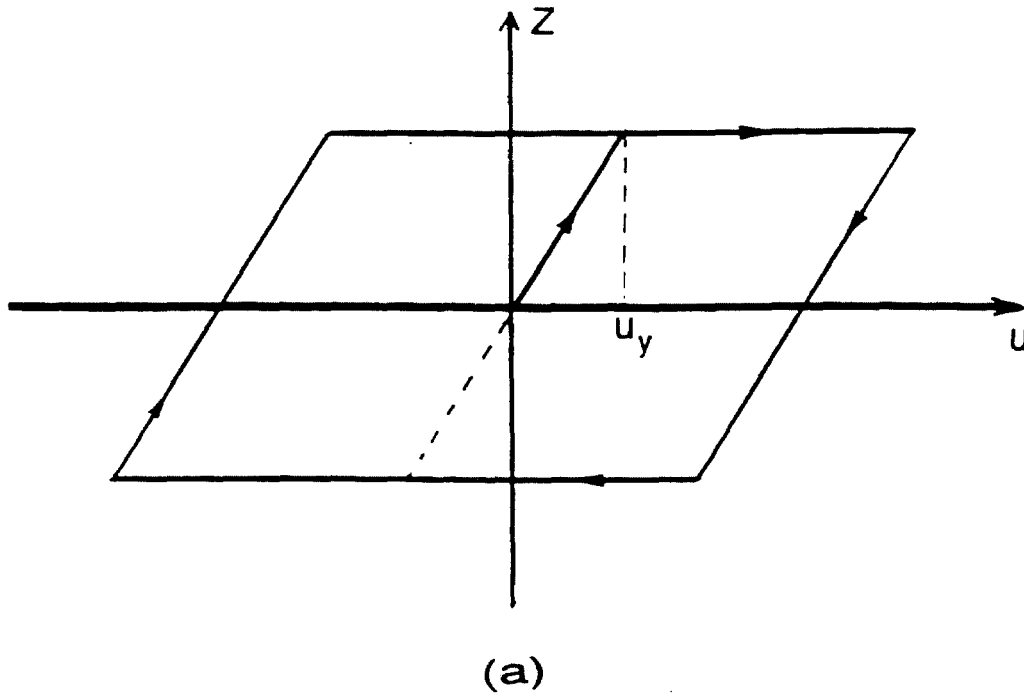
Figure 2.1:     The elastoplastic model (a) Restoring force characteristic (b) Schematic
representation for the system.
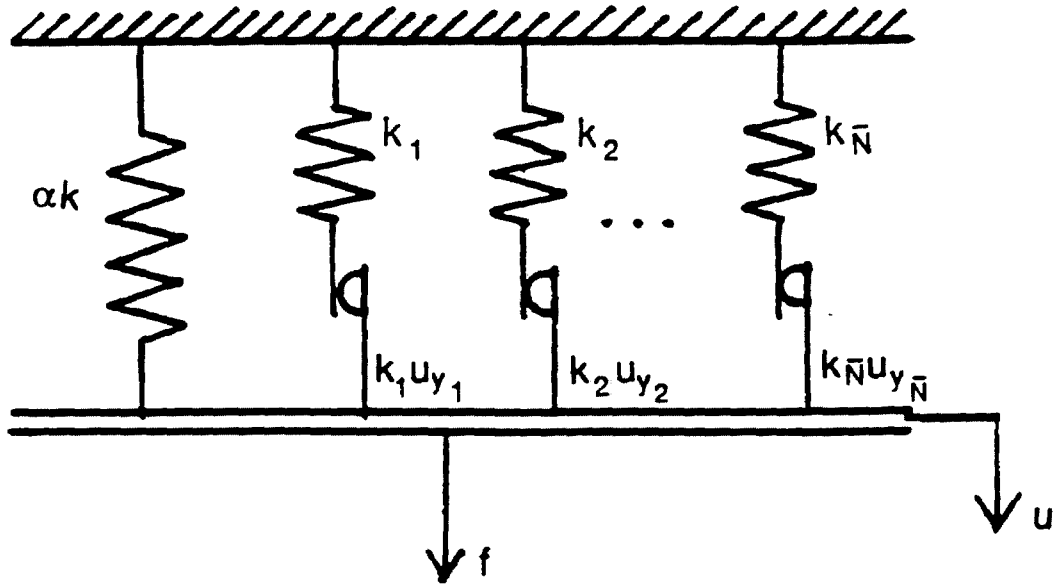
Figure 2.2: Schematic representation for a system with a polylinear hysteretic characteristic.
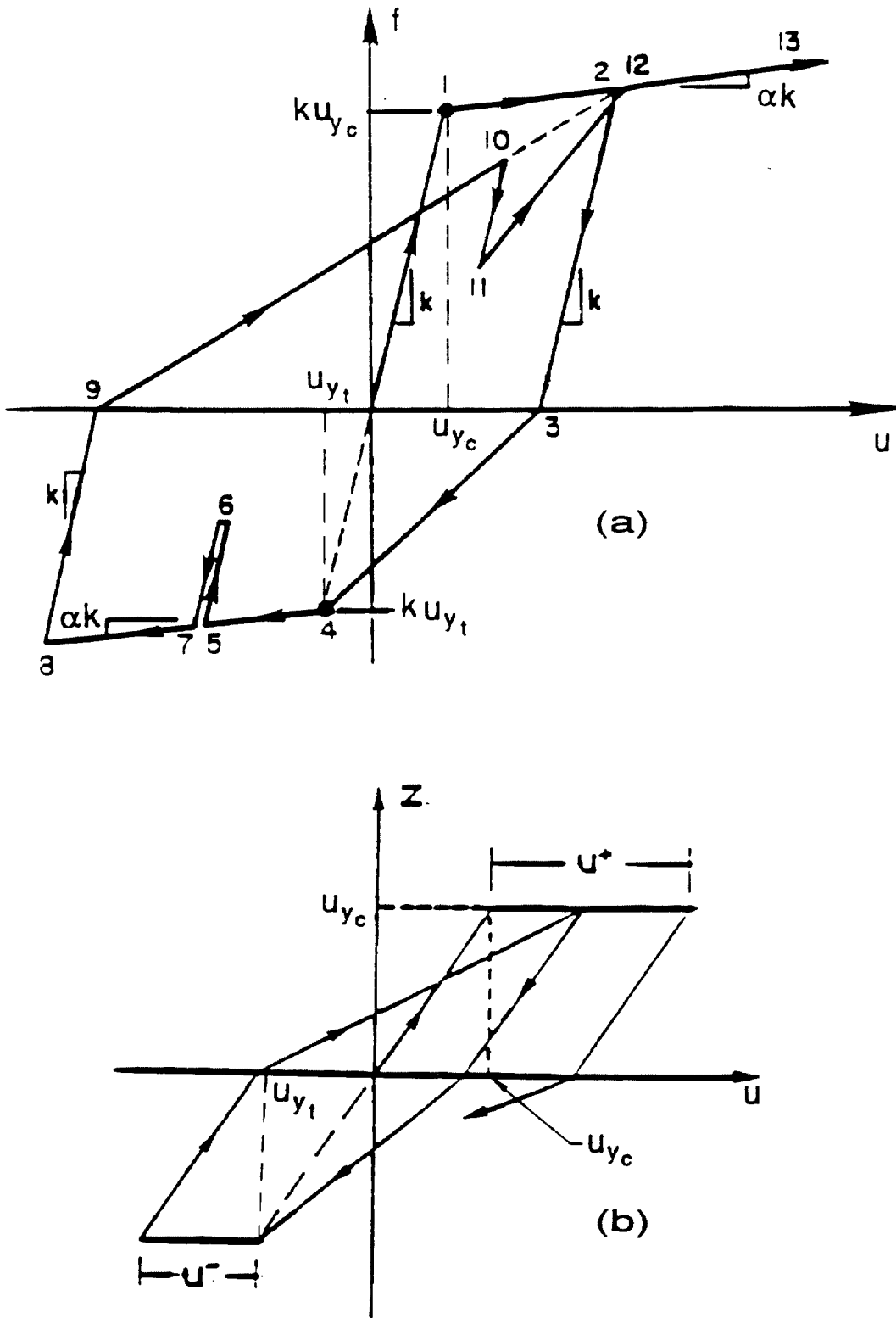
Figure 2.3:     The Clough's hysteretic model for reinforced concrete structures
(a) Restoring force behavior (b) The normalized hysteretic component, z.
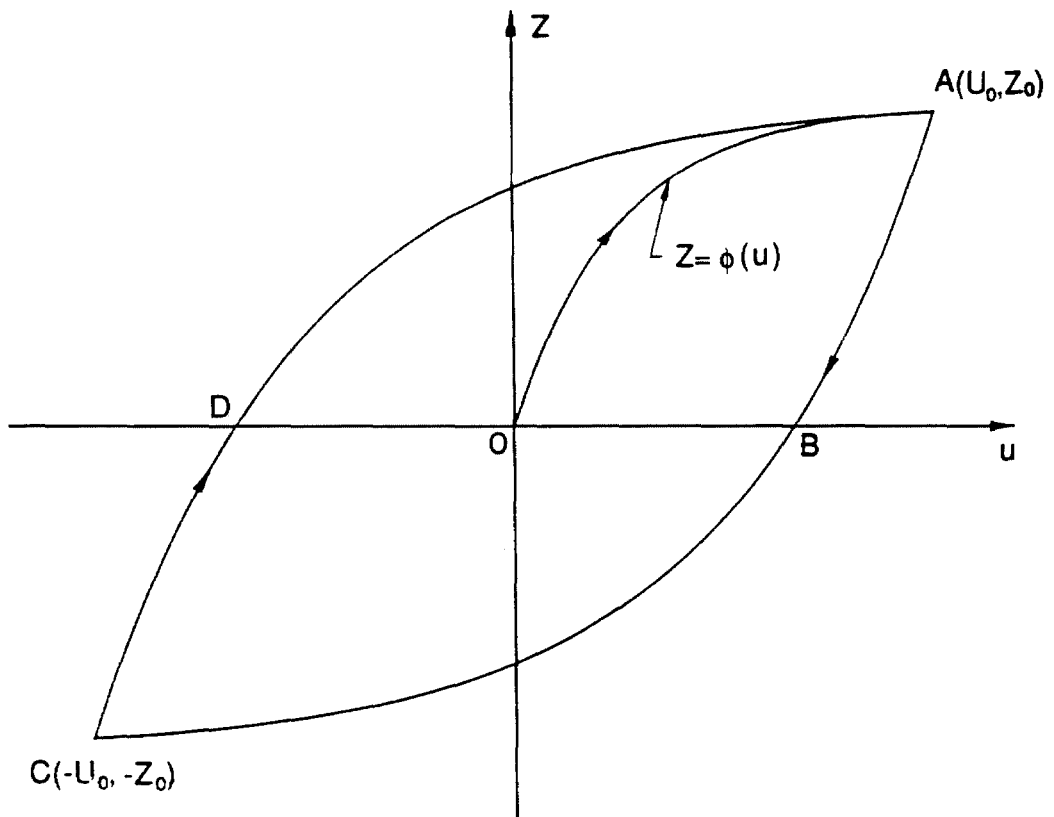
Figure 2.4:    A typical hysteretic loop for steady-state system response.
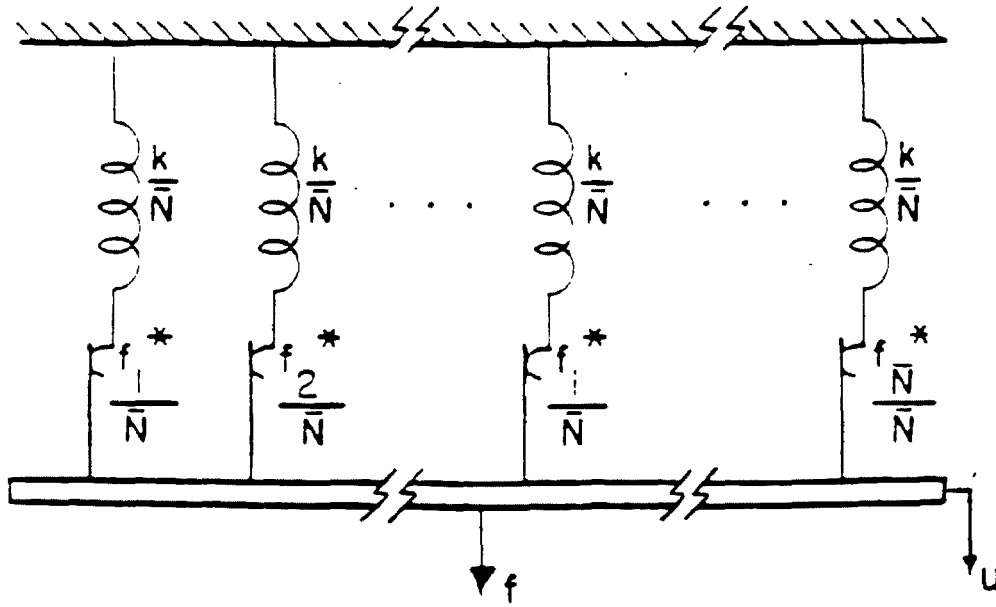
Figure 2.5:    The parallel-series Distributed Element model for hysteresis.
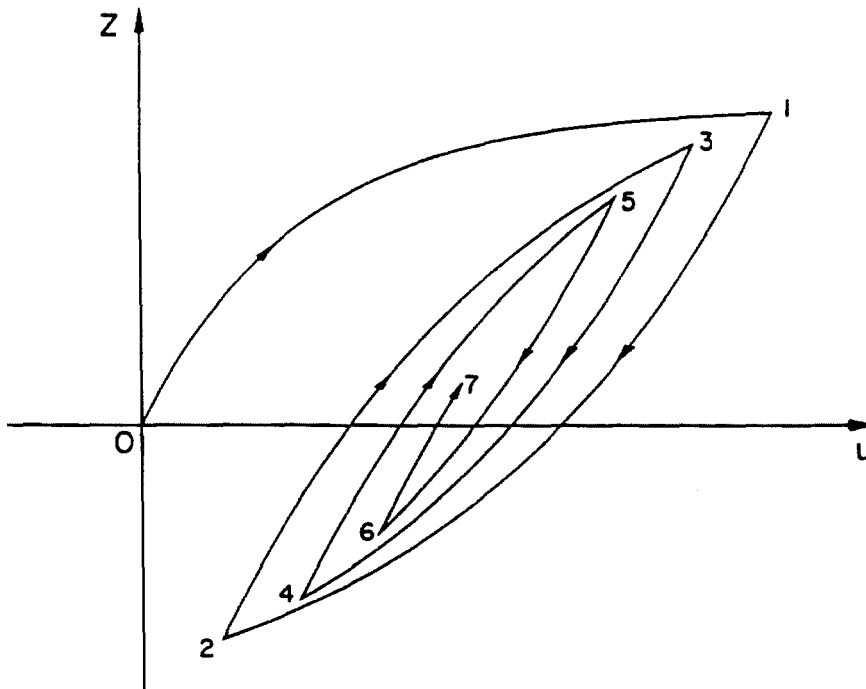


Figure 2.6:    A loading sequence with nested loops subjected on the Distributed Element model.
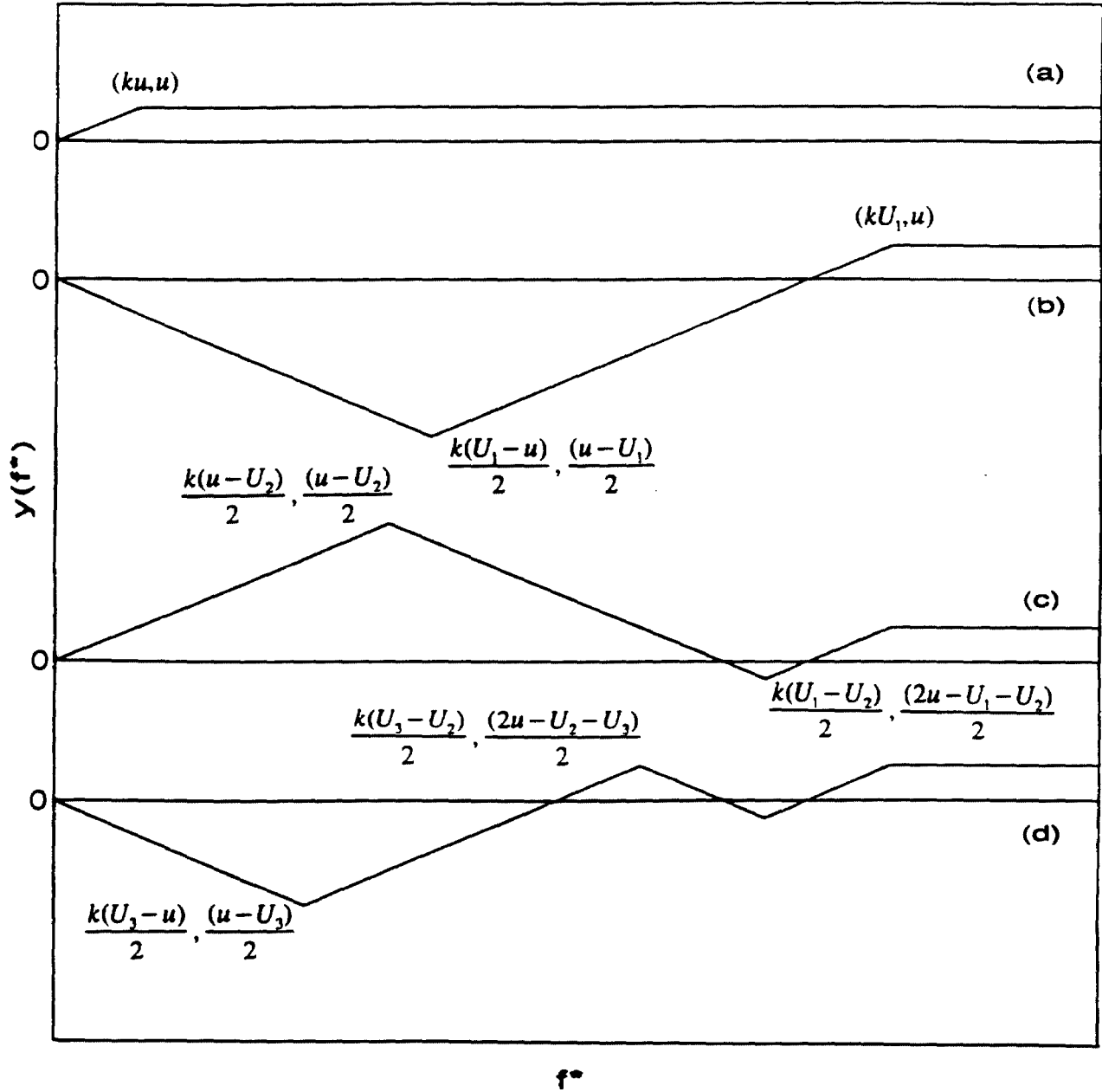
Figure 2.7: The function $y(f^*)$ for (a) path 01 (b) path 12 (c) path 23 (d) path 34 of the loading sequence shown in Fig. 2.6.
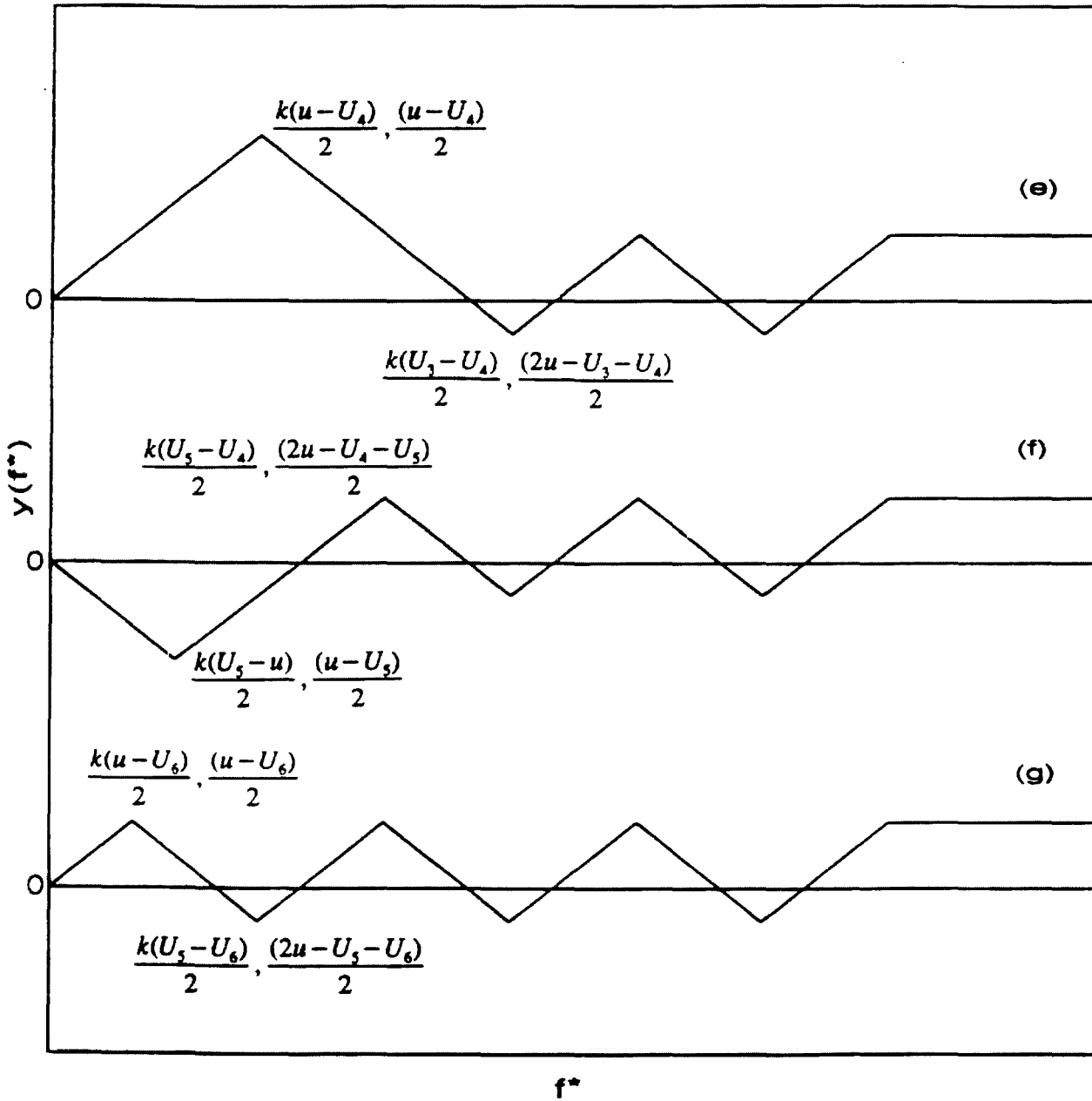
Figure 2.7: (Continued) The function $y(f^*)$ for (e) path 45 (f) path 56 (g) path 67 of the loading sequence shown in Fig. 2.6.

(a)

(b)
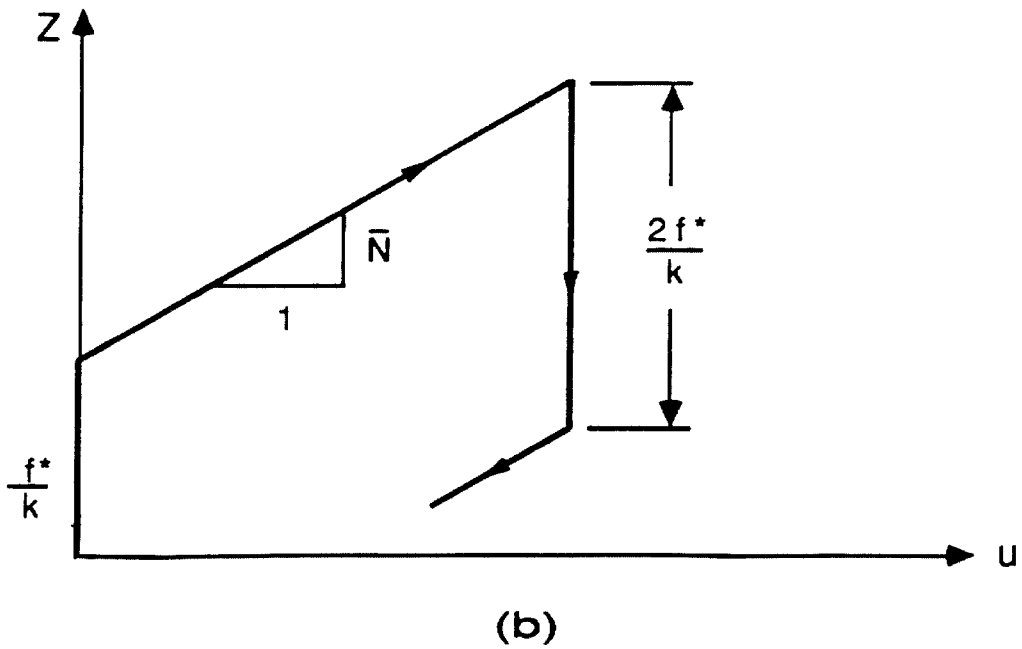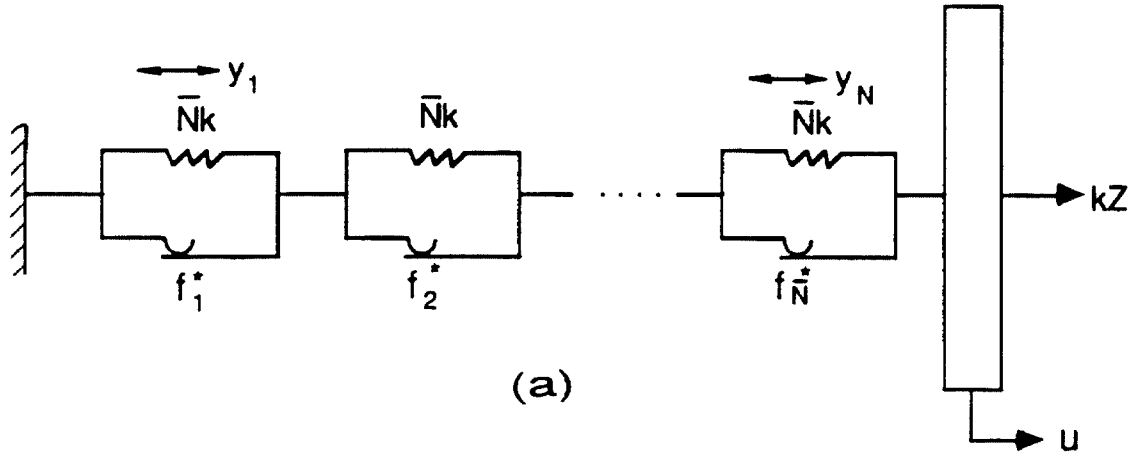
Figure 2.8:    The series-parallel Distributed element model (a) Schematic representation
for the system (b) Restoring force characteristic.
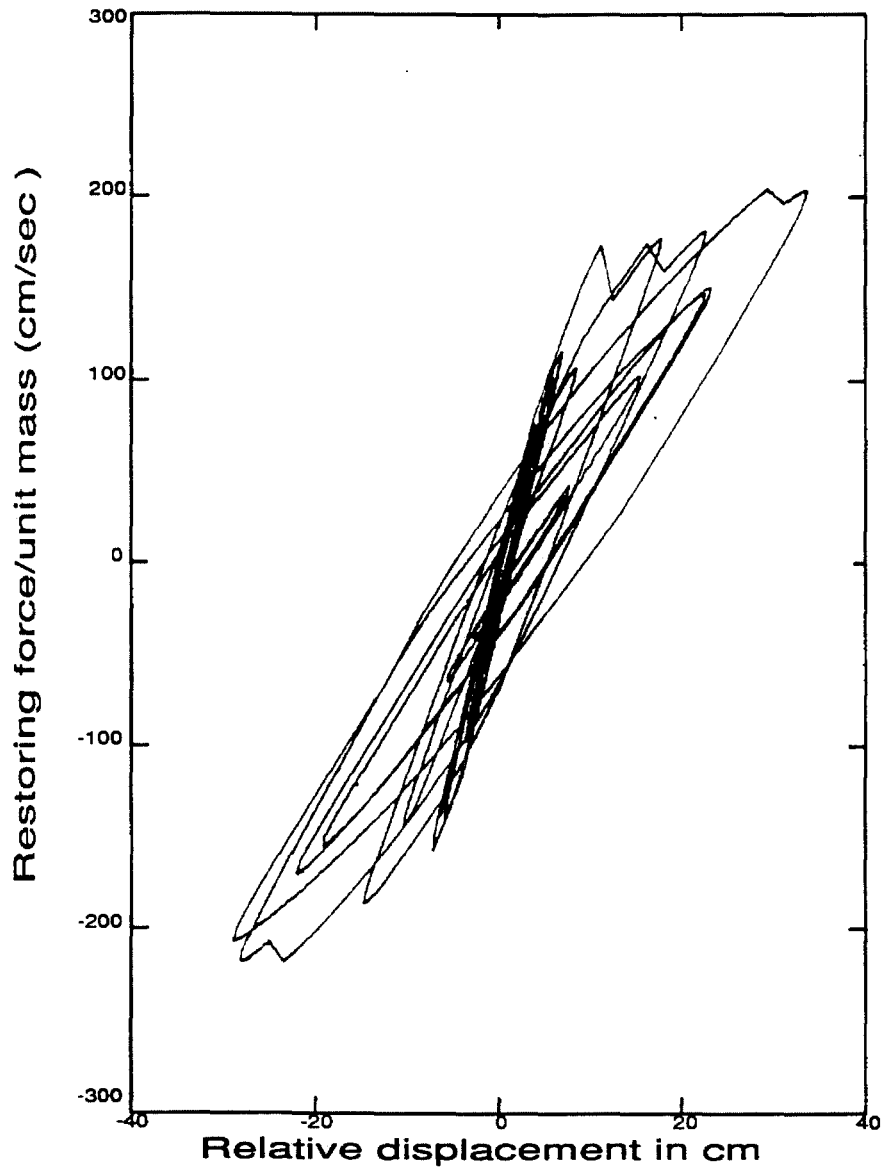
Figure 2.9:   The restoring force behavior of a stiffness- and strength-degrading
Distributed Element model [13].

## CHAPTER 3

# AN IDENTIFICATION METHOD FOR HYSTERETIC SYSTEMS

### 3.1 Introduction

The identification of dynamic models through the use of experimental data is a problem of considerable importance in earthquake engineering. The major goal of the identification process is to characterize or to "identify" accurately the response behavior of a structure subjected to strong ground shaking. Considerable effort has been devoted to determining algorithms and techniques for estimating optimal models from data.

Generally speaking, most of the identification techniques in the past have been parametric; that is, they seek to determine the value of the parameters in an assumed model of the system to be identified. By contrast, nonparametric methods, for example, those by Masri and Caughey [31], Volterra [52], et al., seek the best functional representation of the system without any *a priori* assumptions about the model.

The identification method outlined in this chapter determines a model representation for nonlinear systems in which the slopes of the loading and unloading paths depend only on the instantaneous value of the restoring force. The endochronic models described in Chapter 2 with one additional state variable, for example, the Wen-Bouc hysteretic model, have such a representation. So does the bilinear system. The method involves a search in function space to determine an optimal representation of the system. For this reason, the method can be thought of as a nonparametric identification technique.

The following section describes the technique used for identifying the nonlinear behavior of a system. Examples of the identification of three different hysteretic systems are then enumerated. In each case, the adequacy of the optimal model to describe the original system is examined by comparing their respective responses to a second excitation.

Some of the significant advantages of the identification method are listed in the final section.

## 3.2 The identification procedure:

Let the equation of motion of a single-degree-of-freedom oscillator be given by the following equations

$$m\ddot{u} + c\dot{u} + \alpha k u + (1 - \alpha)kz = -ma(t) \tag{3.1}$$

$$\dot{z} = \dot{u}H(\dot{u})f_1(z) + \dot{u}H(-\dot{u})f_2(z) \tag{3.2}$$

where $u$ is the relative displacement of the oscillator subjected to the base excitation $a(t)$, $z$ is the normalized hysteretic restoring force, $m$ is the mass, $k$ is the initial stiffness, $\alpha k$ is the post-yielding stiffness, $c$ is the viscous damping coefficient, $H$ is the Heaviside's unit step function, and $f_1$ and $f_2$ are single-valued functions of $z$. For a given value of $z$, it may be noted that $kf_1(z)$ and $kf_2(z)$ are the instantaneous system stiffnesses when $\dot{u}>0$ and $\dot{u}<0$, respectively.

The endochronic models with one additional state variable described in Chapter 2 can be represented in the above fashion. For instance, for the Wen-Bouc hysteretic model (Eqn. 2.38), the functions $f_1$ and $f_2$ are given by

$$f_1(z) = \frac{1}{\eta}[A - v|z|^{n-1}(\beta z - \gamma|z|)] \tag{3.3.1}$$

$$f_2(z) = \frac{1}{\eta}[A + v|z|^{n-1}(\beta z + \gamma|z|)] \tag{3.3.2}$$

where $A$, $\beta$, $\gamma$, $v$, $\eta$ and $n$ have the same meaning as in Eqn. (2.38).

Similarly, for the bilinear model (Eqn. 2.2), the functions $f_1$ and $f_2$ are given by

$$f_1(z) = 1 - H(z - u_y) \tag{3.4.1}$$

$$f_2(z) = 1 - H(-z - u_y) \tag{3.4.2}$$

Assume that the measurements for $a(t)$ and $\ddot{u}$ are available over a certain time interval $[0,T]$. The corresponding displacement, $u$, and the velocity, $\dot{u}$, can be found either by direct measurement or by integration of $\ddot{u}$. Assume also that the values of $m$, $c$, $k$ and $\alpha$ have already been obtained by other measurements. For instance, the values of $k$ and $\alpha$ may be determined by performing a monotonic loading test. Eqn. (3.1) can be rearranged to write

$$z = -\frac{ma(t) + m\ddot{u} + c\dot{u} + \alpha ku}{(1 - \alpha)k} \tag{3.5}$$

which yields $\dot{z}$ on differentiation. Eqn. (3.2) can be used to obtain $f_1$ and $f_2$, as follows:

$$f_1(z) = \frac{\dot{z}}{\dot{u}} H(\dot{u}) \tag{3.6.1}$$

$$f_2(z) = \frac{\dot{z}}{\dot{u}} H(-\dot{u}) \tag{3.6.2}$$

Let the normalized value of $z$, namely $\xi$, be defined as:

$$\xi = \frac{(z - \bar{z})}{z_a} \tag{3.7.1}$$

where

$$\bar{z} = (z_{max} + z_{min})/2, \quad z_a = (z_{max} - z_{min})/2 \tag{3.7.2}$$

$z_{min}$ and $z_{max}$ being the minimum and maximum measured values of $z$. Thus, $\xi$ varies from $-1$ to $+1$.

Let the normalized functions $g_1(\xi)$ and $g_2(\xi)$ corresponding to $f_1(z)$ and $f_2(z)$ be defined as

$$g_i(\xi) = f_i(z), \quad i = 1,2 \tag{3.8}$$

where $\xi$ and $z$ are related as in Eqn. (3.7).

The main idea behind the identification methodology used in this chapter is to estimate the functions $g_1$ and $g_2$ (and hence $f_1$ and $f_2$) by approximate functions $\hat{g}_1$ and $\hat{g}_2$, respectively, where $\hat{g}_1$ and $\hat{g}_2$ are expressed in terms of a set of orthogonal polynomials.

Without loss of generality, the set of Legendre polynomials, $P_n(\xi)$, will be used for the remainder of this chapter. Thus,

$$g_1(\xi) \approx \hat{g}_1(\xi) = \sum_{i=0}^{N} a_i P_i(\xi) \qquad (3.9.1)$$

$$g_2(\xi) \approx \hat{g}_2(\xi) = \sum_{i=0}^{N} b_i P_i(\xi) \qquad (3.9.2)$$

The Legendre polynomials, $P_n(\xi)$, which are solutions of the Legendre's differential equation, are given by Rodrigues' formula to be

$$P_n(\xi) = \frac{1}{2^n n!} \frac{d^n}{d\xi^n} (\xi^2 - 1)^n \qquad (3.10)$$

and they satisfy the following orthogonal property with respect to the weighting function of unity,

$$\int_{-1}^{1} P_n(\xi) P_m(\xi) d\xi = \begin{cases} 0 & \text{if } m \neq n \\ \dfrac{2}{2n+1} & \text{if } m = n \end{cases} \qquad (3.11)$$

The next step is to estimate the coefficients, $a_i$ and $b_i$, using some error-minimization criteria. Once these coefficients are determined from the measurements, the system is completely identified for subsequent analysis. Let the error functions be defined as

$$E_i^{(N)} \equiv \int_{-1}^{1} [g_i(\xi) - \hat{g}_i(\xi)]^2 \, d\xi \quad \text{for } i = 1,2 \qquad (3.12)$$

In order that the optimum choice of the coefficients minimize the errors $E_1^{(N)}$ and $E_2^{(N)}$, the following relations must be satisfied:

$$\frac{\partial E_1^{(N)}}{\partial a_j} = 0 \quad \text{for } j = 0,1,2,\ldots,N \qquad (3.13.1)$$

$$\frac{\partial E_2^{(N)}}{\partial b_j} = 0 \quad \text{for } j = 0,1,2,\ldots,N \qquad (3.13.2)$$

Use of Eqn. (3.12) in Eqn. (3.13) yields

$$a_i = \frac{1}{h_i} \int_{-1}^{1} g_1(\xi) P_i(\xi) d\xi \quad \text{for } i = 0,1,2,\dots\dots,N \tag{3.14.1}$$

$$b_i = \frac{1}{h_i} \int_{-1}^{1} g_2(\xi) P_i(\xi) d\xi \quad \text{for } i = 0,1,2,\dots\dots,N \tag{3.14.2}$$

where

$$h_i = \frac{2}{2i+1} \quad \text{for } i = 0,1,2,\dots\dots,N \tag{3.14.3}$$

Either because the data are available only at discrete points and/or because the computation of the coefficients is done on a digital computer, the trapezoidal algorithm may have to be used to replace the integrals in Eqn. (3.14) by finite sums.

In summary, given an identification excitation $a(t)$ and the corresponding acceleration, $\ddot{u}$, of a single-degree-of-freedom system, a model representation of the type described by Eqns. (3.1) and (3.2) can be identified by the optimal choice of the coefficients $a_i$ and $b_i$ given by Eqn. (3.14). For this choice of coefficients, the functions $\hat{f}_1$ and $\hat{f}_2$ are the best approximation in the least-squares sense to the functions $f_1$ and $f_2$, respectively. Using Eqns. (3.7) and (3.8), it is possible to write

$$f_1(z) \approx \hat{f}_1(z) = \sum_{i=0}^{N} a_i\, P_i(\frac{z-\bar{z}}{z_a}) \tag{3.15.1}$$

$$f_2(z) \approx \hat{f}_2(z) = \sum_{i=0}^{N} b_i\, P_i(\frac{z-\bar{z}}{z_a}) \tag{3.15.2}$$

with $\bar{z}$ and $z_a$, as in Eqn. (3.7.2).

It may be mentioned here that the identification data for $f_1$ and $f_2$ need not be obtained necessarily from the response of the system to a dynamic excitation. It could also be obtained from the slopes of the restoring force diagram when the system is subjected to quasi-static loading. Once the data are obtained, the method of identification of the

nonlinear restoring force behavior of the system using orthogonal polynomials is unchanged.

## 3.3 Identification examples

In this section, three examples of the identification of hysteretic systems by the method described above are illustrated. The three systems considered are the Wen-Bouc, the Bilinear and the Distributed Element hysteretic systems. In each case, the system response to two base excitations is determined. The first of these base excitations, $a_1(t)$, shown in Fig. 3.1 is a sinusoidal function with a linearly increasing amplitude and serves as the identification excitation. The response of the system to this excitation is used to obtain the coefficients $a_i$ and $b_i$, and hence the functions $\hat{f}_1$ and $\hat{f}_2$ which define the optimal model.

The second base excitation, $a_2(t)$, shown in Fig. 3.2, is the N-S component of the 1940 El Centro earthquake, which serves as the verification excitation. The response of the optimal model to this excitation is compared with that of the original system to the same excitation. A favorable comparison is an indication that the optimal model is an adequate mathematical representation for the original system.

### 3.3.1 Example 1: The Wen-Bouc hysteretic system

A system whose hysteretic behavior is governed by the Wen-Bouc model (Eqn. 2.38) is considered with the following values of the parameters: the ratio $k/m$=10.0, post-yielding stiffness ratio $\alpha$=0.10, viscous damping coefficient $c$=0.0, $A$=1.0, $\beta$=30.0, $\gamma$=-20.0, $n$=1.5. For these values of the parameters, the maximum or yield value of $z$ is about 0.074.

When this system is subjected to the identification excitation $a_1(t)$, its response displacement and velocity are as shown in Fig. 3.3. Substitution of $u$ and $\dot{u}$ in Eqn. (3.5)

yields $z$ and hence $\dot{z}$. Eqn. (3.6) can then be used to obtain the identification data for $f_1$ and $f_2$, which are used in the determination of the coefficients $a_i$ and $b_i$.

The identification data for $f_1$ thus obtained are shown in Fig. 3.4; also shown in the figure is $\hat{f}_1$, the optimal polynomial fit for $f_1$ when $N=3$ (third-order polynomial). Similarly, the identification data for $f_2$ and the corresponding best fit, $\hat{f}_2$, are shown in Fig. 3.5. $\hat{f}_1$ and $\hat{f}_2$ are found to be

$$\hat{f}_1(z) = 0.975 - 4.660z - 76.647z^2 - 726.313z^3 \qquad (3.16.1)$$

$$\hat{f}_2(z) = 0.976 + 4.598z - 76.800z^2 + 738.973z^3 \qquad (3.16.2)$$

$\in$, a measure of the goodness-of-fit between the actual function, $f_i$, and the approximate one, $\hat{f}_i$, can be obtained in the following manner. Define $\in_1$ and $\in_2$ as

$$\in_i = \frac{\left\{ \dfrac{1}{n} \displaystyle\sum_{j=1}^{n} [f_i(z_j) - \hat{f}_i(z_j)]^2 \right\}^{1/2}}{\left\{ \dfrac{1}{n} \displaystyle\sum_{j=1}^{n} [f_i(z_j)]^2 \right\}^{1/2}} \quad \text{for } i = 1, 2 \qquad (3.17.1)$$

and let

$$\in \equiv \sqrt{\in_1^2 + \in_2^2} \qquad (3.17.2)$$

where $z_j, j=1,2,3,.....,n$ are the $n$ data points at which the identification data are available. In this example, $\in$ is found to equal 0.043.

To determine how satisfactorily the optimal model predicts the response behavior of the original Wen-Bouc system, the optimal model and the original system are subjected to the verification excitation, $a_2(t)$, and the displacement, velocity and hysteretic restoring force diagram are plotted in Figs. 3.6, 3.7 and 3.8, respectively. It can be seen that the prediction by the optimal model of the response of the original system is very good.

## 3.3.2 Example 2: The Bilinear hysteretic system

The bilinear hysteretic system (Eqn. 2.2) is considered next with the following values of the parameters: the ratio $k/m$=10.0, post-yielding stiffness ratio $\alpha$=0.10, viscous damping coefficient $c$=0.0 and the slip level $u_y$=0.08. The maximum or yield value of $z$ is thus 0.08.

When subjected to the identification excitation, $a_1(t)$, the displacement and velocity of this system are as shown in Fig. 3.9. As in Example 1, the identification data for $f_1$ and $f_2$ are evaluated, and the results shown in Figs. 3.10 and 3.11, respectively. The functions, $\hat{f}_1$ and $\hat{f}_2$, the optimal polynomial fits for $f_1$ and $f_2$, are also shown in the corresponding figures for $N$=6 (sixth-order polynomial). A higher-order polynomial is required here in order to capture the step discontinuity in the functions $f_1$ and $f_2$. The goodness-of-fit parameter, $\epsilon$, is found to equal 0.374.

If a further reduction in the value of $\epsilon$ is desired, $N$ would have to be increased. There are three reasons why a large $N$ is undesirable. Firstly, as $N$ becomes very large, the number of parameters required to describe the optimal model becomes large as well. Since the objective of the identification process is to obtain simple optimal models, which can be described by as few parameters as possible, $N$ should be kept small. Secondly, the higher the order of a polynomial, the more rapidly it oscillates within any interval, and the polynomial interpolation between data points may lead to misleading values of the target function. Thirdly, when $N$ is large, noise in the data can significantly alter the optimal polynomial.

The displacement and velocity prediction of the optimal model when subjected to the verification excitation, $a_2(t)$, are compared with the displacement and velocity of the original bilinear system to the same excitation in Figs 3.12 and 3.13, respectively. It can be seen that agreement is very good, even though the value of $\epsilon$ is relatively large when compared to Example 1.

The hysteretic restoring force diagrams for the bilinear system and the corresponding optimal model are as shown in Fig. 3.14. The agreement in the hysteretic behavior is quite satisfactory. A couple of remarks may be made here regarding the hysteresis loops of the optimal model. The approximation of the functions $f_1$ and $f_2$ by their polynomial counterparts $\hat{f}_1$ and $\hat{f}_2$ causes the following two effects:

(1) The transition to yield occurs smoothly, unlike the case of the bilinear system, which has a sharp yield transition.

(2) The maximum or yield value of $z$ is about 0.09, while that of the bilinear system is 0.08. This is because, in the case of the bilinear system, $f_1$ is zero for $z \geq 0.08$. But the corresponding polynomial $\hat{f}_1$ is zero only for $z$ greater than about 0.09. For values of $z$ between 0.08 and 0.09, the extrapolation of $\hat{f}_1$ yields nonzero slopes of the restoring force loops.

As the value of $N$ becomes large, the extent of these two effects is likely to increase.

### 3.3.3 Example 3: The Distributed Element hysteretic system

Unlike the Wen-Bouc and the Bilinear hysteretic systems, the slopes of the hysteretic branches in the response of the Distributed Element system do not depend only on $z$, the normalized hysteretic force, but also on the previous history of the response. That is, the Distributed Element hysteretic systems do not have a representation of the type described by Eqns. (3.1) and (3.2). Given this, it will be interesting to examine how well the identification method works in this case.

Consider the Distributed Element system whose initial loading curve is given by

$$z = z_y(1 - e^{-u/u_y}) \quad \text{for } u \geq 0 \qquad (3.17)$$

Once the initial loading curve is known, the hysteretic behavior of the system for subsequent loading is given by the Extended Massing's hypothesis. For this example, the values of the system parameters are: the ratio $k/m = 10.0$, post-yielding stiffness ratio

$\alpha$ =0.10, viscous damping coefficient $c$=0.0 and $u_y = z_y$=0.03. The maximum or yield value of $z$ is thus 0.03.

When subjected to the identification function $a_1(t)$, the displacement and velocity of the system are as shown in Fig. 3.15. As in the previous examples, $u$, $\dot{u}$ and $z$ are used to obtain the identification data for $f_1$ and $f_2$, which are then plotted against $z$ in Figs. 3.16 and 3.17, respectively. The functions $\hat{f}_1$ and $\hat{f}_2$, the best polynomial fits for $f_1$ and $f_2$, respectively, for $N$=3 are also shown in the figures. The goodness-of-fit parameter, $\epsilon$, for this example is 0.198. As discussed in the previous example, $\epsilon$ may be reduced by increasing $N$, but a large $N$ is considered undesirable for reasons already explained.

The Distributed Element system and the corresponding optimal model are subjected to the verification excitation $a_2(t)$, and the response displacement and velocity are plotted in Figs. 3.18 and 3.19, respectively. It can be seen that the essential features of the displacement response are preserved by the optimal model, but the agreement is not as good as in previous examples. In contrast, the velocity prediction by the optimal model is very good; it will be seen from the results of later chapters that the velocity prediction of an endochronic model is usually more reliable than the displacement prediction.

The restoring force diagrams of the Distributed Element model and the corresponding optimal model are shown in Fig. 3.20. Two distinct features may be observed in the behavior of the optimal model. Firstly, the restoring force behavior of the optimal model sometimes exhibits partial closure as well as nonclosure of loops, and secondly, its hysteresis loops enclose larger areas, indicating larger energy dissipation. Such features in the hysteretic behavior of these models will be examined in greater detail in Chapters 4 and 5.

The identification method can be thought of as yielding the optimal or best fit endochronic representation for the Distributed Element system. Similarly, the identification method proposed in this chapter yields optimal endochronic model representations for real

systems for which data measurements are available. It must be realized that the original Distributed Element system is only approximately represented by the optimal model obtained by the identification procedure. However, the representation so obtained is the optimal or the "best-fit" endochronic model for the original system in the least-squares sense.

## 3.4 Conclusion

A relatively straightforward method has been proposed for the identification of single-degree-of-freedom, nonlinear dynamical systems. Some of the significant advantages of this method are as follows:

(1) Parametric identification techniques usually evaluate the optimal system parameters by minimizing an error that is defined in terms of the time history of the structure's response. This approach has a numerical disadvantage in that it requires the solution of a differential equation each time the error is calculated. The method described in this chapter has a computational advantage since the minimization is based on the restoring force behavior of the structure. Therefore, the execution time requirements of the method are relatively modest.

(2) Even though the identification data may be available only over a certain range of the system response, the extrapolation of the polynomials determined serves as a rational method for the extension of the model to a wider range of the response.

(3) There is no restriction on the type of excitation that can be used for the purposes of identification. For best results, however, the identification excitation must be such that the identification data on $f_1$ and $f_2$ must be available over most of the range of values that the normalized restoring force, $z$, can assume.

(4) The procedure is also applicable to nonlinear, nonhysteretic systems, for example, the Duffing's oscillator. In this case, the technique is simplified if the information of the

nonhysteretic nature is known *a priori*, because the fact that $f_1 = f_2$ implies that only one of these functions needs to be identified.

(5) The method has a fast convergence property, and a small value of $N$ is usually enough to provide satisfactory results.

(6) The identification technique used to determine the coefficients $a_i$ and $b_i$ are not very sensitive to the noise in the data because a minor scatter in the data does not drastically alter the optimal polynomial fit to the data when $N$ is small.

(7) This method offers a simple means for determining the optimal endochronic representation to hysteretic systems. For instance, Example 3 showed how such a representation can be obtained for the Distributed Element hysteretic system.

(8) Once the optimal model representation is obtained for a hysteretic system, it can be used in conjunction with the theory of equivalent linearization to yield approximate statistics on the response of the original hysteretic system when subjected to stochastic excitation.
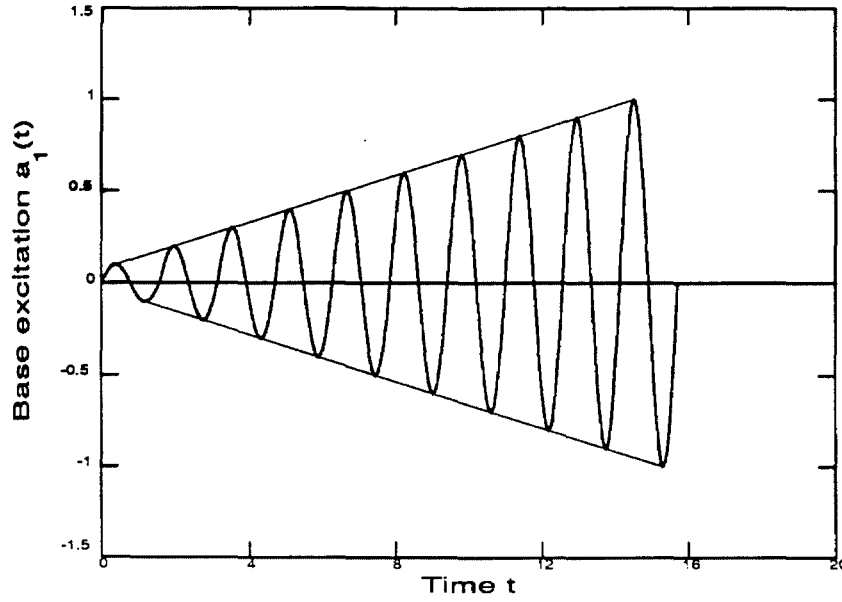
Figure 3.1:　The identification base excitation $a_1(t)$, which is a sinusoidal function with a linearly increasing amplitude.
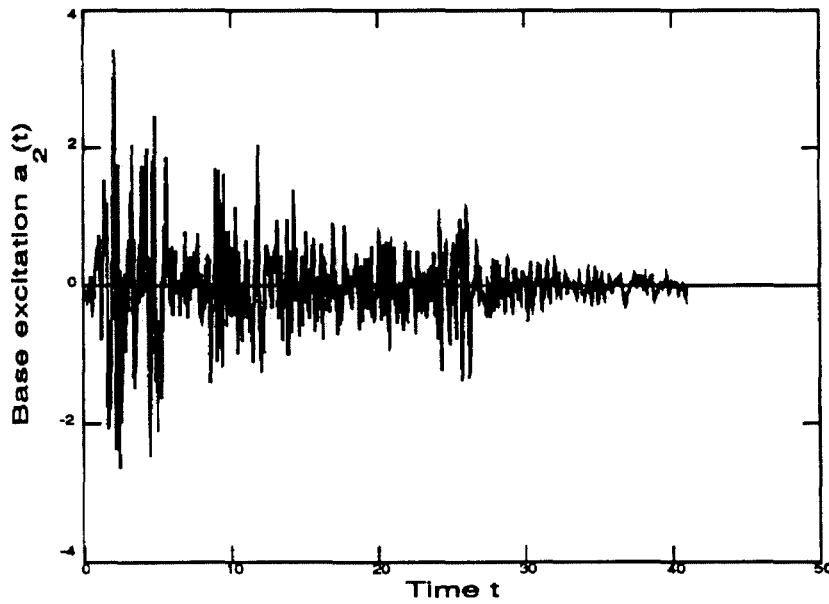


Figure 3.2:　The verification base excitation $a_2(t)$, which is the N-S component of the 1940 El Centro earthquake.
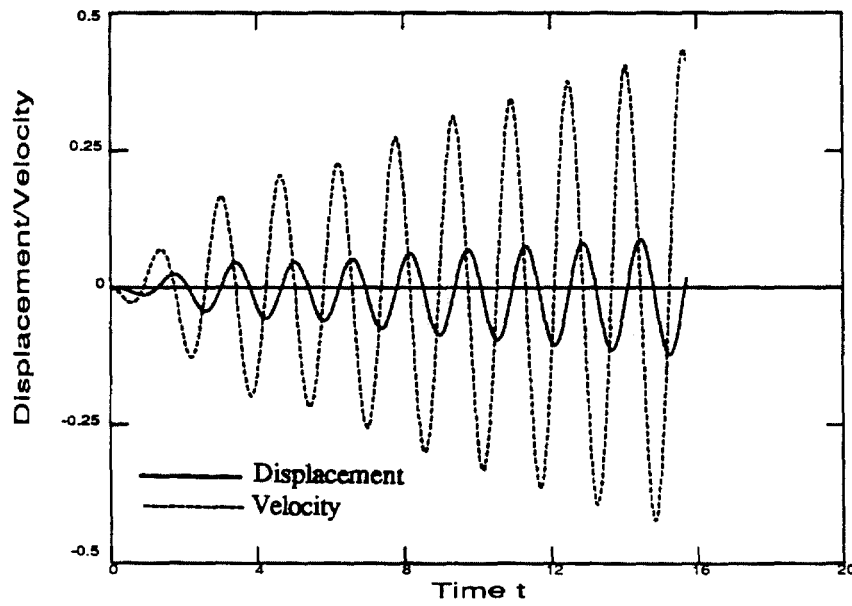
Figure 3.3:    The displacement and velocity of the Wen-Bouc hysteretic system when subjected to the identification excitation, $a_1(t)$.
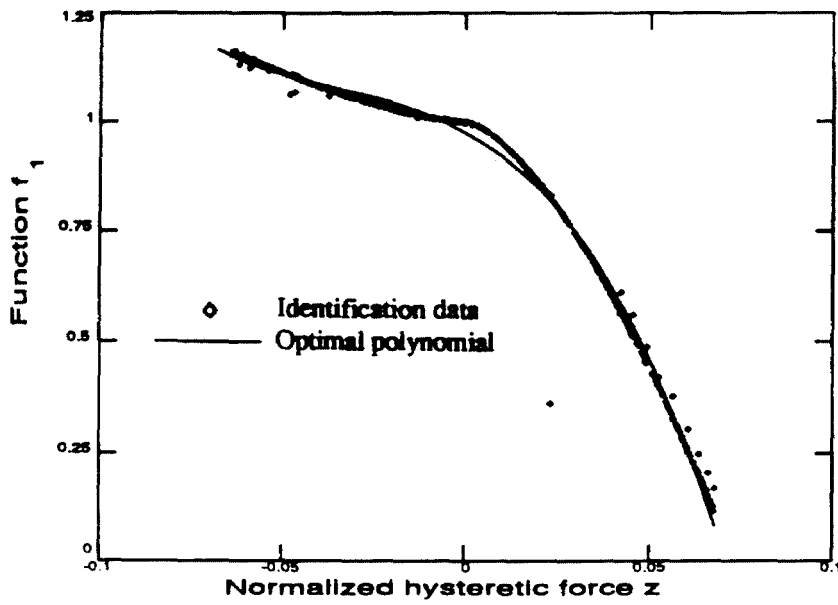
Figure 3.4:   The identification data for $f_1$ and the optimal polynomial fit for the data when the Wen-Bouc hysteretic system is subjected to the identification excitation, $a_1(t)$.
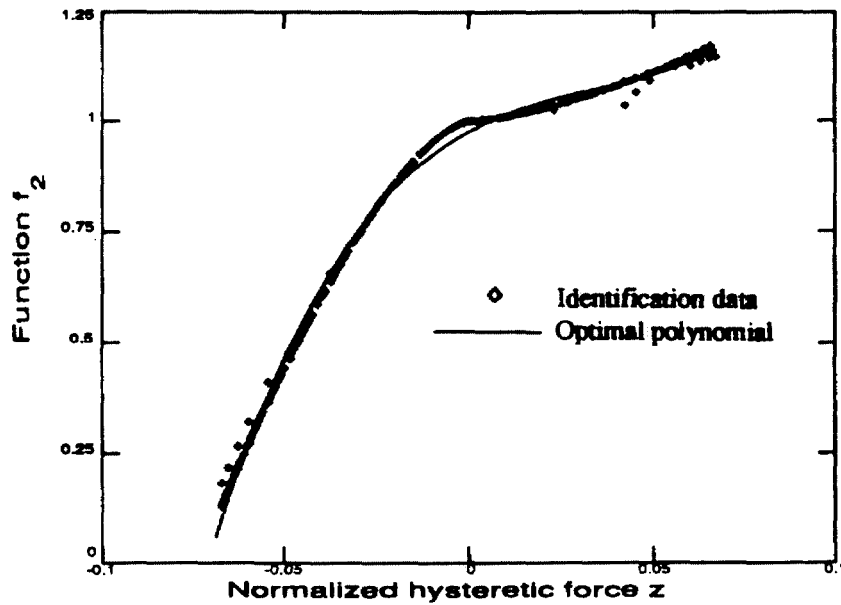


Figure 3.5:   The identification data for $f_2$ and the optimal polynomial fit for the data when the Wen-Bouc hysteretic system is subjected to the identification excitation, $a_1(t)$.
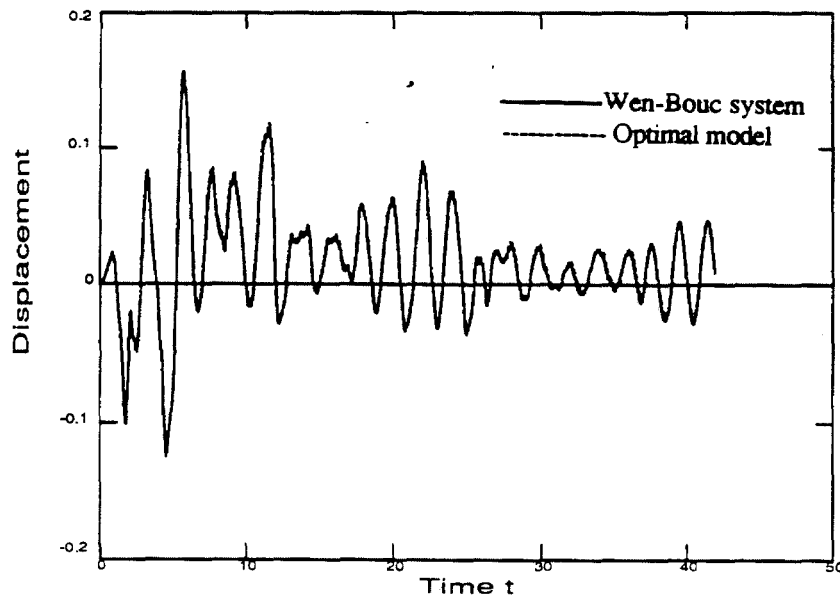
Figure 3.6: The displacement response of the Wen-Bouc hysteretic system and the corresponding optimal model when subjected to the verification excitation, $a_2(t)$.
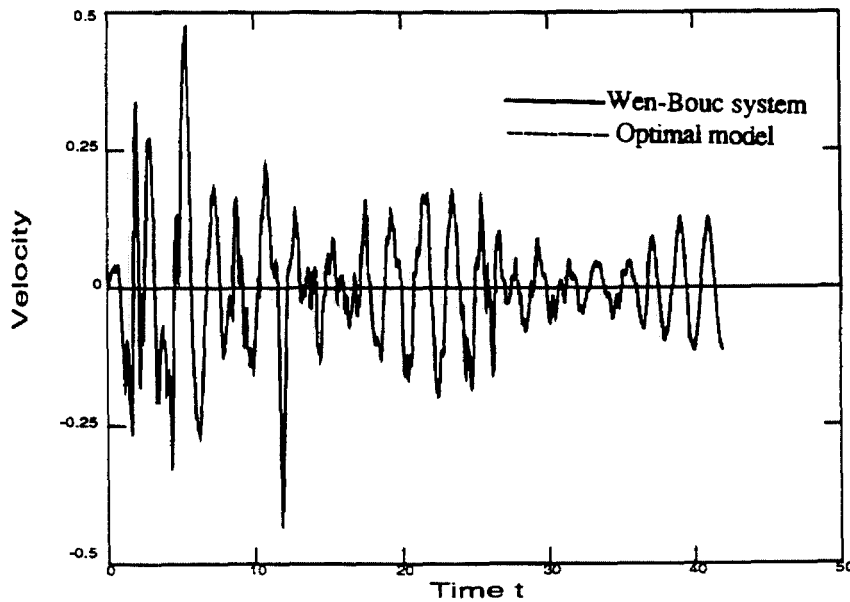


Figure 3.7: The velocity response of the Wen-Bouc hysteretic system and the corresponding optimal model when subjected to the verification excitation, $a_2(t)$.
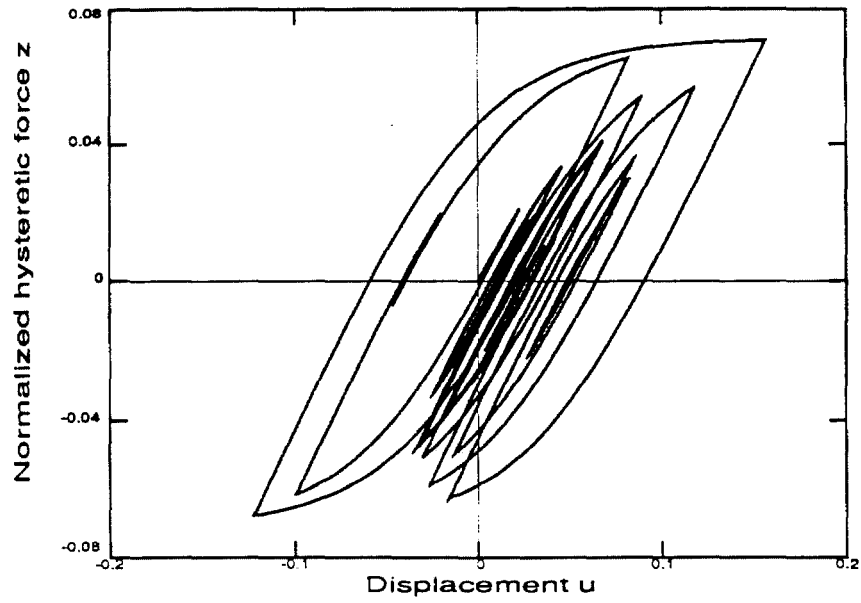
(a)
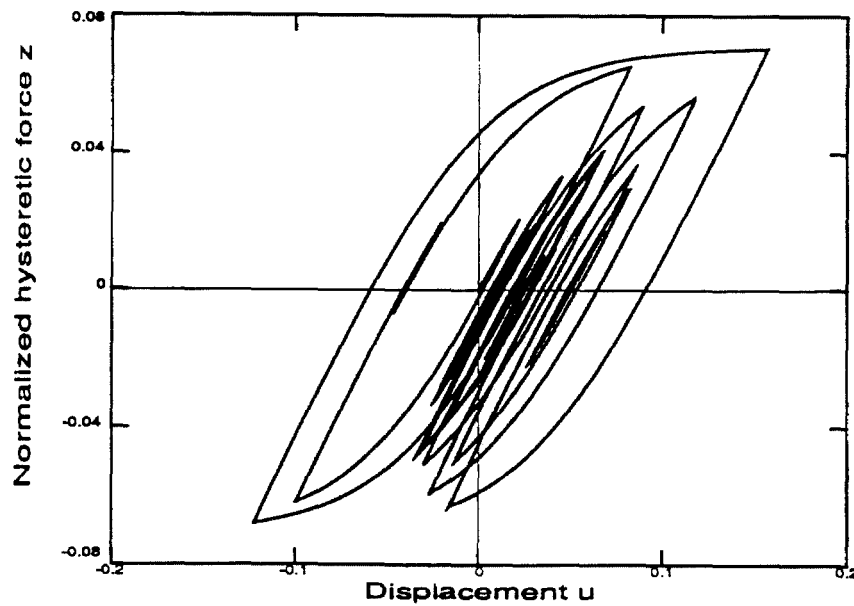


(b)

Figure 3.8:   The hysteretic restoring force diagram for (a) the Wen-Bouc hysteretic system (b) the corresponding optimal model when each is subjected to the verification excitation, $a_2(t)$.
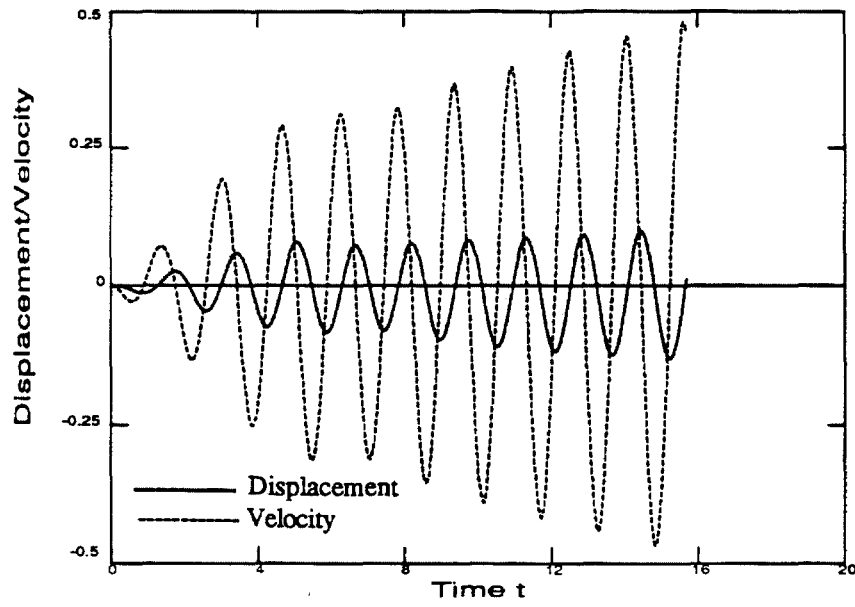
Figure 3.9:    The displacement and velocity of the bilinear hysteretic system when subjected to the identification excitation, $a_1(t)$.
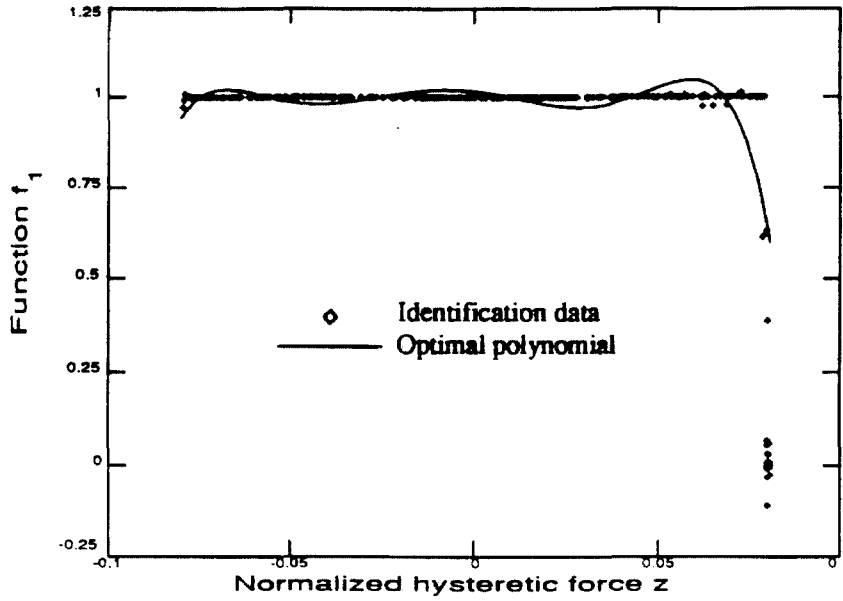
Figure 3.10: The identification data for $f_1$ and the optimal polynomial fit for the data when the bilinear hysteretic system is subjected to the identification excitation, $a_1(t)$.
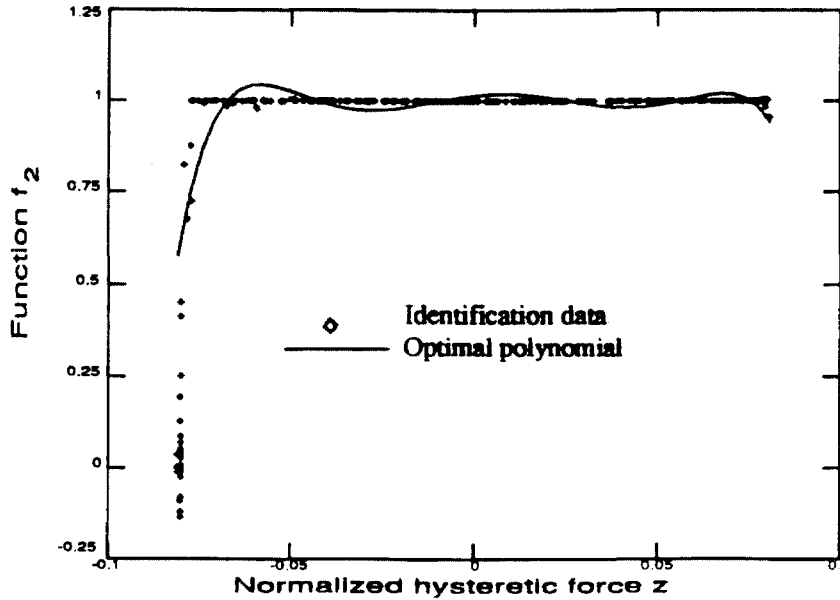


Figure 3.11: The identification data for $f_2$ and the optimal polynomial fit for the data when the bilinear hysteretic system is subjected to the identification excitation, $a_1(t)$.
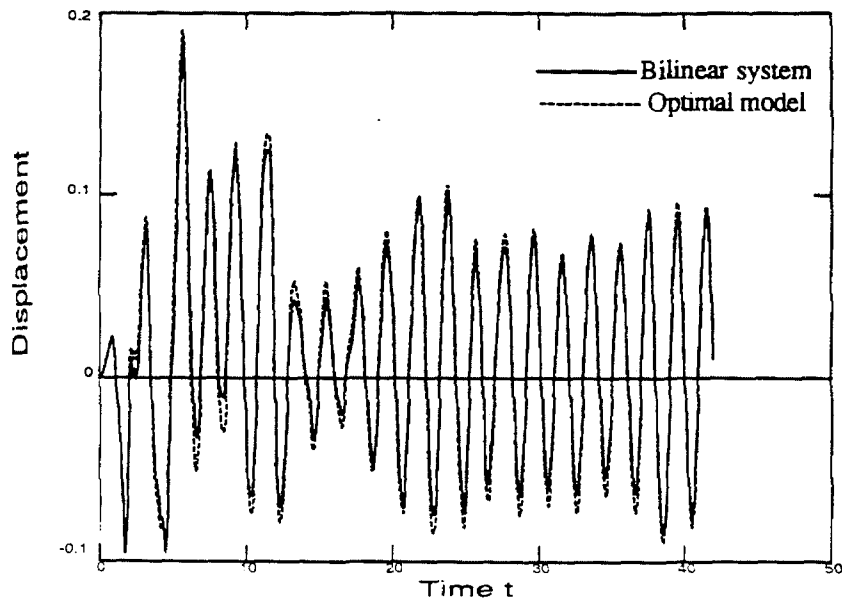
Figure 3.12: The displacement response of the bilinear hysteretic system and the corresponding optimal model when subjected to the verification excitation, $a_2(t)$.
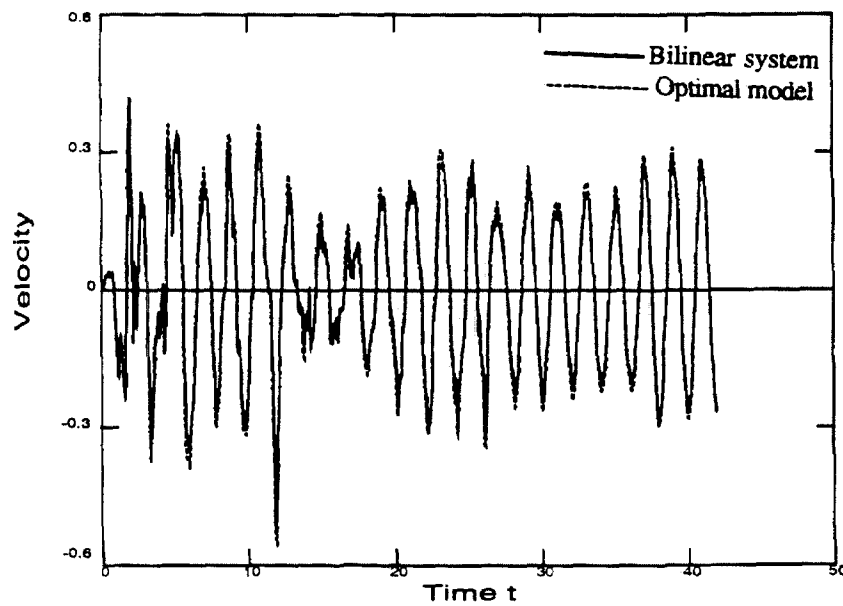


Figure 3.13: The velocity response of the bilinear hysteretic system and the corresponding optimal model when subjected to the verification excitation, $a_2(t)$.
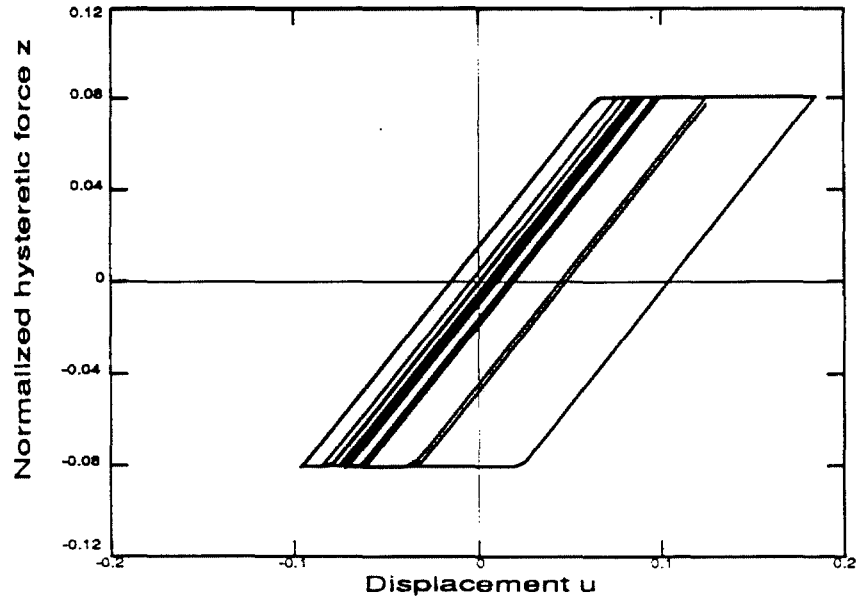
**(a)**
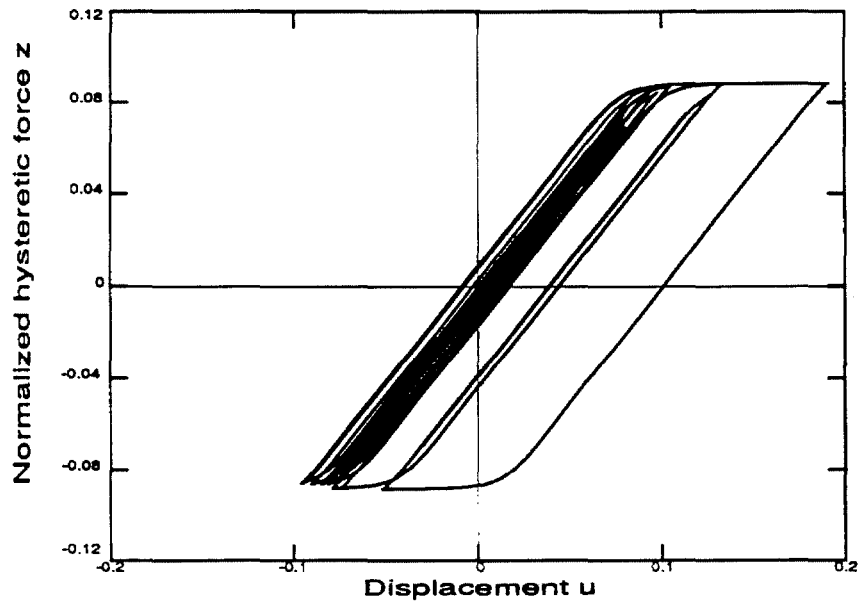


**(b)**

Figure 3.14:   The hysteretic restoring force diagram for (a) the bilinear hysteretic system (b) the corresponding optimal model when each is subjected to the verification excitation, $a_2(t)$.
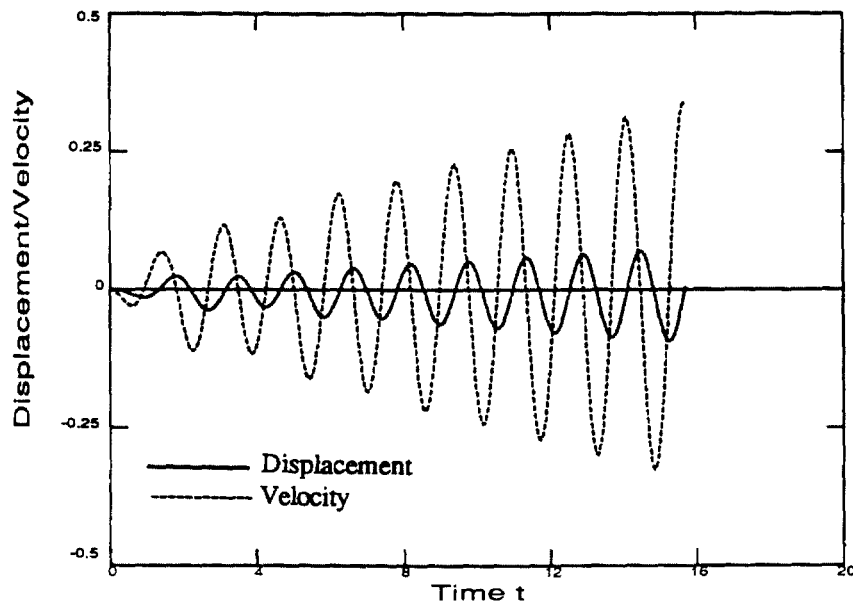
Figure 3.15: The displacement and velocity of the Distributed Element hysteretic system when subjected to the identification excitation, $a_1(t)$.
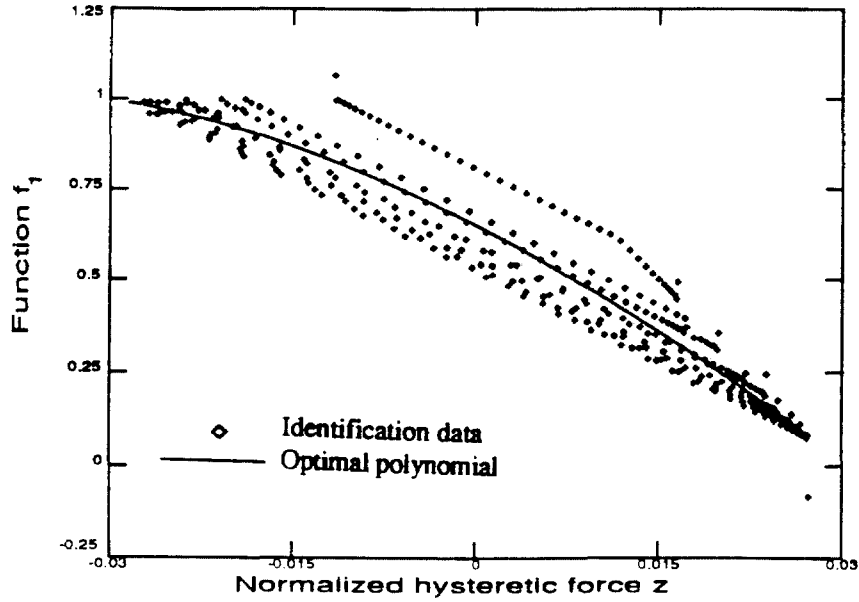
Figure 3.16: The identification data for $f_1$ and the optimal polynomial fit for the data when the Distributed Element hysteretic system is subjected to the identification excitation, $a_1(t)$.
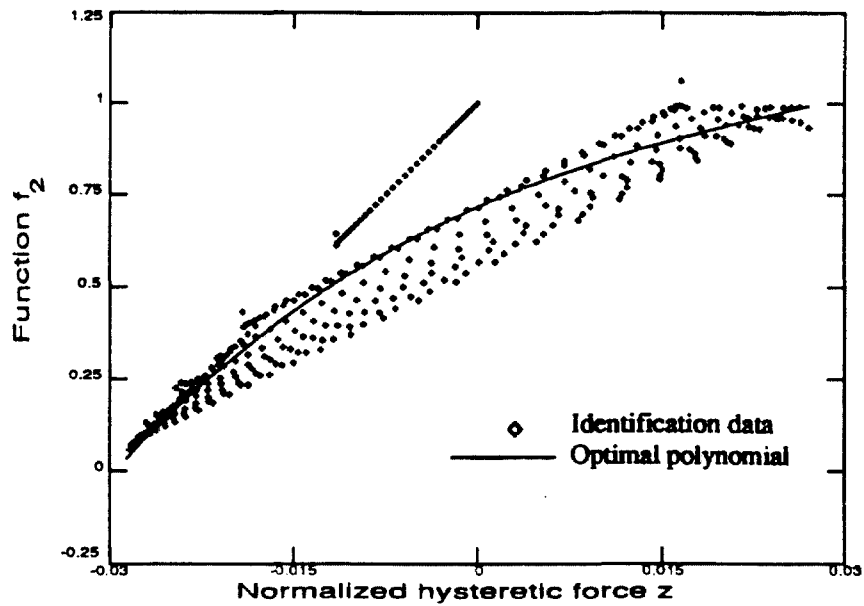


Figure 3.17: The identification data for $f_2$ and the optimal polynomial fit for the data when the Distributed Element hysteretic system is subjected to the identification excitation, $a_1(t)$.
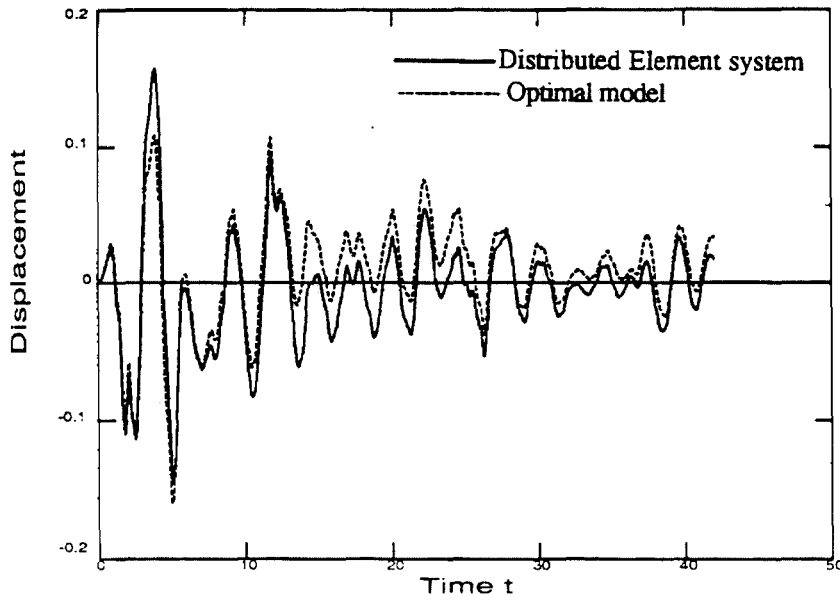
Figure 3.18:   The displacement response of the Distributed Element hysteretic system
and the corresponding optimal model when subjected to the verification
excitation, $a_2(t)$.
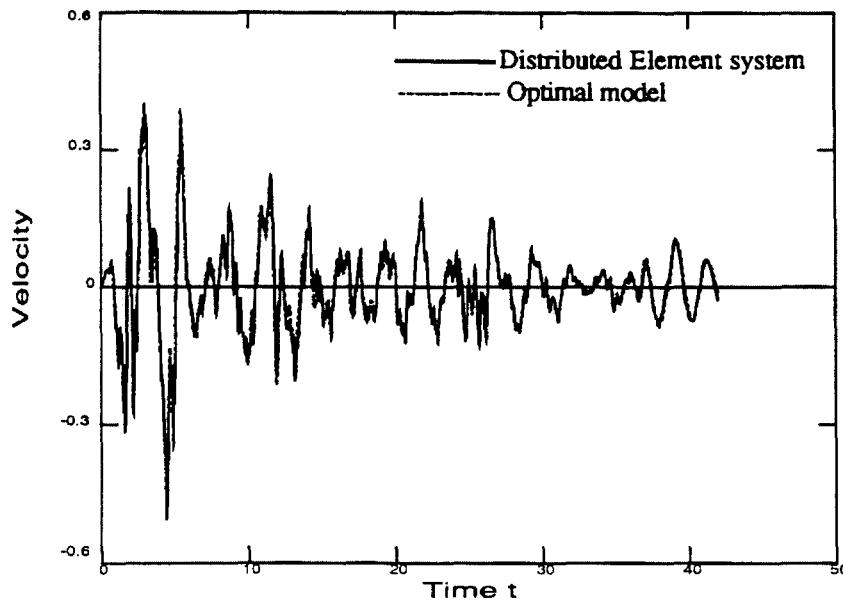


Figure 3.19:   The velocity response of the Distributed Element hysteretic system and
the corresponding optimal model when subjected to the verification
excitation, $a_2(t)$.
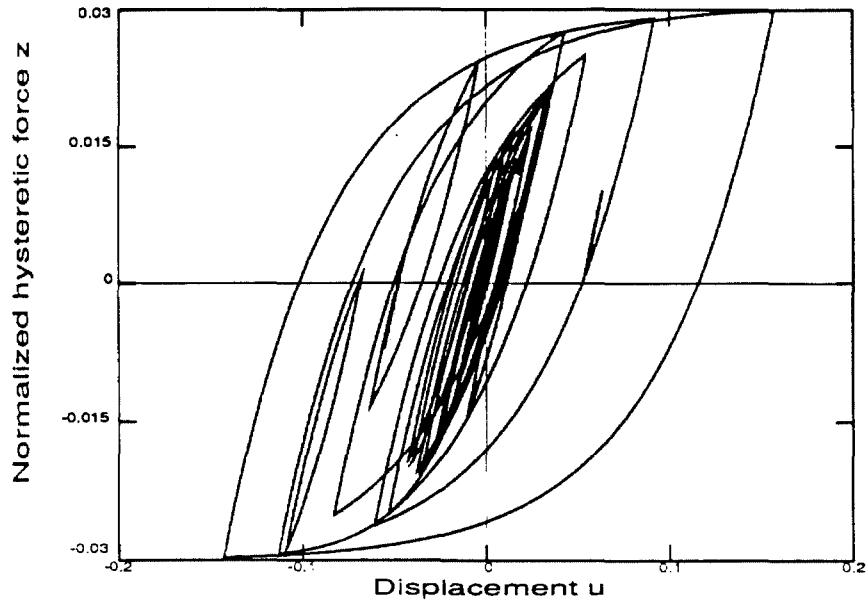
(a)
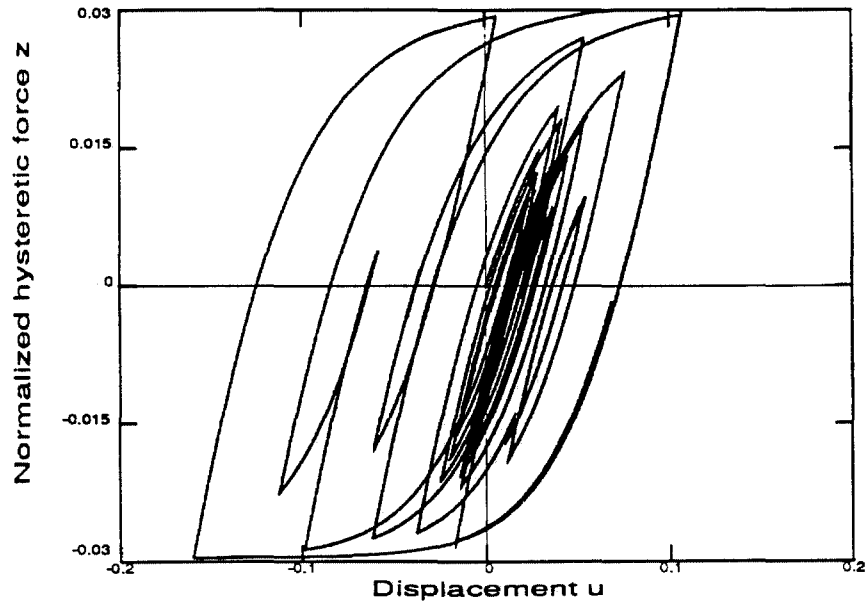


(b)

Figure 3.20: The hysteretic restoring force diagram for (a) the Distributed Element hysteretic system (b) the corresponding optimal model when each is subjected to the verification excitation, $a_2(t)$.

# CHAPTER 4

# COMPARATIVE STUDY OF THE QUASI-STATIC PERFORMANCE OF TWO HYSTERETIC MODELS

## 4.1 Introduction:

In Chapter 2, two classes of curvilinear hysteretic models were described. The first is of the distributed element or assemblage type and the second is of the differential equation type where one additional state variable is introduced in the formulation along with a first-order, nonlinear differential equation that this state variable satisfies. The models belonging to the latter class are also referred to as endochronic models on account of their behavior's being similar to that of the endochronic models used in plasticity. For this reason, the second class of models is herein interchangeably referred to as the endochronic class of hysteretic models.

Certain undesirable behavior exhibited by the endochronic models has been pointed out previously [24,36,44]. However, Wen, Ang, Baber, Casciyati and others have used these models extensively for various applications such as:

- Response analysis by the method of equivalent linearization [10,54],

- Damage evaluation of buildings and the supporting soil systems [54],

- Liquefaction of sand deposits [54],

- System identification of deteriorating systems [46],

- Random vibration of hysteretic systems under bidirectional ground motion [37],

- Nonzero mean random vibrations [5], etc.

The above list is by no means comprehensive: It is given here merely to serve as an indication of how widely used the endochronic formulation has been in structural dynamics.

This chapter performs a comparison of the hysteretic restoring force behavior of the two classes of curvilinear models by carrying out a set of quasi-static tests. These tests pertain to cycling between fixed displacement limits as well as cycling between fixed force limits. This is similar to the cycling of a specimen between fixed strain and stress limits, respectively, in a physical experiment. The results of these tests show some decidedly nonphysical behavior on the part of the endochronic models.

In carrying out these analyses, the two models are adjusted to have identical initial loading curves so as to facilitate direct comparison. For the Distributed Element model, the extended Massing's hypothesis formulation is used because of the relative ease of numerical implementation.

## 4.2 Hysteretic model representations:

The history dependence of the restoring force behavior of a system is characterized by the $z$-$u$ diagrams, where $z$ is the normalized hysteretic force as in Chapter 2 and $u$ is the displacement of the system. The $z$-$u$ relationship for various hysteretic models is given in Chapter 2. In the case of the Wen-Bouc differential equation model, Eqn. (2.38) for $n=1$, $v=1.0, \eta=1.0$ may be written in the following form:

$$\frac{dz}{du} = A - \beta z sgn(du) + \gamma z \tag{4.1}$$

where $\beta$, $\gamma$, $A$ are parameters that control the nature of the hysteretic loops. Given a variation in $u$ or $z$, the corresponding variation in the other may be obtained in closed form by integration of this equation.

In the case of the Distributed Element model in its extended Massing's formulation, $z$ is obtained by

$$\frac{z - Z_N}{2} = \phi(\frac{u - U_N}{2}) \quad \text{for } N \neq 0 \tag{4.2.1}$$

$$z = \phi(u) \quad \text{for } N = 0 \tag{4.2.2}$$

where $U = \{U_1, U_2, U_3, \ldots\ldots, U_N\}^T$ is an array of N nested turning points which is updated continuously depending on the history of $u$ in a manner described in Chapter 2 and where $\{Z_1, Z_2, Z_3, \ldots\ldots, Z_N\}^T$ is the array of the normalized restoring force values at the corresponding turning points. Let $z = \phi(u)$ be the initial loading curve for the model. In order to have the initial loading curve identical to the model in Eqn. (4.1), $\phi$ is defined as follows:

$$\phi(u) = z_y(1 - e^{-u/u_y}) \quad \text{for } u \geq 0 \tag{4.3.1}$$

$$\phi(u) = -\phi(-u) \quad \text{for } u < 0 \tag{4.3.2}$$

where

$$z_y = A/(\beta - \gamma), u_y = 1/(\beta - \gamma) \tag{4.3.3}$$

Given a variation in $u$ or $z$, the corresponding variation in the other may be determined by means of a simple functional evaluation in Eqn. (4.2).

In all the examples of this chapter, the following values are used for the model parameters: $A=1.0$, $\beta=0.6$, $\gamma=-0.4$. For these values of the parameters, $z_y=u_y=1.0$. The initial loading curve has a slope of unity at the origin and rises exponentially to a maximum or yield value of unity.

The hysteretic energy dissipated by the models, $E$, is defined as:

$$E = \int z\,du \tag{4.4}$$

Thus, for a closed loop in the $z$-$u$ plane, the value of $E$ equals the area enclosed by the loop.

In what follows, the Wen-Bouc differential equation model is referred to as the W-B model and the Distributed ELement model with the identical initial loading curve, as the DEL model.

## 4.3 Cyclic loading between fixed displacement limits:

As noted earlier, the cyclic loading of the models between fixed displacement limits simulates the displacement-controlled testing of the corresponding specimens between fixed displacement (or strain) limits in a physical experiment. Two different cases are examined here, one in which the loading is between symmetric limits and another in which the loading is between asymmetric limits.

## 4.3.1 Symmetric cyclic loading:

The following loading sequence is carried out on the two models, which are both assumed to be in the virgin state: Each model is loaded until the displacement has a value of 1.5, and then is cycled between the displacement values of 1.5 and -1.5.

Fig. 4.1 shows the manner in which the normalized restoring force, $z$, of the two hysteretic models behaves for this loading pattern. The following remarks can be made regarding the hysteretic behavior of the two models:

(1) From Fig. 4.1a, it is seen that the DEL model settles to a stable, closed loop after just one load cycle. In the case of the W-B model, since the system returns to 3 instead of to 1 after one cycle, there is a nonclosure of the loop. However, after one more cycle, the loop is essentially closed. For further cycling, the system settles to the stable loop 343. Thus, for displacement loading between fixed symmetric limits, the W-B model exhibits curvilinear, closed hysteresis loops in the steady state.

(2) Unlike the case of the DEL model, it may be noted that the turning points of the stable loop for the W-B model do not lie on the initial loading curve. For cyclic loading between the displacement limits $\pm u_A$, the normalized restoring force values corresponding to the turning points of the stable cycle, $\pm z_A$, can be shown to satisfy the equation

$$2u_A = \begin{cases} \dfrac{1}{(\beta+\gamma)}\log[1+\dfrac{z_A}{A}(\beta+\gamma)]-\dfrac{1}{(\beta-\gamma)}\log[1-\dfrac{z_A}{A}(\beta-\gamma)] & \text{for } \gamma \neq \beta \\ \dfrac{1}{2\beta}\log[1+2\beta\dfrac{z_A}{A}]+\dfrac{z_A}{A} & \text{for } \gamma = \beta \end{cases} \qquad (4.5)$$

Let the locus of points, $(u_A, z_A)$, be defined to be the *turning point curve* for the W-B hysteretic model, with an odd extension being made about the origin as in the case of the initial loading curve. The turning points or the load reversal points of the W-B model for cycling between fixed, symmetric displacement limits lie on the turning point curve in the steady state. As $u_A$ becomes very large, the turning point curve tends to $z_y$, the same value as the initial loading curve. The turning point curve for $A=1.0$, $\beta =0.6$, $\gamma =-0.4$, is shown in Fig. 4.1b.

(3) It can be seen that the W-B model exhibits a stiffness-increase or stiffening, which is apparent from the rotation of the initial loops to a stiffer stable loop. Such a stiffening feature is not present in the DEL model. Thus, for the same displacement, the W-B model has a larger effective stiffness than the DEL model. This stiffening occurs for the the W-B model for all values of $\beta$ and $\gamma$, that is, for both softening and hardening systems. This claim can be verified in the following fashion. The slope of the initial loading curve satisfies

$$\frac{dz}{du} = A - z(\beta - \gamma) \qquad (4.6.1)$$

By differentiating Eqn. (4.5), the following expression can be obtained for the slope of the turning point curve:

$$\frac{dz}{du} = A + z\gamma + O(z^2) \qquad (4.6.2)$$

At $z=0$, the slopes of both curves is $A$. For very small values of $z$, the turning point curve has a slope larger then the initial loading curve if $\beta >0$. The condition $\beta >0$ is essential in the W-B model because it alone ensures that the unloading stiffness is larger

than the loading stiffness at a load reversal point. Thus, the turning point curve has a larger slope than the initial loading curve for small values of $z$ and $u$. Recalling that both curves tend to $z_y$ for large displacements, it can be seen that the turning point curve rises faster to its asymptotic value than the initial loading curve. Therefore, for the same displacement, the turning point curve has a larger vertical ordinate than the initial loading curve. This causes a rotation in the counter-clockwise direction from the initial loops to the stable closed loop for cycling between symmetric displacement limits, thus resulting in the stiffening.

Such stiffening is not very commonly observed in physical systems. The W-B model cannot be used satisfactorily to model systems that do not stiffen in the fashion that the mathematical model does.

(4) The next observation from Fig. 4.1 pertains to the energy-dissipation characteristics of the two systems on repeated cyclic loading. The area enclosed by the stable loops, which yields the energy dissipated by the hysteretic systems, is evidently larger in the case of the W-B model. Evaluation of $E$ for the two models shows that the W-B model dissipates 1.67 times as much energy per cycle as does the DEL model. Fig. 4.2 shows the ratio of the energy dissipated by the W-B model to that dissipated by the DEL model plotted against the amplitude of the displacement cycle, $u_A$. The ratio has a peak at a value of $u_A$ of about 1.5, drops sharply to 1.2 as $u_A$ tends to 0 and drops gradually to 1 as $u_A$ becomes very large. Using Eqns. (4.1) and (4.5), it can be shown that the energy ratio tends to $2\beta / (\beta - \gamma)$ as $u_A$ tends to 0, which is 1.2 for $\beta = 0.6$, $\gamma = -0.4$. As $u_A$ becomes very large, the ratio tends to 1 because the stable loops of both models tend to a parallelogram with two parallel sides that are of length $2u_A$, the distance between them being 2.

There are two factors that contribute to the overestimation of energy dissipated by the W-B model. The first factor is that for the ratio of $\beta / \gamma = -1.5$ selected for the

present analysis, the W-B model has unloading stiffnesses that are larger than those for the DEL model. The second factor is that the W-B model exhibits stiffening, the amount of which is proportional to the vertical distance between the turning point and initial loading curves for the same displacement. As $u_A$ moves from 0 to a very large value, this distance varies from 0 to a maximum value and back to 0 (Fig. 4.1b), which may account for the similar variation of the ratio of energy dissipated. Such an overestimation, though not to the same magnitude, will be shown in Chapter 5 to occur in dynamic problems as well.

### 4.3.2 Asymmetric cyclic loading:

Consider the following loading sequence carried out on the two models, which are again assumed to be initially in a virgin state: Each model is loaded along the initial loading curve until the displacement has a value of 1.5, and is then cycled between the displacement values 1.5 and 1.0.

Fig. 4.3 shows the behavior of the restoring force of the DEL and W-B models when subjected to the above loading sequence. The following remarks can be made regarding the hysteretic behavior of the two models:

(1) The DEL model settles to a stable loop after just one load cycle, while the W-B model requires many cycles before it settles to its stable loop.

(2) One of the most significant differences in the response of the two models is in the observed force relaxation in the case of the W-B model. While the average value of the normalized force of the DEL model for one load cycle is about 0.556 for the loading sequence considered, the corresponding value for the W-B model is 0. The fact that there is a force relaxation in the W-B model is itself not a matter of great concern; this phenomenon has been reported during high cyclic fatigue by Morrow and Sinclair [33]. However, there are two major differences between the W-B model and normally

observed force relaxation. Firstly, the experimentally observed loops close partially during the asymmetric cycling, whereas this is not always so for the W-B model; for instance, loop 123 does not close at 2 at all. Secondly, the physical systems that do exhibit force (or stress) relaxation do not necessarily settle to a zero mean force value.

One serious disadvantage in the use of the W-B model can therefore be seen to be the inbuilt tendency of the model to cause a force relaxation. For physical systems that do not exhibit the phenomenon, the use of the W-B model may result in inaccurate analysis.

(3) During the first cycle of loading, the DEL model moves from 1 to 2 and back to 1 (Fig.4.3a), dissipating positive energy equal to the area enclosed by the closed loop. In comparison, the W-B model moves from 1 to 2 to 3 (Fig. 4.3b) during the same displacement cycle, dissipating negative energy in the process. The amount of negative energy dissipated equals the area of the hatched region in Fig. 4.3b. This is a direct violation of the Ilyushin's postulate, which stipulates that positive energy be dissipated in any displacement (or strain) cycle. More discussion of this violation follows later in this chapter.

It may be noted, however, that the Ilyushin's postulate is violated only for the first few cycles and that the W-B model dissipates positive energy in the steady state (after a large number of cycles).

(4) The stable loop in the W-B model has a larger average stiffness than the loop in the DEL model. This is not readily apparent for the loading case considered, but becomes clearer for larger amplitudes of the load cycle. For instance, Fig. 4.4 shows the stable loops of the two models when cycled between the displacement limits of 2 and 4. The larger average stiffness of the stable loop of the W-B model is readily apparent. Similarly, it can be observed from the areas enclosed by the loops in Fig. 4.4 that the W-B model also dissipates more energy than the DEL model.

(5) As a final remark, the values of the normalized restoring force of the W-B model corresponding to the load reversal points of the stable loop, $\pm z_A$, for cycling between the displacement limits $u_1$ and $u_2$ can be obtained by substituting $u_A = |u_1 - u_2| / 2$ in Eqn. (4.5). That is, the steady-state loops of the W-B model for cycling between the displacement limits $\pm |u_1 - u_2| / 2$, and for cycling between the limits $u_1$ and $u_2$, are identical except for a translation in the horizontal direction by $(u_1 + u_2) / 2$.

## 4.4 Cyclic loading between fixed force limits:

The cyclic loading of the models between fixed force limits simulates the force-controlled testing of the corresponding specimens between fixed force (or stress) limits in a physical experiment. Two different cases are examined here, one in which the loading is between symmetric limits and another in which the loading is between asymmetric limits.

## 4.4.1 Symmetric cyclic loading:

The following loading sequence is carried out in the two models that are assumed to be initially in the virgin state: Each model is loaded along the initial loading curve until the normalized force level is 0.75 and then is cycled between the force levels of 0.75 and -0.75.

Figure 4.5 shows the behavior of the hysteresis loops of the two models. The following observations may be made about the hysteretic behavior of the two models:

(1) Both models settle to a closed, stable loop after only one load cycle. This is unlike the case of cycling between symmetric displacement limits, where the W-B model took a few cycles to settle to the stable loop.

(2) The stiffness of the stable loop of the W-B model is, on an average, larger than that of the DEL model.

(3) The amplitude of the displacement cycle for the W-B·model, $u_A$, can be obtained by substituting the value of the amplitude of the force cycles, $z_A$, in Eqn. (4.5). For the loading sequence considered, $z_A = 0.75$, and $u_A$ from Eqn. (4.5) is 1.04.

(4) The average value of the displacement of the DEL model for each load cycle is 0. This is not so for the W-B model. If the average value of the displacement of the W-B model for each load cycle is $\bar{u}$, and $u_A$ is the value of the amplitude of the displacement cycle, then $\bar{u}$ is given by

$$\bar{u} = -u_A - u_y \log(1 - \frac{z_A}{z_y}) \tag{4.7}$$

There is thus a "drift" with respect to the origin in the displacement of the W-B model that is not observed in the DEL model. It is clear that the W-B model is not suitable for the modeling of a system when the displacement response of the system is expected to respond cyclically between symmetric limits when the system is subjected to force load cycles between symmetric limits.

(5) The energy dissipated by the W-B model is only 0.82 times that dissipated by the DEL model when the models are cycled between the $z$ limits of $\pm 0.75$.

Fig. 4.6 shows the ratio of the energy dissipated by the W-B model to that dissipated by the DEL model plotted against the amplitude of the force cycle. This ratio, as in Sec. 4.3.1, can be seen to tend to 1.2 for very small values of $z_A$. For values of $z_A$ tending to 1, the ratio tends to 0.5 for all values of $\beta$ and $\gamma$. This is because, as $u_A$ becomes very large, the stable loop of the W-B model tends to a parallelogram with two parallel sides that are of length $2u_A$, the distance between them being 2; the corresponding quantities of the DEL model being $4u_A$ and 2 where the value of $u_A$ is obtained by substituting $z_A$ in Eqn. (4.5). For $\beta/\gamma = -1.5$, there is an interval where the energy dissipated is overestimated by the W-B model and one where it is

underestimated. For amplitudes of the force-load cycles tending to unity, the energy dissipation of the W-B model is quite inadequate.

## 4.4.2 Asymmetric cyclic loading:

It is when the W-B model is subjected to cyclic loading between asymmetric force limits that one of the most nonphysical features of the W-B model becomes most evident. Consider the following loading sequence on the two models: Each model is loaded along the initial loading curve until the normalized force level reaches a value of 0.75, and is then subjected to cycles between the force levels of 0.75 and 0.25.

Figure 4.7 shows the manner in which the hysteresis loops behave for the two models. The following observations may be made about the hysteretic behavior of the two models:

(1) The DEL model in Fig. 4.7a settles to a stable loop after just one load cycle, while the W-B model in Fig. 4.7b never does. As a matter of fact, there is no stable loop for W-B model for such a loading situation.

The reason for the absence of the stable loop in the case of the W-B model can be explained in the following manner: Firstly, the W-B model, by its very formulation, namely Eqn. (4.1), does not distinguish between initial loading and reloading. That is, the stiffness of the model during reloading is precisely the same as during initial loading, for the same value of $z$, the normalized force. In Fig. 4.7b, for instance, the initial loading path AB and the reloading path CE have the same value of the slope, $dz/du$. Secondly, $\beta > 0$ ensures that the W-B model has a larger slope for unloading than for reloading or unloading at any $z$. For instance, at B in Fig. 4.7b, the slope of the initial loading path OAB is less than that of the unloading path BC.

The combined effect of these two factors is to cause a loop nonclosure at C. The slope of the reloading path CE at C is the same as the slope of AB at A, and this is less

than the slope of the unloading path BC at C. Thus, there is not even a partial closure of the loop. It can be seen that on completion of one load cycle, the system returns to E instead of to B, thus resulting in a "drift" $d$ per cycle with respect to the displacement of the system at the start of the load cycle, as shown in the figure. The curves CE and AB are identical except for a translation in the horizontal direction by $d$. Similarly, the unloading paths EF and BC are identical except for the same translation. The larger the number of such cycles the W-B model is subjected to, the larger will be the displacement of the system, since the drift increases by $d$ for each additional load cycle.

(2) The stiffness of the reloading paths (when $z$ goes from 0.25 to 0.75) is less for the W-B model than for the DEL model, resulting in a stiffness deterioration.

(3) Fig. 4.8 shows the hysteretic behavior of the W-B model for one load cycle between arbitrary, fixed, asymmetric force limits of $z_1$ and $z_2$ (where $z_1 > z_2 \geq 0$). It can be seen that as in the case of the cycling between asymmetric displacement limits, the Ilyushin's postulate is violated by the model for the path BCD, during which the displacement executes one cycle. The energy dissipated during this cycle is $-A_1$ (where $A_i$ is the area of the region $i$, $i=1,2,3,4$), which is less than 0. The DEL model undergoes a closed loop during the same displacement cycle, and dissipates energy equal to the area enclosed by the loop. Therefore, the DEL model satisfies the Ilyushin's postulate.

The Drucker's postulate requires that the following inequality be satisfied for every force (stress) cycle from $z_1$ to $z_2$ and back to $z_1$:

$$\int (z - z_1) du \geq 0 \qquad (4.8)$$

A simple geometric evaluation of the integral in the above inequality for the path BCE in Fig. 4.8 yields the value of the integral to be $-(A_1 + A_2)$, which is less than 0. Thus, the Drucker's postulate is violated. More discussion on this will follow later in this chapter.

In the case of the DEL model, the integral in inequality (4.8) equals the area enclosed by the stable loop in Fig. 4.7a. Thus, the DEL model satisfies the Drucker's postulate.

The violation of these two postulates by the W-B model does not necessarily mean that the model will have a negative value of $E$, the energy dissipated as defined in Eqn. (4.4), during each force-load cycle. This is so because the value of $E$ for the path BCE, corresponding to the behavior of the system during one force-load cycle, is $(A_4 - A_1)$, which is not necessarily negative. For instance, for the loading sequence BCE, the value of $E$ for the W-B model is 0.373 and for the DEL model is 0.014 (the area enclosed by the closed loop in Fig. 4.7a).

For the case $n=1$ of the W-B model, the value of $d$, the drift per cycle for a force-load cycle from $z_1$ to $z_2$ and back to $z_1$ (where $z_1 > z_2$) can be obtained by the following equation:

$$d = \begin{cases} \dfrac{1}{(\beta - \gamma)}\log\left(\dfrac{A - (\beta - \gamma)|z_2|}{A - (\beta - \gamma)|z_1|}\right) + \dfrac{1}{(\beta + \gamma)}\log\left(\dfrac{A + (\beta + \gamma)|z_2|}{A + (\beta + \gamma)|z_1|}\right) & \text{for } \gamma \neq \beta \\[4mm] \dfrac{|z_1| - |z_2|}{A} + \dfrac{1}{2\beta}\log\left(\dfrac{A + 2\beta|z_2|}{A + 2\beta|z_1|}\right) & \text{for } \gamma = \beta \end{cases} \qquad (4.9)$$

This equation is derived from an integration in closed form of Eqn. (4.1) for the force-load cycle. Fig. 4.9 is a three-dimensional representation of the absolute value of $d$ plotted against $|z_1|$ and $|z_2|$ for $A=1.0$, $\beta=0.6$, $\gamma=-0.4$. The following observations can be made with the help of the figure and the equation:

(1) $d=0$ when $|z_1|=|z_2|$, that is, either when $z_2=z_1$ (trivial case) or when $z_2=-z_1$. Therefore, as was observed in Sec. 4.4.1, symmetric loading in $z$ causes no drift.

(2) There is a nonzero value of $d$ for every asymmetric load cycle in $z$.

(3) The value of $d$ for a cycle between $z'$ and $z''$ ($z'>z''\geq 0$) is the same as the value of $d$ for a cycle between $z'$ and $-z''$. For instance, the behavior of the W-B model for $z'=0.5$,

$z''$=0.3, shown in Fig. 4.10, clearly illustrates this point. For the load cycle between the $z$ values of 0.5 and -0.3, the path of the model is ABCBD, while for the load cycle between the $z$ values of 0.5 and 0.3, the path is ABD. In both cases, the system has the same drift $d$, equalling the distance AD.

(4) For a given value of $z_2$, it can be seen from Fig. 4.9 that $d$ tends to very large values as $z_1$ tends to 1. Thus, the W-B model yields very large displacement drift values when subjected to a nonzero mean force-load cycle if one of the limits tends to the yield level of the system.

(5) For values of $|z_1|$ and $|z_2|$ between 0 and 0.15, it can be seen that the drift surface is quite flat. Thus, for loading between fixed force limits that are small when compared to the yield level, the values of $d$ are also small.

In an effort to make the W-B model satisfy the Drucker's postulate and to minimize the associated drifting, Casciyati [10] has proposed the model described by Eqn. (2.41), wherein a term $\delta|du|sgn(z)$ is added to the right-hand side of Eqn. (4.1), $\delta$ being a parameter intended to control loop closure. Let $z_0$ be defined as follows:

$$z_0 = \frac{\delta}{\beta} \tag{4.10}$$

Figure 4.11 shows the behavior of the hysteresis loops of the Casciyati model ($A$=0.7,$\beta$=0.6,$\gamma$=-0.6,$\delta$=0.3 $\Rightarrow z_0 = 0.5$) when subjected to load cycles between fixed, asymmetric, normalized force limits, $z_1$ and $z_2$ ($z_1 > z_2$). The following features may be observed from the figure:

(1) For $z_1 > z_0 > z_2$, it can be seen that the loops indeed do close, albeit partially. However, the partial loop closure does not necessarily guarantee that the Drucker's postulate will not be violated. To demonstrate this, the Drucker's integral in inequality (4.8) is evaluated by fixing $z_1$=0.75, and letting $z_2$ vary from 0 to $z_1$, the result is plotted against $z_2$ in Fig. 4.12a. It can be observed that for $z_2$ less than about 0.35, the value of

the integral is greater than 0 and thus the Drucker's postulate is satisfied. However, for $0.35 < z_2 < 0.50$, the Drucker's postulate is violated even though the loops do close partially.

For purposes of comparison, the Drucker's integral is also plotted for the W-B model in Fig. 4.12b for $z_2$ between 0 and $z_1$. This plot shows that the Drucker's integral is violated for the entire interval of $z_2$.

(2) Consider the loading situation wherein each of the limits, $z_1$ and $z_2$, is greater than $z_0$. In this case, the behavior of the Casciyati model shown in Fig. 4.11 is exactly the same as the W-B model and the added term, $\delta|du|sgn(z)$, has no effect on cycles in $z$ when both limits are above $z_0$ (and by symmetry, below $-z_0$).

(3) For $z_0 > z_1 > z_2 > 0$, it is seen that the loading-unloading behavior is quite nonphysical, with the unloading slopes being less than the loading and reloading slopes at load reversal points. This actually results in the model's yielding negative displacements when cycled between positive force limits, which is quite unrealistic.

Considering the behavior of the Casciyati model in these three cases, it is arguable whether the model is really an improvement over the W-B model. Even though it does provide partial loop closure in certain loading situations, general dynamic loading is likely to contain other loading situations where the model is not as satisfactory.

## 4.5 The Drucker's and Ilyushin's postulates:

In earlier sections, it was seen that the W-B model may sometimes violate the Drucker's and Ilyushin's postulates. The implication of the Drucker's postulate's not being satisfied is that the W-B model is unstable in the sense that it can be disturbed from an equilibrium state by an external agency that does negative work. This point can be explained in the following manner: Consider the loading situation where the W-B model, initially in the virgin state, is loaded to an equilibrium state $(u_e, z_e)$. This state corresponds

to the point B in Fig. 4.7b. An external agency that causes the model to be disturbed from point B to point E via the path BCE has disturbed the equilibrium state of the system but has done negative work in the process. The fact that the Ilyushin's postulate is not satisfied means that negative energy is dissipated by the system during certain displacement cycles.

Rice points out that these postulates are separate from and do not arise as a consequence of the second law of thermodynamics [41]. He notes that they are instead nothing more than reasonable classifications of behavior for metals[40]. Even though it is true that these postulates are not strict physical or thermomechanical requirements for the behavior of real materials, it is arguable [44] that they play an important role in the construction of rational theories or models of material behavior for use in general dynamic problems. Sandler [44] performed a stability and uniqueness analysis of the simple endochronic model described in Sec. 2.3.5.1. It may be recalled that this model was constructed by starting with a one-dimensional Maxwell model and that its mathematical description is similar to the W-B model. Sandler raises serious doubts about the model by presenting examples of situations where

(a) the Drucker's and Ilyushin's postulates are violated

(b) multiple numerical solutions exist for what should be a reasonable physical problem with a unique solution

(c) introduction of small errors in initial and/or boundary conditions leads to rapid deterioration in the accuracy of the numerical solutions for subsequent computations.

Sandler uses the fact that the model does not distinguish between initial loading and reloading to demonstrate an example of situation (b) and the tendency of the model to drift in displacement when subjected to nonzero mean stress cycles to illustrate an example of situation (c). It was seen earlier in this chapter how these same features in the response behavior of the W-B model also lead to the violation of the Drucker's and Ilyushin's

postulates. Violation of the postulates may thus be used to serve as an indication that other nonphysical behavior may also occur.

The W-B and Casciyati models, being similar in behavior to the model analyzed by Sandler, may also exhibit instances of (b) and (c) in certain loading situations. The presence of nonunique solutions may not be considered to be a matter of grave concern because there are physical systems that exhibit bifurcation and multiple solutions. Bardet [6] provides an example of dense sand which often switches in the triaxial test from an uniform mode of deformation to a localized deformation along a shear plane. In this case, he points out that the Drucker's postulate must not be satisfied, because it is known from classical plasticity that the inequality being satisfied is a sufficient condition to guarantee a unique solution. However, in structural dynamics, unique solutions are expected to exist for reasonable physical problems and hence the possibility that the endochronic models may yield nonunique solutions is alarming.

In summary, it may be concluded that the violation of the postulates by a hysteretic model is an indication that the model may have the tendency to exhibit nonphysical behavior in certain loading situations. The satisfaction of the postulates could be used as a rational basis in the construction of mathematical models for hysteretic behavior. It may be mentioned here that even the widely used Clough-Johnston hysteretic model [14] also violates the Drucker's postulate in certain loading situations.

## 4.6 Conclusion:

The quasi-static loading situations considered in this chapter clearly demonstrate certain differences in the response of the endochronic models from observed physical behavior of hysteretic systems. The W-B model, which was chosen as characteristic of the class of endochronic models, exhibits a tendency to drift, to have unclosed or partially closed hysteretic loops, to cause a force or stress relaxation, and to have a different energy-

dissipation behavior. In addition, the models may not obey the Drucker's and Ilyushin's postulates, thereby possibly yielding inaccurate numerical solutions and/or nonunique solutions. It may be mentioned here that the quantitative results of this chapter have been established only for $A=1.0, \beta=0.6, \gamma=-0.4$. The qualitative nature of the discussions regarding the behavior of the models for other values of the parameters is not expected to be much different.

The tendency of the W-B model to drift may actually be beneficial in the modeling of certain physical behavior, for example, in the portrayal of cyclic creep behavior for cyclic loading with nonzero mean stress, or in the characterization of the settling of sand during cyclic loading. But for structural systems, the instability of the models leading to drifting and to the prediction of unusually large displacements is quite undesirable. Even though an ideal elastoplastic model can also lead to nonunique displacements under a yield load, it cannot be said that the endochronic model is no more unstable than the elastoplastic model for the following reasons. The first reason is that the perfectly elastoplastic model has the instability only at the limit or yield load (which is quite consistent with physical systems), but the endochronic model exhibits the feature at all loads. The second difference is that small amplitude, displacement-controlled cycles cause a force relaxation eventually to a zero mean value in the case of the endochronic model, while they cause well-behaved, stable force levels in the elastoplastic system.

Further analysis on the suitability of the endochronic model for physical systems is examined in the next chapter where a dynamic analysis is conducted.
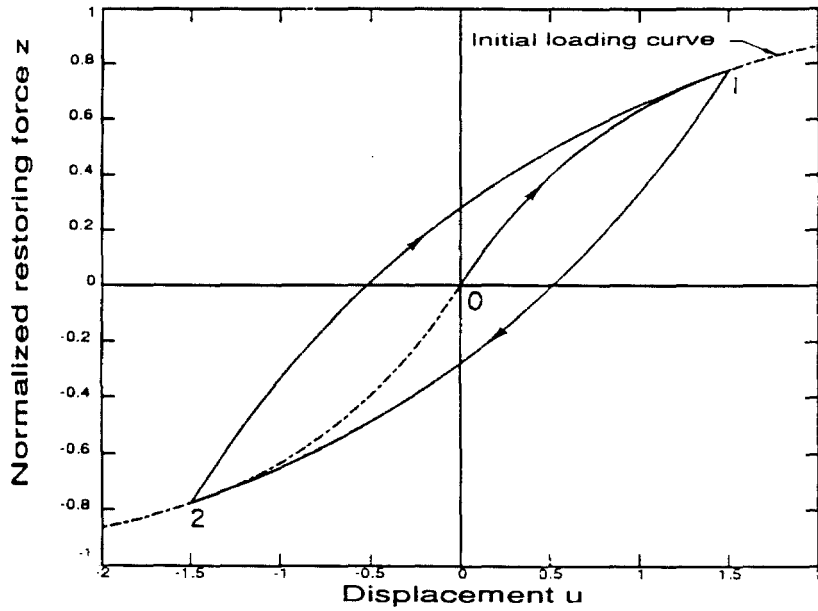
(a)
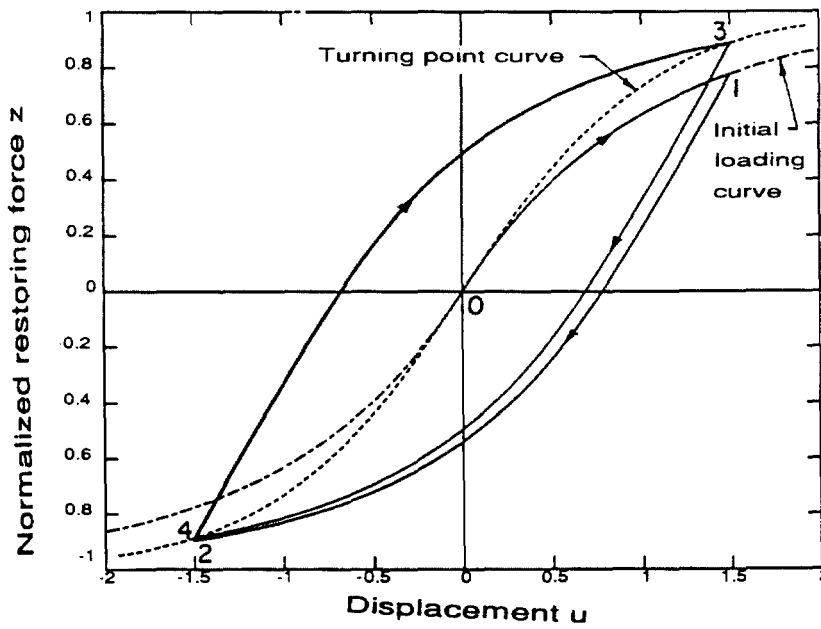


(b)

Figure 4.1:    The hysteretic restoring force behavior of (a) the DEL model (b) the W-B
              model when cycled between fixed, symmetric displacement limits.
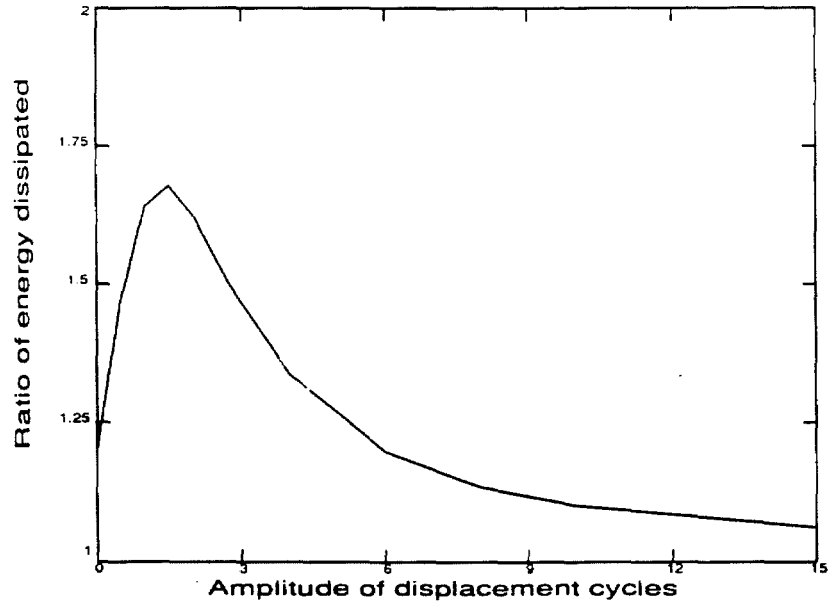
Figure 4.2:    Ratio of the energy dissipated by the W-B model to that dissipated by the
DEL model for cyclic loading between fixed, symmetric displacement
limits.
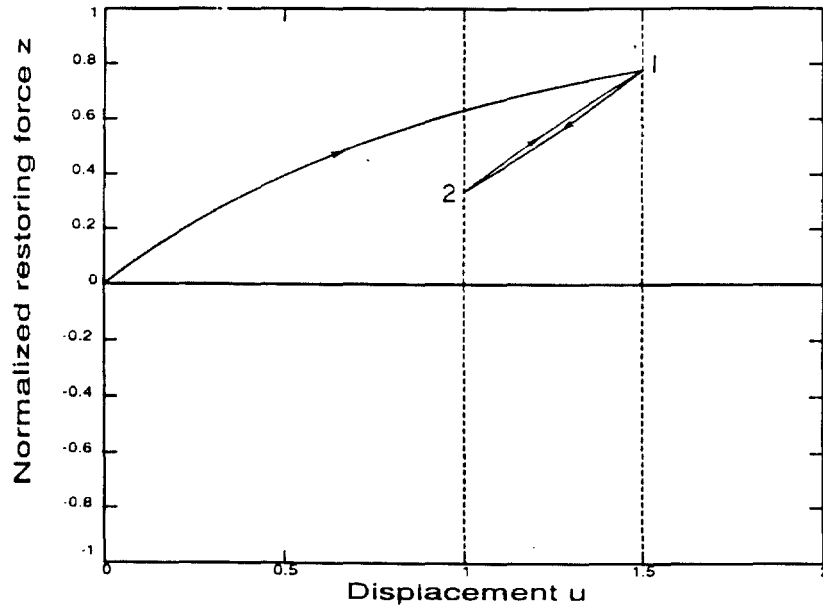
(a)
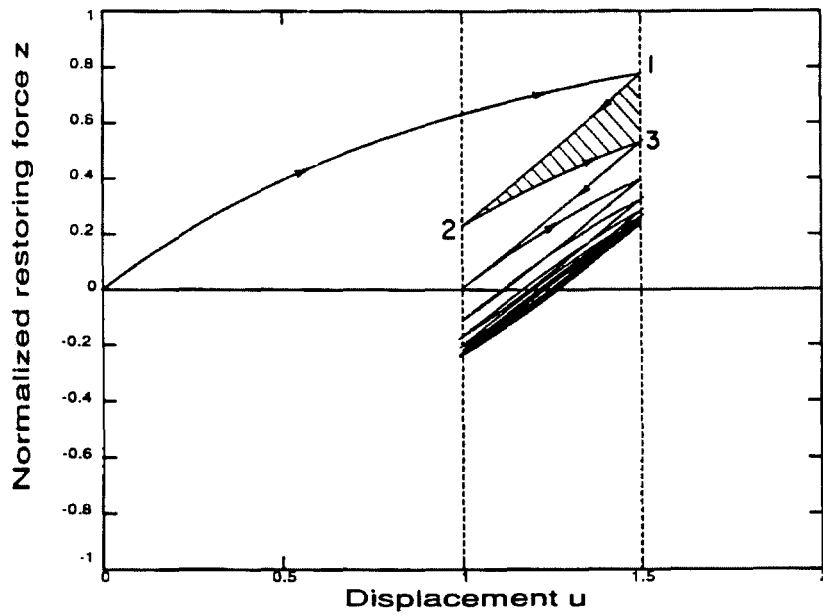


(b)

Figure 4.3:   The restoring force behavior of (a) the DEL model (b) the W-B model
when cycled between fixed, asymmetric displacement limits, 1 and 1.5.
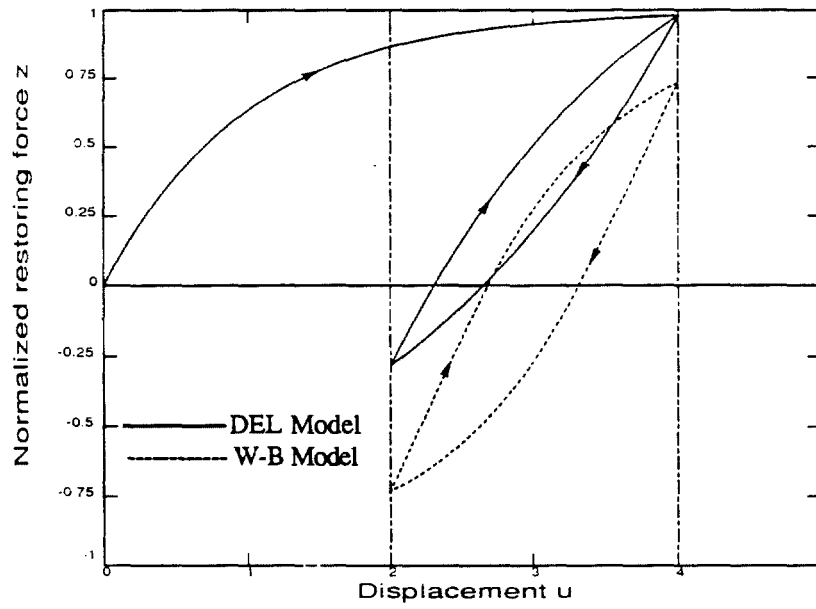
Figure 4.4:    The stable loops corresponding to the two hysteretic models when cycled
between the fixed, asymmetric displacement limits, 2 and 4.
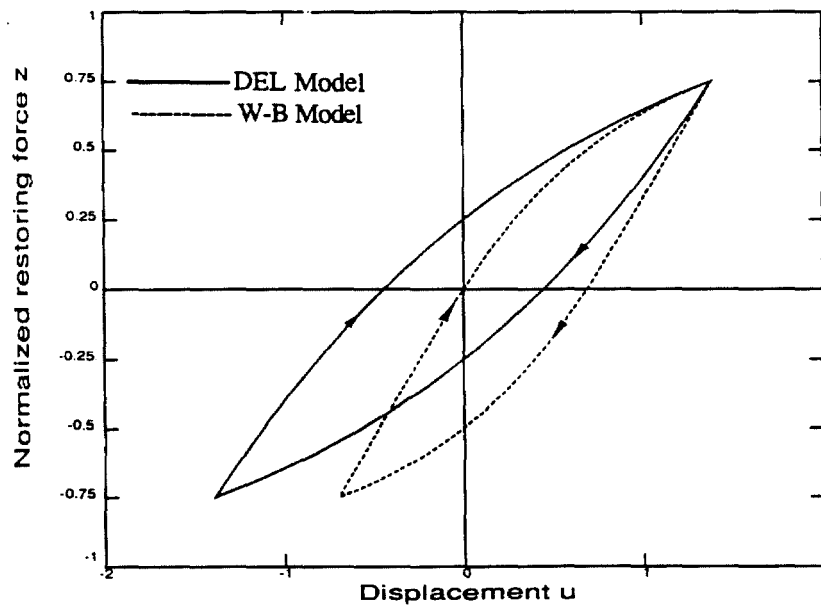


Figure 4.5:    The hysteretic behavior of the two models when subjected to cycling
between fixed, symmetric force limits.
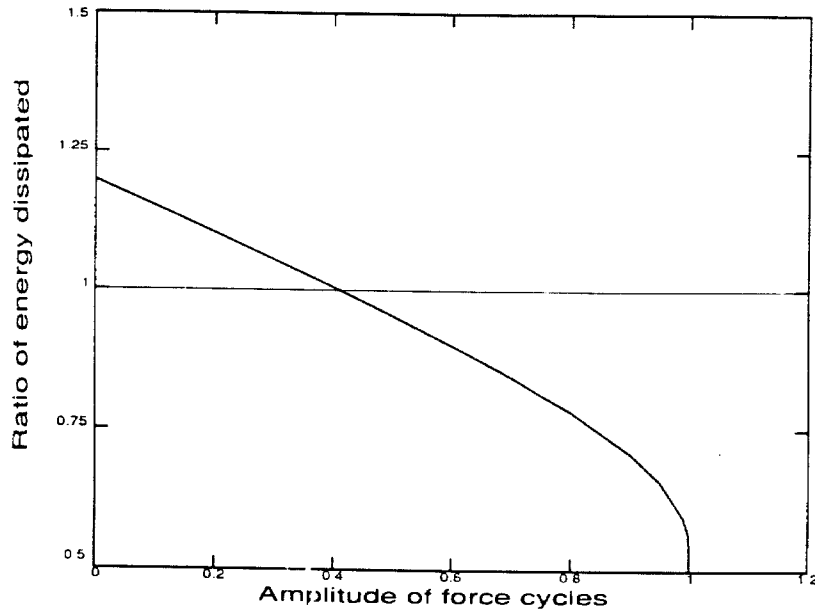
Figure 4.6:  Ratio of the energy dissipated by the W-B model to that dissipated by the DEL model for cyclic loading between fixed, symmetric force limits.
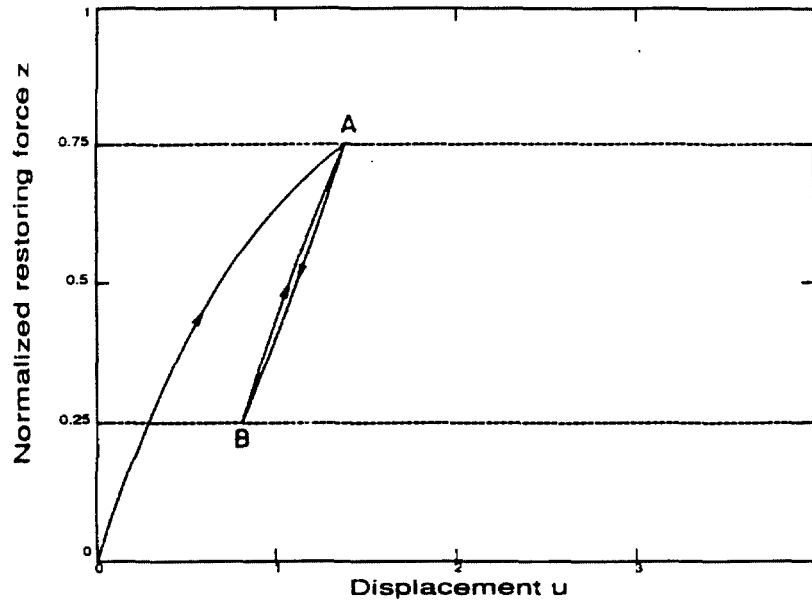
(a)
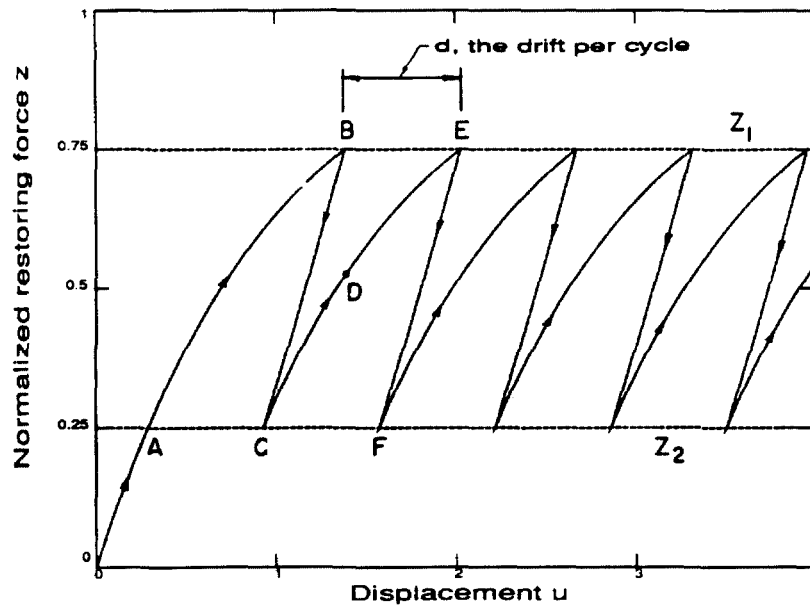


(b)

Figure 4.7:    The hysteretic behavior of (a) the DEL model (b) the W-B model when
subjected to cycling between fixed, asymmetric force limits.
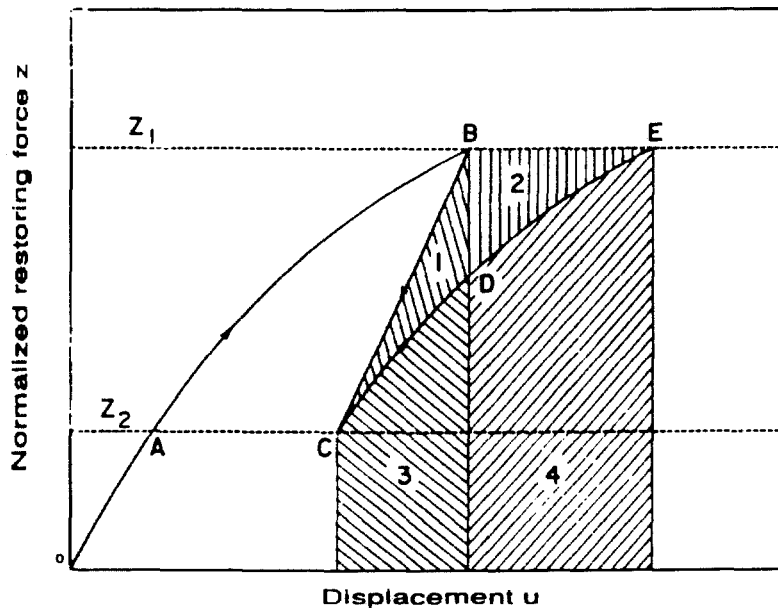
Figure 4.8: The hysteretic behavior of the W-B model when subjected to one load cycle between fixed, asymmetric force limits.
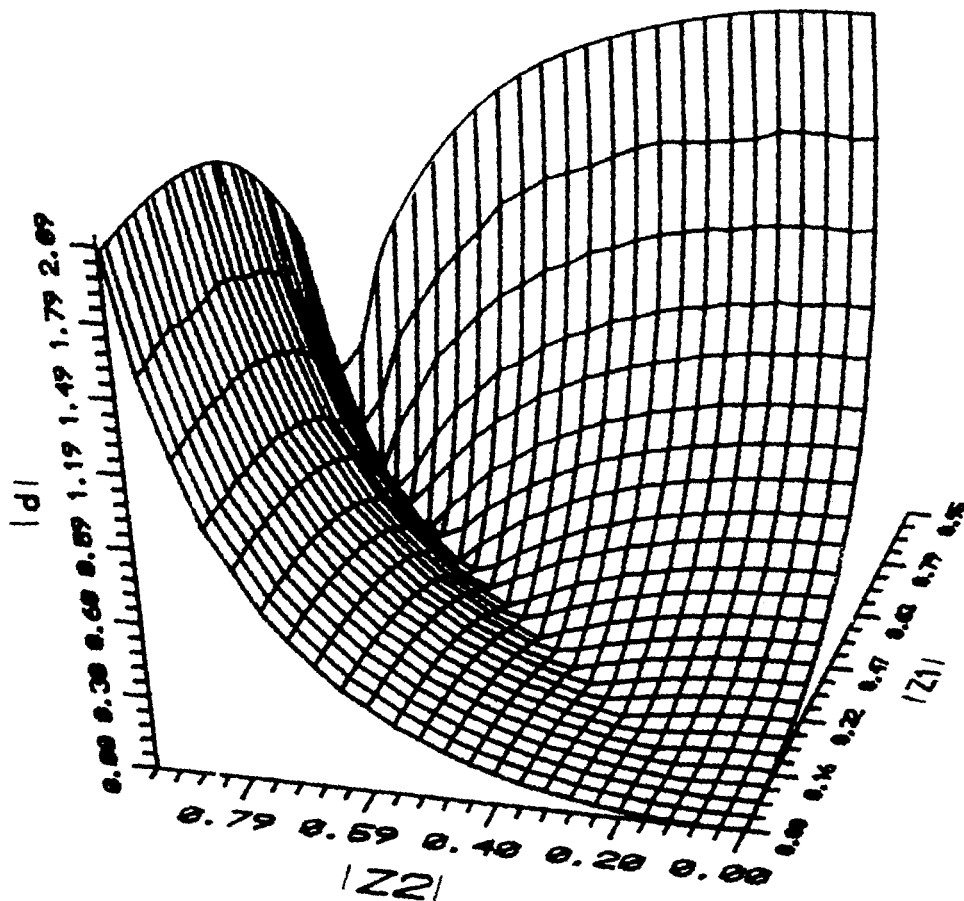
Figure 4.9: Three-dimensional plot of $|d|$, the absolute value of drift per nonzero mean cycle between the fixed limits $z_1$ and $z_2$.
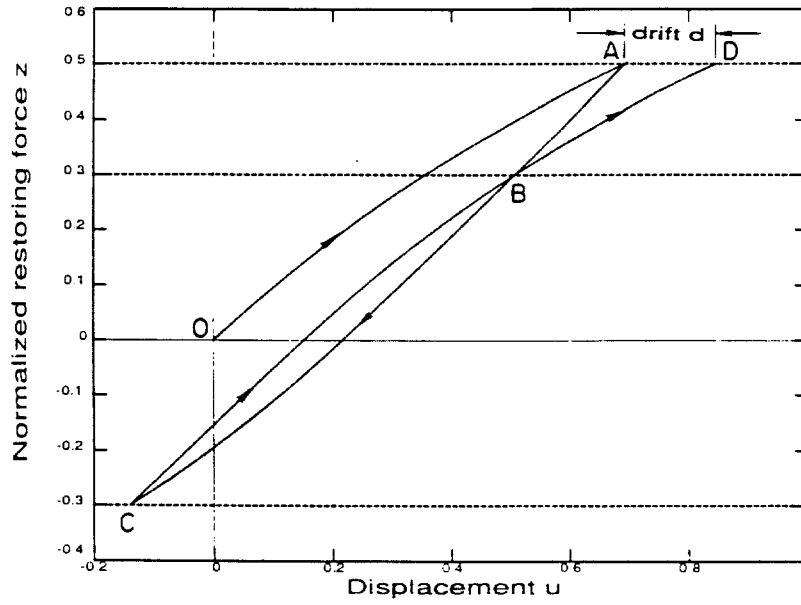
Figure 4.10: The behavior of the drift of the W-B model when subjected to one load cycle between fixed, asymmetric force limits.
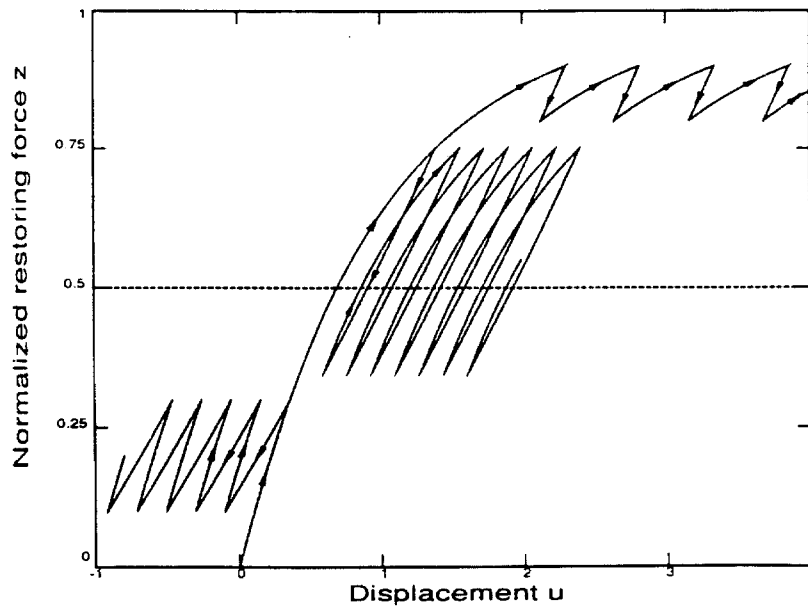


Figure 4.11: The hysteretic behavior of the Casciyati model when subjected to load cycles between fixed, asymmetric force limits.
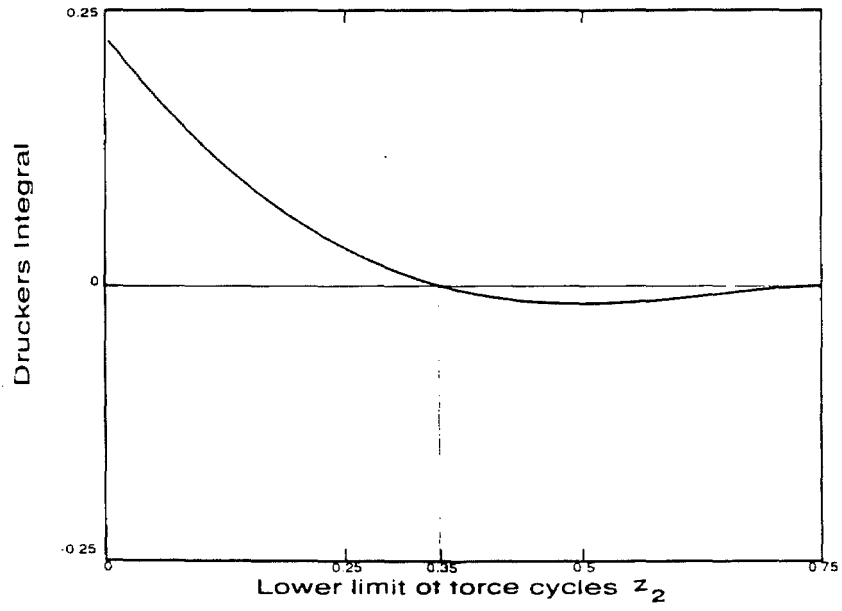
(a)
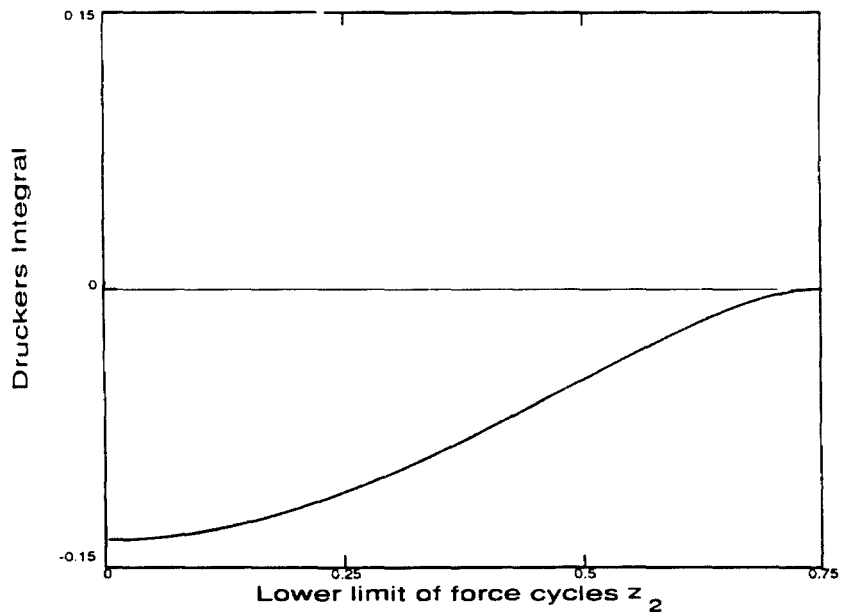


(b)

Figure 4.12:   The Drucker's integral for (a) the Casciyati model (b) the W-B model
when subjected to a load cycle in $z$ from $z_1$ to $z_2$ and back to $z_1$. The
value of $z_1$ is 0.75.

# CHAPTER 5
# COMPARATIVE STUDY OF THE DYNAMIC PERFORMANCE
# OF TWO HYSTERETIC MODELS

## 5.1 Introduction:

In Chapter 4, a set of quasi-static tests was performed on two classes of curvilinear hysteretic models, namely, the Distributed Element type and the endochronic type. The results presented indicated the difference in the behavior of the hysteretic restoring force diagrams for the two classes of models in such features as loop closure, force relaxation, energy dissipation and drift. In addition, it was shown that the endochronic models may sometimes violate the Drucker's and Ilyushin's postulates. Such decidedly nonphysical behavior exhibited by these models has also been pointed out previously [24,36,44]. However, these models have been used extensively for various applications in dynamics, a few of which were listed in Chapter 4, with the most significant application being in the response analysis of hysteretic systems by the method of equivalent linearization [10,54].

So far, no systematic investigation has been undertaken to determine how appropriately the endochronic models represent real physical systems when subjected to dynamic excitations such as earthquakes. Most comparisons so far, including those in Chapter 4, have been carried out in a quasi-static manner and not dynamically where inertial, viscous and other effects are present. This chapter compares the two model responses when they are subjected to a variety of dynamic excitations, including deterministic functions, recorded earthquake time histories, stochastic excitation, and simulated earthquakes. The differences in some of the characteristic response quantities serve as a measure of how satisfactory the endochronic model representation is for physical systems.

In carrying out these analyses, the two models are adjusted to have identical initial loading curves so as to facilitate direct comparison. For the Distributed Element model, the extended Massing's hypothesis formulation is used because of the relative ease of numerical implementation.

## 5.2 Hysteretic model representations:

Let $f(u,\dot{u},\mathbf{Z})$ be the total restoring force in a system (Fig. 5.1) because of $u$, the instantaneous relative displacement at instant $t$, $\dot{u}$, the instantaneous relative velocity at instant $t$, and $\mathbf{Z}$, a vector that accounts for the dependence of $f$ on the history of $u$ up to the instant $t$.

For a linear system,

$$f(u,\dot{u},\mathbf{Z}) = c\dot{u} + ku \tag{5.1}$$

where $c$ is the viscous damping coefficient, and $k$ is the stiffness of the system. Since the restoring force is dependent only on instantaneous quantities in the case of a linear system, $\mathbf{Z}$ is the null vector.

In the case of the Wen-Bouc differential equation model,

$$f(u,\dot{u},\mathbf{Z}) = \alpha ku + (1-\alpha)kz + c\dot{u} \tag{5.2}$$

where $k$ is the initial stiffness of the system, $c$ is the viscous damping coefficient and $\alpha$ is the ratio of the post-yielding stiffness to the initial stiffness. The only quantity accounting for history dependence is the instantaneous value of $z$, which itself satisfies

$$\dot{z} = A\dot{u} - \beta|\dot{u}|z + \gamma\dot{u}|z| \tag{5.3}$$

Thus, $\mathbf{Z} = \{z\}$. Eqn. (5.3) is obtained by setting $n=1$, $v=\eta=1.0$ in Eqn. (2.38).

The initial loading behavior in the positive direction (i.e., $\dot{u} > 0$) is given by the equation

$$z = z_y(1 - e^{-u/u_y}) \tag{5.4}$$

where

$$z_y = \frac{A}{(\beta - \gamma)} \ , \quad u_y = \frac{1}{(\beta - \gamma)} \tag{5.5}$$

For $(\beta - \gamma) > 0$, the initial loading behavior as shown in Fig. 5.2 has a limiting value of $z_y$

and an initial slope of $A$, i.e., $\left. \dfrac{dz}{du} \right|_{u=0} = A$.

The ductility factor of the response, $\mu$, may be defined with respect to $u_y$ as

$$\mu = \frac{u_m}{u_y} \tag{5.6}$$

where $u_m$ is the maximum absolute value of $u$, the response displacement to an excitation. To be capable of withstanding an excitation without failing, a structure must be designed to meet the ductility demand of the response that is due to the excitation. Generally speaking, the larger the value of $\mu$ that a structure can withstand without failing, the more ductile it is. This factor plays a dominant role in the seismic design of a structure.

Popov [39] has reviewed experimental hysteresis loops for different structural members and subassemblages constructed from different materials like steel, reinforced concrete, etc. Maximum ductility demands of about 6.0 could be met by a steel cantilever beam with welded connections as well as by an eccentrically braced steel frame. A reinforced concrete cantilever beam and a framed reinforced concrete wall could meet maximum ductility demands of about 4.0 and 3.5, respectively. A ductility ratio of 4.0 is often used in design and analysis of structures, and this value has been adopted for several examples in this chapter.

For the Distributed Element model in its extended Massing's hypothesis formulation (Differential form), $f$ satisfies Eqn. (5.2); i.e.,

$$f(u,\dot{u},Z) = \alpha k u + (1 - \alpha)kz + c\dot{u} \tag{5.2}$$

where $\alpha$, $k$ and $c$ have the same meaning as in Eqn. (5.2), and

$$\dot{z} = \dot{u}\psi[sgn(\dot{u})\frac{(u - U_N)}{2}]$$ (5.7.1)

$\mathbf{U} = \{U_1, U_2, \ldots\ldots, U_N\}^T$ is an array of $N$ nested turning points, which is updated continuously depending on the history of $u$ in a manner set forth in Chapter 2. $\psi$ is defined as

$$\psi(u) \equiv Ae^{-u/u_y}, \quad u \in (0, \infty)$$ (5.7.2)

In this case, $\mathbf{Z} = \{z, U_1, U_2, \ldots\ldots, U_N\}^T$.

It may be recalled that if $\mathbf{U}$ is the null vector, as in the case of virgin loading,

$$\frac{dz}{du} = \psi[u\, sgn(\dot{u})], \quad u \in (-\infty, \infty)$$ (5.7.3)

It can be seen that for initial loading in the positive direction ($\dot{u} > 0$), the two hysteretic models have the value of $\frac{dz}{du}$ given by $\psi$ as defined in Eqn. (5.7.2), leading to identical initial loading behavior.

In what follows, the Wen-Bouc differential equation model will be referred to as the W-B model, and the corresponding Distributed ELement model with the same initial loading curve as the DEL model.

## 5.3: Simple structural models:

### 5.3.1: Single-Degree-of-Freedom (SDOF) system:

Consider the simple structural model as shown in Fig. 5.3. This model consists of a concentrated mass $m$ in a gravitational field $g$ at a height $h$ above the ground. Assume that the restoring force in the horizontal direction, $f$, can be described as in Sec. 5.2, and that there is an external force $F(t)$ acting on the mass. Assume also that there is a horizontal excitation $a(t)$ applied to the base of the structure. Let $u$ and $y$ be the horizontal and vertical displacements of the mass, respectively. The equation of motion for $u$ can be derived in the following manner:

The Lagrangian of the system, $L$, can be written as:

$$L = \frac{1}{2}m[(\dot{u} + \dot{a}_g)^2 + \dot{y}^2] - mg(h - y)$$ (5.8.1)

where $a_g$ is the displacement of the ground; that is, $\ddot{a}_g(t) = a(t)$. From the Lagrange's equations,

$$\frac{d}{dt}\left(\frac{\partial L}{\partial \dot{u}}\right) - \frac{\partial L}{\partial u} = \text{net force in the horizontal direction,}$$

$$= F(t) - f(u, \dot{u}, \mathbf{Z})$$ (5.8.2)

If $\theta$ is the angle of rotation of the concentrated mass, the following relations can be written for $u$ and $y$:

$$u \approx h\,Sin\theta, \quad y \approx h(1 - Cos\theta)$$ (5.8.3)

For small angles $\theta$,

$$u \approx h\theta \text{ and } y \approx h\theta^2 / 2 \Rightarrow y \approx u^2 / 2h$$ (5.8.4)

Using this result in the Lagrange's equation yields the following equation of motion for $u$, the horizontal displacement of the mass with respect to the ground:

$$m\ddot{u} + f(u, \dot{u}, \mathbf{Z}) - \frac{mg}{h}u = F(t) - ma(t)$$ (5.9.1)

with

$$f(u, \dot{u}, \mathbf{Z}) = \alpha ku + (1 - \alpha)kz + c\dot{u}$$ (5.9.2)

and $z$ satisfies either Eqn. (5.3) or Eqn. (5.7), depending on the hysteretic model used.

The first-order effect of the gravitational field is to cause a reduction in stiffness. There is thus a toppling effect, which may have a significant effect on the stability of the system. More will be said about this in Sec. 5.5.2.

### 5.3.2 The Multi-Degree-of-Freedom (MDOF) system:

A model for a multistory structure is shown in Fig. 5.4. Here the mass of the structure is concentrated at only a few characteristic points along its height, usually at each

floor. Neglecting gravity, and assuming that there is a horizontal base excitation $a(t)$, the equations of motion for the interstory displacements $u_1, u_2, \ldots\ldots, u_n$ can be written as:

$$m_i(a + \sum_{j=1}^{i} \ddot{u}_j) + f_i(u_i, \dot{u}_i, Z_i) - f_{i+1}(u_{i+1}, \dot{u}_{i+1}, Z_{i+1}) = 0 \quad \text{for } i=1,2,3,\ldots,(n-1) \quad (5.10.1)$$

$$m_n(a + \sum_{j=1}^{n} \ddot{u}_j) + f_n(u_n, \dot{u}_n, Z_n) = 0 \quad (5.10.2)$$

with each restoring force, $f_i$, satisfying

$$f_i(u_i, \dot{u}_i, Z_i) = \alpha_i k_i u_i + (1 - \alpha_i) k_i z_i + c_i \dot{u}_i \ , \ i=1,2,3,\ldots,n \quad (5.10.3)$$

$z_i$ satisfies either Eqn. (5.3) or Eqn. (5.7), and $m_i$ is the mass of the $i^{th}$ story.

The equations of motion can also be expressed as:

$$\ddot{u}_1 + \frac{1}{m_1} f_1(u_1, \dot{u}_1, Z_1) - \frac{1}{m_1} f_2(u_2, \dot{u}_2, Z_2) = -a(t) \quad (5.11.1)$$

$$\ddot{u}_i - \frac{1}{m_{i-1}} f_{i-1}(u_{i-1}, \dot{u}_{i-1}, Z_{i-1}) + (\frac{1}{m_{i-1}} + \frac{1}{m_i}) f_i(u_i, \dot{u}_i, Z_i) - \frac{1}{m_i} f_{i+1}(u_{i+1}, \dot{u}_{i+1}, Z_{i+1}) = 0$$

$$\text{for } i=2,3,\ldots.(n-1) \quad (5.11.2)$$

$$\ddot{u}_n - \frac{1}{m_{n-1}} f_{n-1}(u_{n-1}, \dot{u}_{n-1}, Z_{n-1}) + (\frac{1}{m_{n-1}} + \frac{1}{m_n}) f_n(u_n, \dot{u}_n, Z_n) = 0 \quad (5.11.3)$$

where

$$f_i(u_i, \dot{u}_i, Z_i) = \alpha_i k_i u_i + (1 - \alpha_i) k_i z_i + c_i \dot{u}_i \ , \ i=1,2,3,\ldots,n \quad (5.11.4)$$

## 5.4 Time integration procedure

The time integration of the equations of motion is accomplished by writing these equations as a set of three first-order, ordinary differential equations (ODE) in the quantities $u$, $\dot{u}$ and $z$ for each degree of freedom and then performing a fourth-order Runge-Kutta integration with adaptive stepsize control. The technique employed is best explained in the case of one independent variable, $y$, and one dependent variable, $x$.

Let the system be

$$\frac{dy}{dx} = f(x,y) \tag{5.12}$$

where $f$ is a known function of $x$ and $y$. If $y(x_n) = y_n$, then the function $y$ at $x_{n+1} = x_n + h$ is estimated as follows:

$$k_1 = hf(x_n, y_n) \tag{5.13.1}$$

$$k_2 = hf(x_n + \frac{h}{2}, y_n + \frac{k_1}{2}) \tag{5.13.2}$$

$$k_3 = hf(x_n + \frac{h}{2}, y_n + \frac{k_2}{2}) \tag{5.13.3}$$

$$k_4 = hf(x_n + h, y_n + k_3) \tag{5.13.4}$$

$$y_{n+1} = y_n + \frac{1}{6}(k_1 + 2k_2 + 2k_3 + k_4) + O(h^5) \tag{5.13.5}$$

In the case of a vector of unknown functions, a similar representation holds [17]. The fourth-order Runge-Kutta is very commonly used in ODE integration.

Quite often, the step size $h$ may be too large, and the truncation errors introduced may be unacceptable. In dynamics, this may occur, for example, when finding the response of an oscillator with a very short natural period compared to the integration time step $h$. A good ODE integrator should exercise some adaptive control over its own progress, making changes in step size, $h$, so as to keep the truncation error within bounds. The most straightforward technique for the control of $h$ is step-doubling. Each step is traversed twice, once as a full step, and once as two consecutive half-steps. The following procedure is then used to determine whether the step size should be reduced.

Let $y(x+2h)$ be the exact solution for an advance from $x$ to $(x+2h)$, $y_1$ the approximate solution from Eqn. (5.13) for one step of size $2h$, and $y_2$ the approximate solution from Eqn. (5.13) for 2 steps of size $h$. Then,

$$y(x + 2h) = y_1 + (2h)^5 \phi + O(h^6) \qquad (5.14.1)$$

$$y(x + 2h) = y_2 + 2h^5 \phi + O(h^6) \qquad (5.14.2)$$

The difference of the two numerical estimates, $\Delta$, is a convenient indicator of the truncation error

$$\Delta = (y_2 - y_1) \qquad (5.15)$$

This error, $\Delta$, must be kept less than some specified tolerance by adjusting $h$. Since $\Delta$ is proportional to $h^5$ and a step $2h$ results in an error $\Delta$, the required step size $2h_0$ for an acceptable error $\Delta_0$ can be estimated by

$$2h_0 = 2h \left| \frac{\Delta_0}{\Delta} \right|^{0.2} \qquad (5.16)$$

For $\Delta_0 < \Delta$, Eqn. (5.16) provides an estimate of how much to decrease the step size when the present step is repeated. For $\Delta_0 > \Delta$, there is no need to decrease the present step size $2h$.

For a system of first-order ODEs, the quantity $\Delta_0$ is actually a vector of desired accuracies, one for each dependent variable. Eqn. (5.16) is used to get an estimate for $2h_0$ for each dependent variable, and the step size is decreased according to the smallest of the estimates.

## 5.5 Example 1: SDOF Structure with a suddenly applied external load:
## 5.5.1 Gravitational effects neglected:

Consider an SDOF oscillator of the type described in Sec. 5.3.1 with a $k/m$ ratio corresponding to a nominal natural frequency of 1 Hz, no viscous damping and a value of $\alpha$ of 0.05. The parameters of the nonlinear system, $A$, $\beta$, $\gamma$ are taken to be 1.0, 0.12 $cm^{-1}$, and -0.08 $cm^{-1}$, respectively. The ratio of $\beta / \gamma$ =-1.5 is a typical value for the W-B model, the parameter $A$=1.0 means $dz/du$ =1.0 at $u$=0 , and $\beta$ is chosen such that $u_{st}$, the

nominal static displacement of the oscillator because of its self-weight $mg$, corresponds to a

ductility ratio of 5.0. That is, $\dfrac{u_{st}}{u_y} = 5.0$, where $u_y = \dfrac{1}{(\beta - \gamma)}$ and $u_{st} = \dfrac{mg}{k}$.

In the absence of a base excitation and neglecting gravitational effects, the equation of motion becomes

$$\ddot{u} + \frac{1}{m}f(u,\dot{u},\mathbf{Z}) = \frac{F(t)}{m} \tag{5.17}$$

where $f(u,\dot{u},\mathbf{Z})$ has the usual meaning. The objective is to compare the response of the two hysteretic models to a suddenly applied load. Such a situation could arise, for example, when a steady gust of wind starts acting on a structure, or because of a sudden current on ocean structures.

The increase in static pressure $p$ that is due to a steady gust of wind may be expressed as [1,43]:

$$p = C_e C_g C_p \frac{1}{2}\rho V^2 \tag{5.18.1}$$

where $\rho$ is the mass density of air, $V$ is the wind velocity, $C_e$ is the exposure factor depending on the height of the building, $C_g$ is the gust factor, and $C_p$ is the shape factor for the building as a whole. Assuming $\rho=1.26$ kg/m$^3$, $C_e=1.5$, $C_g=2.0$, $C_p=1.3$, it can be shown that an 80 kmph wind causes an equivalent pressure of about 1250 N/m$^2$. That is,

$$p = 1250\left(\frac{V}{80}\right)^2 \text{ N/m}^2 \tag{5.18.2}$$

where $V$ is the wind speed in kmph. Assuming a 10 story structure with a plan area of 20 m by 20 m, a height of 35 m, a mass density for the structure of 1000 kg/m$^2$/story, and a wind velocity of 80 kmph, the wind force per unit mass $F(t)/m$ is found to be equal to be about 0.02 $g$. This wind force might be assumed to be a step function in time acting on the structure that is initially quiescent .

The two models respond quite differently when subjected to the step forcing function. Fig. 5.5 compares the displacements of the two models relative to the ground. The drifting characteristic in the displacement of the W-B model is clearly evident. After 140 seconds, the displacement for the W-B model is about 6 times that of the DEL model.

In Fig. 5.6, a comparison is made of the hysteretic restoring force diagrams. The same drifting is again quite evident in the response of the W-B model. By comparison, the DEL model settles down to a stable closed loop. The distinguishing feature noticeable in Fig. 5.6 is that there is a gradual hysteretic force relaxation in the W-B model. As a matter of fact, if the motion is observed for a long enough time, the mean hysteretic restoring force in the W-B model will settle down to a zero value. If $\bar{u}$ and $\bar{z}$ are the steady-state mean values of $u$ and $z$, then on neglecting inertial effects, the equation of motion yields

$$\alpha k \bar{u} + (1 - \alpha)k\bar{z} = 0.02mg \tag{5.19}$$

Since $\bar{z}=0$ for the W-B model, $\bar{u}=0.50633/\alpha$. For $\alpha=0.05$, Eqn. (5.19) is satisfied in the case of the W-B model by $\bar{z}=0$, $\bar{u}=10.127$ cm. By comparison, in the case of the DEL model, the equation is satisfied in steady state by $\bar{z}=0.503$ cm and $\bar{u}=0.570$ cm as seen in Fig. 5.6.

Fig. 5.7 compares the relative velocity response of the two models for $\alpha=0.05$. The agreement is very good. For the first 25 seconds, the behavior is almost identical. For the next 50 seconds, a slight elongation in the period of the system is observed for the W-B model, but is otherwise satisfactory.

Fig. 5.8 shows the displacement response of the W-B model for different values of $\alpha$, namely, 0.0, 0.05, 0.25 and 0.50. The corresponding steady-state values, $\bar{u}$, are $\infty$, 10.127, 2.025 and 1.013 cm., respectively.

In summary, for suddenly applied loads, it can be said that there is good agreement in response quantities like relative velocity (Fig. 5.7) and maximum hysteretic force (Fig. 5.6), but there can be large discrepancies in relative displacement and ductility. Whether the

use of the Wen-Bouc model is appropriate therefore depends on what response quantity is being elicited from the model.

## 5.5.2 Gravitational effects included:

In the presence of a gravitational field, a structure of the type described by Sec. 5.3.1 has a term $-mgu/h$ on the left-hand side of the equation of motion (Eqn. 5.9). This results in a reduced system stiffness that introduces a negative restoring force tending to topple the structure, a phenomenon often described as the $P - \delta$ effect. This tendency to collapse is not due to the deterioration of the mechanical properties of the members, but rather is due to the large geometrical changes that take place. For large displacements, the experimental hysteresis loops for subassemblages in [39] display negative slopes associated with the motion of the subassemblage as a mechanism aided by the $P - \delta$ effect.

In the absence of a base excitation, the equation of motion can be written as:

$$\ddot{u} + \frac{1}{m} f(u, \dot{u}, \mathfrak{Z}) - \eta \frac{k}{m} u = \frac{F(t)}{m} \qquad (5.20)$$

where $f$ has the usual meaning, and where $\eta \frac{k}{m} = \frac{g}{h}$. As in Sec. 5.5.1, let the nominal natural frequency=1.0 Hz, $A$=1.0, $\beta$=0.12 cm$^{-1}$, $\gamma$=-0.08 cm$^{-1}$, $F(t)/m$=0.02 $g$, $h$=35 m. Thus, $\eta$=0.071. There is assumed to be no viscous damping.

For $\alpha > \eta$, no change is expected from the results in Sec. 5.5.1, since the post-yielding stiffness is reduced but is still greater than 0. However, for $\alpha < \eta$, the post-yielding stiffness has a negative value. Given the manner in which the displacement drift of the W-B model increased when the post-yielding stiffness was decreased in Sec. 5.5.1 (Fig. 5.8), the drift for the system with negative post-yielding stiffness may be expected to be even larger. Figs. 5.9 and 5.10 compare the displacements and restoring force diagrams respectively, for the case $\alpha$=0.05. After 140 seconds, the displacement of the W-B model

is about 8 times that of the DEL model. As a matter of fact, $u$ for the W-B model will keep increasing as the time of observation increases. The other difference observed is that the W-B model does not exhibit the hysteretic force relaxation in Fig. 5.10 as was noted in Fig. 5.6. Actually, to counter the decrease in the restoring force that is due to the $P - \delta$ effect, $z$ and therefore the hysteretic force increase. This will go on until the increase of $z$ will no longer be enough to offset the destabilizing force, $\eta ku$, and the W-B model will predict catastrophic failure, even though from the DEL model, it is seen that a constant force of 0.02 $g$ per unit mass of the structure does not, in fact, lead to the failure of the structure.

These features are more evident for larger values of $\eta$. For example, Figs. 5.11 and 5.12 compare the relative displacement history and restoring force diagram for $\eta = 0.25$. It can be seen that the W-B model predicts collapse at about 90 seconds after the load is first applied. This is not the case with the DEL model, which has a steady-state mean offset of about 1 cm. From a physical viewpoint, it seems highly unlikely that a 80 kmph wind would lead to the collapse of the structure. Hence, the failure predicted by the W-B model can be attributed to the instability of the mathematical representation of the model rather than to the inability of the structure to withstand the load.

It is concluded that extreme caution must be exercised when the Wen-Bouc model is used to study the response of structures exhibiting unstable behavior. If the Wen-Bouc model is used to describe the hysteretic nature of a system and the ensuing analysis predicts failure, it might not be possible to tell whether the result is spurious, arising from the inherent instability of the mathematical representation of the model, or whether the structure actually failed because of excessive loading. It may be prudent not to employ the Wen-Bouc model representation for any nonlinear hysteretic system with a negative post-yielding stiffness.

## 5.6 Example 2: Structure subjected to earthquake excitation:

### 5.6.1 SDOF system:

Consider an SDOF oscillator of the type described in Sec. 5.3.1 with a $k/m$ ratio corresponding to a nominal natural frequency of 1.0 Hz, $c$ such that the viscous damping coefficient is 5% of critical, and a value of $\alpha$ of 0.05. The parameters describing the nonlinear behavior, $A$, $\beta$ and $\gamma$ are 1.0, 25.25 m$^{-1}$ and -18.15 m$^{-1}$ (i.e., $\beta/\gamma$ =-1.5), respectively. The value of $\beta$ is such that the maximum displacement of the oscillator with the hysteresis described by the DEL model corresponds to a ductility value of 4.0 when subjected to the NS component of 1940 El Centro earthquake (Fig. 5.13). For the selected values of A, $\beta$ and $\gamma$, $u_y=z_y=0.022$ m. There is no external force $F(t)$, gravitational effects are neglected and the structure is assumed to be initially quiescent. The response of the two models is numerically computed for a duration of $T=50$ seconds.

Figs. 5.14-5.17 show the hysteretic restoring force diagrams, $u$ vs. $t$, $z$ vs. $t$ and $\dot{u}$ vs. $t$, respectively. The following observations may be noted:

(1) The restoring force diagrams are qualitatively and quantitatively different as seen from Fig. 5.14. Firstly, nonclosure of some loops is quite evident in the W-B model. Secondly, it is observed that the unloading branches are stiffer for the W-B model than for the DEL model. The consequence of the first difference is that there may be portions of the response where negative energy is dissipated by the W-B model, while that of the second difference is that the loops in the W-B model enclose larger areas and hence result in a larger dissipation of energy.

(2) The basic nature of the displacement response time histories for the W-B and DEL models is quite similar (Fig. 5.15). There is close agreement in the absolute value of the maximum displacement (0.087 and 0.088 m, respectively), and in the dynamic amplitude, which is the difference between the largest and smallest values of the

displacement (0.1219 and 0.1218 m, respectively). Some features are different: Notably, the final offsets for the W-B and DEL models are 0.034 and 0.025 m, respectively.

(3) The time histories of $z$ and $\dot{u}$ (Figs. 5.16 and 5.17) match very well, especially in the maximum values. For instance, the maximum values of the relative velocity for the W-B and DEL models are 0.359 and 0.362 m/sec, respectively. Even in the later stages of the excitation ($t>30$ seconds), when the displacement of the W-B model drifts away from the displacement of the DEL model, the agreement in the velocity response is very good. Generally, the agreement in the velocity response of the two models can be expected to be better than that in the displacement response.

It is instructive to carry out a comparison of the time histories of the system response for the duration of interest $[0,T]$ as in Figs. 5.14-5.17. Such a comparison is, however, an inefficient way to compare the performance of the two models, for two reasons. Firstly, the volume of data involved in such a comparison is large and secondly, it is not so easy to see the most important features to facilitate the comparison. Comparison of a few important quantities characterizing the response yields useful information on the differences in the response behavior of the two models. Listed below are eight quantities that have been selected for comparison purposes henceforth:

(1) $u_m$, the maximum relative displacement (absolute value) in $[0,T]$

(2) $\mu$, the ductility factor of the response displacement that is due to the excitation

(3) $(u_{max} - u_{min})$, the dynamic amplitude, which is the difference between the largest and smallest values of the relative displacement in $[0,T]$

(4) $t_{max}$, the instant in time at which $u_m$ occurs

(5) $\dot{u}_m$, the maximum relative velocity (absolute value) in $[0,T]$

(6) $C_b$, the base shear coefficient. This is the maximum absolute acceleration of the oscillator in $[0,T]$ expressed as a fraction of $g$, the acceleration due to gravity

(7) $u_{off}$, the final displacement offset

(8) $E(T)$, the hysteretic energy dissipated during the time period $T$ normalized by $(1 - \alpha)k$. That is,

$$E(T) = \int_0^T z\dot{u}\, dt \tag{5.21}$$

The maximum displacement, velocity and acceleration are often used to compute response spectra; the dynamic amplitude is a quantity used in damage evaluation; the time of maximum displacement is a useful quantity in random vibration for purposes of reliability calculations; the base shear coefficient is used to determine the maximum force that the structure must withstand during the excitation and hence is necessary in the selection of member sizes; the energy dissipated plays a dominant role in reducing the vibration of the structure; the final offset serves as an indication of the residual drift or tilt of the structure; and the ductility factor is an indication of the maximum deformation that the structure should be able to undergo without failing during the excitation. Individual members will have to be detailed in a manner that allows for this deformation.

Table 5.1 presents a comparison of these eight quantities for the two hysteretic models. Most of the entries may be inferred from Figs. 5.14-5.17. The relative error shown in the table is defined as follows: If $q_a$ and $q_b$ are the values corresponding to the W-B and DEL models, respectively, for a particular quantity, then

$$\text{Relative Error } (\%) = \left( \frac{q_a - q_b}{q_b} \right) * 100 \tag{5.22}$$

From the table, it can be seen that five quantities (four of which are independent) have errors less than 2%. This is quite remarkable. It remains to be seen how well this holds up for cases with different levels of nonlinearity. It will be seen that the agreement in $u_m$ noted here is not observed for most of the cases considered later in this chapter. Another observation that may be made here is that it appears that the agreement in the response

behavior of the two models subjected to a zero mean earthquake excitation is much better than in Example 1, where the models were subjected to a nonzero load.

The analysis presented so far in this section has been for a ductility ratio of 4.0 in the response of the DEL model. In order to carry out a comparison in the eight characteristic quantities for a range of ductilities of the DEL model, the yield level $z_y$ of the nonlinear model is varied so as to achieve a variation of the ductility ratio in the response of the DEL model. For each $z_y$, both models with the same initial loading curve are then subjected to the 1940 El Centro earthquake. Keeping $A=1.0$ and $\beta/\gamma=-1.5$, $\beta$ is changed such that $z_y$ varies from 0.005 to 0.90 m; the ductilities in the case of the response of the DEL model vary from 0.10 to about 30.

Figs. 5.18-5.25 show the eight characteristic quantities defined earlier in this section plotted against the normalized hysteretic force yield level, $z_y$. The case $z_y=0.022$ was the one treated in detail in Figs. 5.14-5.17. As $z_y$ decreases, the ductility ratio of the response increases for both models (Fig. 5.19) and hence the nonlinearity increases. For very large values of $z_y$ (i.e., for very small values of $\beta$ and $\gamma$), the response of both models will tend to the linear model response. The following observations may be made from Figs. 5.18-5.25:

(1) For most of the range of $z_y$ under consideration, the maximum displacement of the W-B model is less than that of the DEL model (Fig. 5.18). This means that the predicted ductilities are also lower for the W-B model (Fig. 5.19). The difference in the ductilities becomes more noticeable as the nonlinearity increases. For $z_y=0.005$, the largest nonlinearity considered, the relative error in ductility is as much as 15% (compared to about 2% for the case $z_y=0.022$).

(2) The behavior of dynamic amplitude (Fig. 5.20), $\ddot{u}_m$ (Fig. 5.21) and $C_b$ (Fig. 5.22) of the two models is similar, and the relative errors for the three quantities at $z_y=0.005$ are each less than 6%.

(3) The agreement of the models in $t_{max}$, the instant in time at which $u_m$ occurs, is very poor at large nonlinearities (Fig. 5.23).This is also true for the final offset, $u_{off}$ (Fig. 5.24). At $z_y$=0.005, the final offsets for the W-B and DEL models are about 0.005 and -0.045 m, respectively.

(4) The energy dissipated, $E(T)$, is larger for the W-B model for the entire range of ductilities under consideration (Fig. 5.25). At a value of $z_y$=0.022 (corresponding to a ductility of about about 4.0 for both models), the relative error in $E(T)$ is about 20%. This may be because the unloading stiffnesses are larger in the case of the W-B model.

(5) It is interesting that the quantities $u_m$, dynamic amplitude, $t_{max}$, $u_{off}$, $E(T)$ do not vary monotonically with respect to $z_y$. For example, from Fig. 5.25, it can be seen that there is a certain level of nonlinearity (at $z_y$=0.031 m) where maximum energy is dissipated. That is, lowering the value of $z_y$ may lead to larger levels of ductility but not necessarily to larger levels of energy dissipation.

In summary, it may be stated that the response of the W-B model when subjected to a zero mean earthquake excitation is not in complete agreement with that of the DEL model, especially in the response quantities displacement, ductility and final offset, even though it must be said that the agreement is much better than in the case when the two models were subjected to a nonzero mean load. Generally speaking, it seems as though the prediction of the base shear, velocity and dynamic amplitude by the W-B model can be expected to be better than its displacement prediction.

## 5.6.2: MDOF system:

It was seen in Chapter 4 how any nonzero mean cycle in $z$ causes a drift in the displacement of the W-B model, resulting in a nonclosure of the loop. In an SDOF oscillator, the response is essentially at one predominant frequency, while in the case of an MDOF system, the response is likely to have significant components at the first few natural

frequencies of the system. A similar situation may also arise in the case of an SDOF oscillator when the excitation is predominantly at a frequency different from that of the natural frequency of the oscillator, resulting in a response with two peaks in its frequency spectrum. In either case, the tendency of the W-B model to drift, have nonclosure of loops, etc., may be more pronounced because the response will have high-frequency components superposed over a low-frequency component, and these high-frequency components cause additional cycles in $z$ over a nonzero mean. A hysteretic restoring force is frequency-independent; thus, a nonzero mean cycle in $z$ will result in the same amount of drift irrespective of the frequency associated with that cycle. Therefore, in an MDOF system, the drift in the displacement of the W-B model is likely to be larger than in an SDOF system.

To demonstrate this qualitatively, the two-story structure shown in Fig. 5.26 is considered. The initial stiffness-to-mass ratios are such that the nominal natural frequencies of the system are 0.5 and 1.5 Hz. There is assumed to be no viscous damping, and the post-yielding stiffness ratio $\alpha$ equals 0. The nonlinear parameters describing the nonlinear behavior are: $A_1 = A_2 = 1.0$, $\beta_2 / \gamma_2 = \beta_1 / \gamma_1 = -1.5$, $\beta_2 = \beta_1 = 18.00$ m$^{-1}$. The $\beta$ s are chosen such that the maximum displacement of the first story of the DEL model to the El Centro earthquake corresponds to a ductility of about 4. For the purposes of this comparison, gravity effects are neglected, and there are no external forces acting on the structure.

Figs. 5.27 and 5.28 compare the interstory displacements of the first and second stories, respectively. The maximum displacement in the first story is 0.130 m (a ductility ratio of 3.90) in the case of the DEL model and is 0.180 m (a ductility ratio of 5.40) in the case of the W-B model.

It is also interesting to compare the first story's restoring force diagrams of the two models (Fig. 5.29). In Fig. 5.29a, two segments in the restoring force diagram of the W-B model associated with drift and nonclosure of loops are shown in dashed lines. These

occur at about 3 seconds and 12 seconds after the earthquake commences. By observing the displacement of the first story (Fig. 5.27) at these instants in time, it can be seen that the segments are due to the high-frequency component of the response. In addition, the usual contribution to drift due to the nonzero mean cycling corresponding to the low frequency component is also present, as in the case of the SDOF system.

It may be noted that the discussions in this section are for one specific base excitation. While useful information can be gathered about the nature of the responses of the two hysteretic models to earthquake excitations from the example considered, for more quantitative comparisons, a stochastic analysis will be performed in the next section with ensembles belonging to different families of excitations.

## 5.7 Stochastic excitation:

### 5.7.1 Introduction:

If the state of stress, the material properties, location and history of fractures and other requisite details are known, and the tectonic mechanisms causing earthquakes are completely understood, the ground motion $a(t)$ at a given site can be theoretically computed in advance. Since all the required information is rarely available, engineers and scientists must accept a certain level of uncertainty or randomness in describing the earthquake ground motion. For this reason, earthquake motion is often represented by a stochastic process. Use of a stochastic model to describe earthquake motion is appropriate in much the same way as the use of probabilistic models in the characterizations of errors in measurements of physical quantities such as structural stiffnesses.

One suitable approach in the selection of stochastic models to describe earthquake motion is in defining the excitation as belonging to a general class of time histories. The class of time histories should have time- and frequency-domain properties that will realistically reflect the features of an actual earthquake, like the frequency content, duration

of shaking, peak acceleration, etc. The larger the number of features the earthquake model has to include, the larger will be the number of parameters to describe the model. The only limitation in the selection of the complexity of the stochastic models is that the analytical methods for the analysis of nonlinear systems subjected to random excitation are much more complex than in the case of a simple deterministic input. Therefore, the stochastic model description for earthquake motion must be as simple as possible. Also, from the point of view of numerical simulation analysis such as carried out here, the stochastic models need to be simple enough so that only a small computational effort is spent in generating the ensemble of excitation time histories.

In this section, two classes of stochastic excitation are chosen for which a comparative response study is performed of the eight characteristic quantities defined in Sec. 5.6. The two types of random processes are stationary white noise and response spectrum-consistent time histories. The following two sections explain the manner in which the ensembles are generated and compare the response of the two hysteretic models to the ensembles.

### 5.7.2 Example 3: SDOF system with stationary white noise base excitation:

One of the simplest random processes is a zero mean, Gaussian stationary process. Because stationary processes are well understood and the theory is well developed, much effort has been devoted in earthquake engineering research to model earthquakes as stationary processes. One such approach has been to use stationary white noise; Housner [18] suggested a model that was essentially white noise - a large number of impulses arriving at random times. The white noise model has been used extensively to investigate structural behavior during earthquakes [9,42]. Clearly, stationary excitations can be used only to represent the strong shaking portion of an earthquake record, not for the buildup or

tail of the ground motion. The simplicity of the white noise random process has ensured its continued use in current research as a stochastic model to describe earthquake motion.

Let the base excitation $n(t)$ be a zero mean, stationary, Gaussian white noise with a spectral density $S_0$. Let there also be a constant external force per unit mass $\bar{F}$ on the structure and let gravitational effects be neglected. For the purpose of carrying out a Monte Carlo simulation with white noise, an ensemble of $\bar{N}$ sample functions is generated for $n(t)$. Each sample function is constructed in the following manner: A sequence of independent Gaussian distributed numbers with a zero mean and unit variance is generated. The numbers are used as ordinates of the function at equally spaced intervals in time, $\Delta t$. The function is then assumed to vary linearly within each time interval. On multiplying the function by $(2\pi S_0 / \Delta t)^{1/2}$, it can be shown [15] that the power spectral density of the function approaches $S_0$ as the $\omega \Delta t$ approaches zero and remains within 5% of $S_0$ for $\omega \Delta t < 0.57$, $\omega$ being the frequency. Therefore, to approximate a white noise process to within a given tolerance up to a desired frequency, the time interval chosen must be appropriately small. In this example, $\Delta t = 0.02$ seconds.

Most digital computers have only a library subroutine that generates pseudo-random numbers uniformly distributed on $[0,1]$. From two such numbers $x_1$ and $x_2$, two independent numbers, $z_1$ and $z_2$, belonging to a Gaussian distribution with zero mean and unit variance can be generated using the following relations [15]:

$$z_1 = \sqrt{-2\ln x_1}\, Cos(2\pi x_2), \quad z_2 = \sqrt{-2\ln x_1}\, Sin(2\pi x_2) \tag{5.23}$$

In this manner, $\bar{N}$ samples of zero mean, stationary, Gaussian white noise, each lasting 20 seconds, are generated, this time period being a typical earthquake duration. A simulation analysis is performed for each of the six cases listed in Table 5.2. For each case, a comparison is made between the two models of the eight characteristic response quantities described in Sec. 5.6. For all six cases, the following are kept constant: nominal natural

frequency of 1 Hz, viscous damping as a fraction of critical 5%, the ratio $\beta/\gamma$ of

-1.5 and $A$=1.0. The parameters that are varied in the six cases of Table 5.2 are $\alpha$, $\bar{F}$, and

$\beta$. In Cases I, II and III, there is no post-yielding stiffness, there is no external force

($\bar{F}$=0), and $\beta$ is changed so as to vary the level of nonlinearity; for the three values of $\beta$

considered, the mean values of the predicted ductilities in the response of the DEL model

are about 2.0, 4.0 and 8.0. Thus, the manner in which the response statistics of the two

hysteretic models vary over a range of ductilities may be observed. The motivation behind

the choices of the remaining cases listed in Table 5.2, namely, Cases IV, V and VI is to

study the effect of positive post-yielding stiffness, nonzero mean loading, and combined

positive post-yielding stiffness and nonzero mean loading, respectively.

To examine the convergence rate of the mean and standard deviation of $u_m$ in Case

III, statistics are obtained for a variation of the number of samples, $\bar{N}$, from 5 to 1000. For

both models, the means converge faster than the standard deviations, as should be

expected. After 250 simulations, the standard deviations for the W-B and DEL models are

within 3% and 8% of their respective values after 1000. For the remainder of this section,

$\bar{N}$=250 samples are considered large enough for the calculation of the response statistics.

For each case listed in Table 5.2, the two systems with hysteresis described by the

W-B and DEL models and initially at rest with zero velocity are subjected to the ensemble

of ground acceleration and external force $\bar{F}$, and the responses are computed for a time

duration of $T$=30 seconds. From the respective responses, statistics of the eight

characteristic response quantities under consideration are calculated and tabulated in detail

in Tables 5.3 through 5.8, respectively, for the six cases. The statistics displayed for each

quantity are the mean, the standard deviation and the median. For a symmetric distribution,

the mean and the median are the same. Also recorded in the tables are the statistics of the

relative error for all eight quantities except $u_{off}$. This is because the final offset for zero

-116-

mean loading has a zero mean, and the values of $u_{off}$ close to zero will cause a large relative error in Eqn. (5.22), leading to misleading figures.

Values from Tables 5.3, 5.4 and 5.5 are used to plot Figs. 5.30-5.35, which show $u_m$, $\mu$, $\ddot{u}_m$, $C_b$, $u_{off}$ and $E(T)$, respectively, vs. the yield level of the normalized hysteretic force, i.e., $z_y$. The three values of $z_y$ corresponding to Cases I, II and III, are 7.82, 5.00 and 3.42 cms, respectively. The smaller the value of $z_y$, the larger is the ductility (Fig. 5.31) and hence larger the nonlinearity. In Figs. 5.30-5.35, three curves are drawn for each hysteretic model, corresponding to the values of (i) mean minus one standard deviation, (ii) mean, and (iii) mean plus one standard deviation of the response quantity. Thus, an idea can be obtained not only of the mean value comparison but also of the standard deviation. The following observations may be made from Figs. 5.30-5.35 and Tables 5.3, 5.4 and 5.5:

(1) From Figs. 5.30 and 5.31, it is seen that the values of $u_m$ and ductility are likely to be larger for the W-B model. For both models, the standard deviation increases as the nonlinearity increases. The mean and standard deviation in $u_m$ for the W-B model are about 1.25 and 1.75 times that of the DEL model for Case II, and the mean relative error is 27%. The use of the W-B model would therefore lead to a more conservative design with structures designed for larger ductilities than would be necessary according to the DEL model.

(2) The relative error in the dynamic amplitude for Case II has a mean value of about 7%, meaning that on an average, the W-B model overestimates the dynamic amplitude value of the DEL model by about that amount. In specific instances, however, the estimation may be more or less since the error has a standard deviation of about 22%.

(3) The relative errors involved in the estimation of $t_{max}$ by the W-B model are very large (mean of 76% and standard deviation of 222% for Case II). This means that the use of the W-B model in reliability calculations will lead to erroneous results.

(4) The maximum velocity ($\dot{u}_m$) values for the W-B model are somewhat less than for the DEL model (Fig. 5.32). For Case II, the mean and standard deviation of $\dot{u}_m$ are about 60 cms/sec and 7 cms/sec, respectively, for the W-B model and 65 cms/sec and 8 cms/sec respectively for the DEL model, and the mean relative error is about -7.5%. Given this information, one may make the decision that $\dot{u}_m$ predictions by the W-B model are quite acceptable, but this is a subjective matter requiring some consensus on what is "acceptable" error.

(5) Among the eight quantities under discussion, the one in which by far the best agreement is observed among the two hysteretic models is in $C_b$, the base shear coefficient (Fig. 5.33). The means of $C_b$ for Case II are 0.214 and 0.216, respectively, for the W-B and the DEL models, and the mean relative error is about -1%.

(6) The final offset is a quantity that should be expected to have a zero mean and from Fig. 5.34, this is seen to be essentially true for both models. However, the standard deviations are much larger for the W-B model than for the DEL model, especially at higher levels of nonlinearity. For Case II, the standard deviation of the W-B model is more than 2.25 times that of the DEL model; i.e., the final offset value is likely to be larger for the W-B model, and that would imply that larger damage has occurred than actually did according to the DEL model.

(7) The values of the energy dissipated, $E(T)$, for the W-B model are consistently larger than those for the DEL model (Fig. 5.35). This overestimation by the W-B model was observed in Sec. 5.6, too. In Fig. 5.36, it appears that there is only a translational shift in curves: for the three values of $z_y$ considered, the means differ by a constant value, while the standard deviations are essentially the same. For Case II, the mean value estimate of $E(T)$ by the W-B model is 1.07 times that of the DEL model.

On the basis of these observations, a few remarks may be made here. For systems with no post-yielding stiffness, the W-B model provides an excellent estimate of the value

of the base shear coefficient $C_b$, while estimates by the W-B model of the maximum

velocity $\dot{u}_m$, the dynamic amplitude and the energy dissipated $E(T)$, appear to be adequate.

But the estimates by the W-B model of the maximum displacement, $u_m$ (and hence of the

ductilities), the final offset, $u_{off}$, and the time of maximum displacement, $t_{max}$, are much

less reliable. It is not immediately apparent if the trends noted here are unchanged for

systems with different nonlinear parameters (different $\beta/\gamma$, $A$, etc.), but the analysis

performed here gives an idea of how the two models compare.

For complete information on the statistical nature of each response quantity, it would

be necessary to know the probability density function. For Case III, a comparison of the

probability density functions for a few quantities is carried out. Fig. 5.36 shows the

probability density function of $u_m$, the maximum absolute value of the relative

displacement. The two models exhibit similar behavior in the probability density, but it can

be seen that the mean value and standard deviation for the W-B model (about 34 cms and

14.5 cms, respectively) are larger than for the DEL model (about 28 cms and 11 cms,

respectively). The density functions resemble Rayleigh distributions even though there is

not enough information on the behavior for values of $u_m$ less than 15 cms.

If $u_m$ for each hysteretic model is normalized by subtracting the respective mean and

dividing by the respective standard deviation and the probability density functions plotted

as in Fig. 5.37, it can be seen that they follow the same basic distribution. This would

seem to suggest that the differences in the means and standard deviations of the two models

are adequate to characterize the differences in their probability densities.

Fig. 5.38 shows the cumulative probability function (the integral of the probability

density function) of $u_m$. The medians for the W-B and DEL models are about 31 cms and

25.5 cms, respectively. In random vibration, the reliability function $W(T)$ is defined as the

probability that the magnitude of $u$ does not exceed a specified level $b$ throughout the time

interval $[0,T]$ . Fig. 5.38 is therefore also the plot of $W(30)$ for values of $b$ on the

horizontal axis from 0 to 100 cms. Thus, the reliability function used in the first passage problem is different for the two hysteretic models, and the probability that $u_m$ is less than any specified value $b$ (also called the "safe" probability) is larger for the DEL model than for the W-B model.

Figs. 5.39 and 5.40 show the probability density functions for Case III of the maximum relative velocity, $\dot{u}_m$, and the base shear coefficient, $C_b$, respectively. These probability densities are more symmetric than $u_m$, and the predictions of $C_b$ by the two models match very closely. For $\dot{u}_m$, the mean relative error is about -7%; this accuracy may or may not be enough depending on the allowable error tolerance.

Fig. 5.41 is the probability density function of $u_{off}$, the final offset which is almost zero mean for both hysteretic models, but the spread or standard deviation for the W-B model is 1.5 times that of the DEL model. The final offset of the W-B model is therefore likely to be larger than that of the DEL model. For example, it can be seen from Fig. 5.41 that the probability that $u_{off}$ will between 49 and 51 cms is larger for the W-B model.

Case IV is the same as Case II in every aspect except that $\alpha$ is 0.05 for Case IV instead of 0 as in Case II; i.e., the system has a post-yielding stiffness equal to 5% of the initial stiffness and thus there is a positive linear restoring force. The effect of such a linear spring is to control the displacement drift of the W-B model, and one should therefore expect that $u_m$ (and $\mu$) values of the W-B model for this case should be closer to those of the DEL model than in Case II. This indeed is true. From Tables 5.4 and 5.6, it is seen that though there is some marginal improvement in most of the eight quantities, the most dramatic is in $u_m$. The mean and standard deviation of this quantity are about 18 cms and 4.5 cms, respectively, for both models. This would suggest that for systems with positive post-yielding stiffnesses ($\alpha > 0$), the W-B model may be a more suitable description of hysteresis than for systems without ($\alpha = 0$).

In Case V, an external static load ($\bar{F} \neq 0$) is added to the zero mean white noise ensemble in order to study the effect of nonzero mean loading. $\bar{F}$ is 2% g which, as was seen in Sec. 5.5.1 would correspond approximately to a 80 kmph wind on a 10 story structure. Cases II and V have the same parameters; the only difference is that Case V has a nonzero $\bar{F}$. Direct comparison of Tables 5.4 and 5.7 will thus show the effect of the static load. From the example in Sec. 5.5.1, one should expect the $u_m$ differences to be much larger for Case V than for Case II. A look at Table 5.7 confirms this. For Case V, the mean and standard deviation in $u_m$ of the W-B model are almost 1.75 and 2.25 times that of the DEL model (compared to the corresponding factors 1.25 and 1.75 for Case II). The external static load has the effect of increasing the mean value of the ductility $\mu$ from 3.94 to 4.42 for the DEL model and from 4.93 to 7.59 for the W-B model. The following conclusion may therefore be drawn: The hysteretic representation given by the W-B model provides unreliable estimates of the response statistics of systems with no post-yielding stiffness subjected to a nonzero mean loading. The case of nonzero mean loading is not a favorable one for the use of the W-B model as description of system hysteresis.

Case VI involves having a nonzero mean loading as well as a positive $\alpha$ ($\alpha = 5\%$). This enables the combined effect of having a nonzero mean loading condition (unfavorable for the W-B model) and a positive post-yielding stiffness (favorable for the W-B model). Considering Tables 5.4, 5.7 and 5.8, it can be seen that the effect of $\alpha > 0$ not only reduces the detrimental effect of the nonzero mean loading in the response of the W-B model, but actually provides a better agreement in the response statistics than in Case II (but not as good as in Case IV).

### 5.7.3 Example 4: Comparison of inelastic response spectra:

The response spectrum is a common means of specifying earthquake ground motion for structural response studies. It is appealing because it gives some of the most important

features of the response without requiring knowledge of the time history of the excitation. In spite of its advantages, the response spectrum has one glaring shortcoming as a design specification. It is normally defined only in relationship to linear systems. This can be a severe limitation because most modern building structures are designed to behave in a nonlinear, ductile manner during a major earthquake. One way to overcome this difficulty may be in the definition of an inelastic response spectrum associated with a given elastic response spectrum. It is believed that for many buildings, satisfactory approximations to the design forces and deformations can be obtained from the modal method by using the corresponding inelastic response spectrum. Veletsos and Newmark [51] , Iwan [23] and others have given methods for estimation of inelastic response spectra from their elastic counterparts for simple piecewise-linear hysteretic models.

Because it is desired to determine the inelastic response spectra of the two models corresponding to a linear elastic spectrum, an ensemble of histories consistent with the specified elastic response spectrum should be generated. The NRC Reg. Guide 1.60 horizontal mean response spectrum [34] for a damping value of 2% (Fig. 5.42) is chosen to be the specified design spectrum. The theory used for the generation of response spectrum-consistent histories established by Mason and Iwan [29,30], is briefly summarized below.

The mathematical model of the earthquake process is that of a zero mean, stationary, Gaussian random process $n(t)$ modulated by a deterministic envelope $\theta(t)$. One such envelope is shown in Fig. 5.43. The quadratic time-dependence phase, the constant phase and the exponentially decaying phase model the buildup, strong shaking and tail parts of earthquakes. The base excitation $a(t)$ can therefore be written as

$$a(t) = \theta(t)n(t) \qquad (5.24)$$

Given a displacement response spectrum $SD(\omega,\xi,P_s)$ and an excitation envelope function $\theta(t)$, the spectral density $S_{nn}(\omega)$ of $n(t)$ is found such that the response of a linear SDOF oscillator satisfies the equation:

$$\text{Prob}\{u_m(\omega,\xi) \leq SD(\omega,\xi,P_s)\} = P_s \quad \text{for } \omega_{min} \leq \omega \leq \omega_{max} \tag{5.25}$$

where $\omega$ is the natural frequency of the oscillator, $\xi$ is the damping ratio, $u_m(\omega,\xi)$ is the maximum value of the relative displacement of the system that is due to the acceleration $a(t)$, $SD(\omega,\xi,P_s)$ is the specified displacement response spectrum value at frequency $\omega$, and $P_s$ is the safe probability or the confidence level, i.e., the probability of not exceeding the target spectrum. The procedure to find $S_{nn}(\omega)$ involves the application of the two-state Markov process approach to compute first passage probabilities and is clearly explained in [27,29].

The second step in the generation of $\bar{N}$ time histories, $a_k(t)$, uses the formula [55]:

$$a_k(t) = \theta(t) \sum_{j=1}^{M} \sqrt{2A_j} Cos(\bar{\omega}_j t + \phi_{jk}) \quad \forall t \in [0,T] \tag{5.26}$$

$$k = 1,2,....,\bar{N}$$

where

$\omega_j = \omega_{min} + (j-1)(\omega_{max} - \omega_{min})/M$ , $j = 1,2,...,(M+1)$

$A_j$ = the area under the one-sided spectral density function $S_{nn}(\omega)$ in the interval $(\omega_j,\omega_{j+1})$

$M$ = the number of intervals $(\omega_{min},\omega_{max})$ is divided into

$\bar{\omega}_j = (\omega_j + \omega_{j+1})/2$ =the central frequency of the interval $(\omega_j,\omega_{j+1})$

$\phi_{jk}$ = a random phase uniformly distributed on $[0,2\pi]$

The following values of the parameters are used in the generation of 250 ($\bar{N}$=250) samples comprising the ensemble: $\xi$=2%, $P_s$=50%, $\omega_{min}/2\pi$=0.10 Hz, $\omega_{max}/2\pi$=33 Hz, the number of divisions $M$=250, earthquake duration $T$=30 seconds; the envelope parameters are $t_0$=4 seconds, $t_1$=15 seconds, $t_2$=30 seconds, and the exponential rate of

decay is 0.10. For these envelope parameter values, the modulating envelope $\theta(t)$ is similar to the Caltech B-type earthquake envelope [26], which was designed to represent shaking close to the fault of an earthquake of a Richter magnitude of 7.0 or greater.

Assume that there are no external forces, and neglect gravitational effects. The system parameters are: viscous damping as a fraction of critical=2%, $\alpha=0$, $A=1.0$, $\beta/\gamma=-1.5$, and $k/m$ is varied so as to achieve a range of nominal natural frequencies $f$ from 0.1 to 9.0 Hz. For each value of $k/m$, the yield level $z_y$ is varied until a mean ductility value of about 4.0 is achieved in the response of the DEL model to the generated ensemble of earthquake excitations. Then the W-B model with the same yield level $z_y$ is subjected to the ensemble.

In this way, the pseudovelocity $(PSV)$, velocity $(SV)$ and acceleration $(SA)$ spectra of the two models are determined and plotted vs. the natural frequency on a log-log scale in Figs. 5.44, 5.45 and 5.46, respectively. The quantities spectral displacement $(SD)$, spectral velocity $(SV)$, spectral acceleration $(SA)$, pseudovelocity $(PSV)$ and pseudoacceleration are defined in the following manner:

$$SD = u_m, SV = \dot{u}_m, SA = gC_b, PSV = (2\pi f)SD, PSA = (2\pi f)^2 SD \qquad (5.27)$$

The three curves shown for each model in these figures correspond to the values of (i) the mean minus one standard deviation, (ii) the mean and (iii) the mean plus one standard deviation. In Fig. 5.46, only the mean values of $SA$ are shown because in this case, the standard deviations are only about 5% of the mean values. It may be mentioned here that since the elastic NRC spectrum in Fig. 5.42 is scaled to a maximum ground acceleration of 1 $g$, the inelastic response spectra shown in Figs. 5.44-5.46 are also normalized to a maximum ground acceleration level of 1 $g$. For other excitation levels, these spectra can be scaled accordingly. For instance, for a maximum ground acceleration level of 0.40 $g$, the normalized inelastic spectra are to be multiplied by a scale factor of 0.40.

The following observations can be made from Figs. 5.44-5.46:

(1) For both models, the $SV$ curves shown in Fig. 5.45 are similar in shape to the NRC elastic spectrum (Fig. 5.42), whereas the $PSV$ curves shown in Fig. 5.44 have shapes quite different from that of the NRC spectrum. For values of $f$ of about 0.10 Hz, for example, the $PSV$ values are smaller than the corresponding $SV$ values by a factor of about 2.0. Using the $SV$ spectrum as the design criterion may thus lead to a more conservative design for tall structures than the $PSV$ spectrum. In the frequency range of 0.30 to 9.0 Hz, the $PSV$ values are larger than the corresponding $SV$ values by a factor of almost 2.0. For instance, the mean values of PSV and SV for the DEL model at a natural frequency of 1 Hz are about 141 and 73 in/sec, respectively. Thus, unlike a linear system where $PSV{\approx}SV$, in the case of nonlinear systems, the spectral velocity and pseudovelocity are quite different from one another.

(2) From Fig. 5.44, it is seen how the two hysteretic systems compare with each other in the pseudovelocity, $PSV$. For values of the frequency of about 0.10 Hz, and larger than about 1.50 Hz, the mean $PSV$ values of the DEL model are less than those of the W-B model, which means that the W-B model leads to a more conservative design than the DEL model. But in the intermediate range of 0.25 to 1.50 Hz, the W-B model with smaller $PSV$ values than the DEL model, leads to a nonconservative design when compared to the DEL model. Therefore, caution must be exercised while using the inelastic $PSV$ design spectrum produced by the W-B model.

(3) Consistent with a trend observed in the white noise simulations (Sec. 5.7.1), the $SV$ values for the W-B model are lesser than those for the DEL model (Fig. 5.45). If a design procedure should entail use of the spectral velocity as a design parameter, then the lower $SV$ values of the W-B model will lead to nonconservative designs.

(4) The mean $SA$ curves for the two models shown in Fig. 5.46 agree quite well over the entire range of $f$ under consideration. This may have been expected from earlier

observations. It would seem from this observation that either hysteretic model may be used to produce the inelastic *SA* response spectrum for design purposes.

The ATC 3-06 recommendations for the procedures to be used in the analysis of forces and deformations in buildings subjected to earthquake ground motion are listed in [2] in the order of increasing rigor and expected accuracy. These procedures range from an equivalent lateral force procedure to an inelastic response history analysis involving step-by-step integration of the equations of motion. A comparison of the design base shear values from (i) the ATC 3-06 lateral force procedure, (ii) the elastic NRC spectrum, (iii) the W-B model and (iv) the DEL model will now be offered.

The ATC 3-06 prescription for the base shear coefficient, $C_b$ (also called the seismic design coefficient), is given by the lesser of the two following values [2]:

$$C_b = \frac{1.2A_v S}{RT_n^{2/3}}$$
(5.28.1)

$$C_b = \frac{2.5A_a}{R}$$
(5.28.2)

where

$A_v$ = the coefficient representing Effective Peak Velocity (*EPV*)-related acceleration

$A_a$ = the seismic coefficient representing the Effective Peak Acceleration (*EPA*)

$S$ = the site coefficient depending on the soil profile characteristics of the site

$R$ = the response modification factor and

$T_n$ = the fundamental natural period of the structure.

$A_v$ and $A_a$ are two parameters used to characterize the intensity of design ground shaking and they are representative of the *EPV* and *EPA*, respectively. The *EPA* and *EPV* are determined in the following manner from the elastic PSV response spectrum. The *EPA* is proportional to the *PSA* ordinates for periods in the range of 0.1 to 0.5 seconds, while the *EPV* is proportional to the *PSV* ordinates at a period of 1 second. (The proportionality

constant in both cases is 2.50.) Sites with the largest seismic exposure have values of $A_a$ and $A_v$ of 0.4 each, corresponding to a EPA and EPV of 0.4 $g$ and 12 in/sec, respectively.

In the response modification factor $R$, the ATC provisions recognize the fact that structures have a reserve capacity to absorb energy beyond the elastic strain energy at significant yield. $R$ thus takes into account the ductility of the structural system. The value of $R$ depends on the structural system and on the kind of mechanism used to resist seismic forces. It ranges from a value of 1.25 for a bearing wall system of unreinforced masonry walls to a value of 8 for a moment-resisting frame system with special steel moment frames.

Assuming $A_a=A_v=0.4$, a site with shallow, stiff soil over rock ($S=1.0$) and an ordinary moment-frame-resisting system made of steel ($R=4.5$), the design coefficient is determined from Eqn. (5.28).

To facilitate direct comparison of the values of $C_b$ for the elastic and inelastic spectra with the code values, scaling of the spectra needs to be performed. The normalized NRC spectrum (Fig. 5.42) has PSA ordinates of about 4 $g$ in the period range 0.1 to 0.5 seconds and a PSV ordinate of about 120 in/sec at a period of 1 second. Using the normalizing factor of 2.5, the corresponding EPA and EPV values are 1.6 $g$ and 48 in/sec. Thus, to be consistent with the ATC 3-06 values 0.4 $g$ and 12 in/sec respectively, a scaling factor of 0.25 is applied for the elastic spectrum and the inelastic spectra associated with the elastic spectrum. For the elastic NRC spectrum,

$$C_b = PSA / g = (2\pi f)PSV / g \qquad (5.29)$$

where $f=1/T_n$. For the inelastic models, the base shear coefficient $C_b$ is the maximum absolute acceleration of the system (SA) expressed as a fraction of $g$.

Fig. 5.47 shows the design base shear coefficient as given by the elastic NRC spectrum, the inelastic spectrum corresponding to the W-B and DEL models, and the ATC 3-06 recommendation as a function of the fundamental natural period of the structure. It is

immediately apparent why it is beneficial to design structures with an ability to perform in a ductile manner. The values of $C_b$ according to a linear elastic design are quite high and will lead to expensive designs. For example, at a natural period of 1.0 Hz, designing the structure to deform elastically when subjected to strong ground motion will require a seismic design coefficient of about 0.48. But a structure detailed in a manner to meet a ductility demand of about 4 needs to be designed only for a value of the seismic coefficient of about 0.14.

The second observation that may be made is that even the least rigorous of the ATC 3-06 recommended analysis procedures yields design coefficients that are quite comparable to those predicted by a stochastic analysis of the dynamic behavior of the two nonlinear models. It must be kept in mind that there is some flexibility in the choice of $R$, the response modification factor, and the foregoing discussions must be viewed in that context. A good choice of the factor involves a lot of experience on the part of the designer.

The ATC 3-06 determines the value of the design displacement drift, $\delta$ (for an SDOF system, $\delta$ is the displacement of the mass relative to the ground), as follows:

$$\delta = C_d \delta_e \tag{5.30}$$

where

$C_d$ = the deflection amplification factor, which, like $R$, depends on the structural system

$\delta_e$ = the deflections determined from an elastic analysis.

For an ordinary moment-frame-resisting system made of steel, $C_d=4.0$. Taking $\delta_e$ to be the SD value of the elastic NRC spectrum, the ATC 3-06 values for design drift can be determined from Eqn. (5.30). These values are plotted in Fig. 5.48 along with the mean values of $u_m$ for the two hysteretic models. For almost the entire range of the natural periods under consideration, the design values of the displacement drift for the W-B model are less than those for the DEL model. In this context, the ATC 3-06 values are slightly on the high side, especially at longer natural periods.

### 5.7.4 A note on the maximum displacement prediction by the two models:

In the six cases of Example 3 where an SDOF structural model was subjected to white noise base excitation, the maximum displacement and ductility values of the W-B model are generally higher than those of the DEL model. On the other hand, in Example 4 where the SDOF model was subjected to simulated earthquake base excitations, the values of the said quantities of the W-B model are generally lower than the corresponding values of the DEL model. The reason for this may perhaps be explained thus. One of the differences in the two ensembles is in the duration of strong shaking, with the durations for the white noise and spectrum-consistent ensembles being 20 seconds and 11 seconds, respectively. Keeping in mind that the W-B model tends to cause larger permanent offsets, it is likely that at the end of 11 seconds of white noise excitation in Example 3, the residual offset for the W-B model is larger than for the DEL model. The additional 9 seconds of strong shaking is likely to bias the displacement in the direction of the residual offset, thus causing larger displacements in the case of the W-B model.

It may be concluded that increasing the duration of strong shaking (i.e., increasing the likely number of severe excitation pulses) may have the effect of increasing the displacement of the Wen-Bouc model more than the corresponding Distributed Element model.

### 5.8 Conclusion:

Several examples have been considered in this chapter in which the relative dynamic performance of two curvilinear hysteretic models has been evaluated. Depending on the type of loading (zero mean, static loading, gravity, earthquake-like excitations, etc.), the type of system (nature of post-yielding stiffness, number of degrees of freedom, etc.), the adequacy of the endochronic model to depict real hysteretic systems varies. For earthquake-

like excitations, the agreement between the W-B and DEL models is favorable in such response quantities as base shear, maximum velocity, energy dissipated and dynamic amplitude, but not as reliable in displacement quantities such as ductility, final offset, etc. The agreement is usually enhanced as the post-yielding stiffness becomes larger. Indeed, given the differences in the behavior of the two models quasi-statically, the degree of agreement in some of the dynamic response quantities is quite surprising.

In the final analysis, the decision as to which hysteretic model to employ rests with the individual user. The relative simplicity of the mathematical description of the W-B model has to be weighed against the deviation in the values of predicted response quantities from true behavior. Given the large memory capacities and high speeds of today's computers, the more physical DEL model in its Extended Massing's formulation could be used, at least for moderate-sized systems. In the modeling of hysteretic systems with large numbers of degrees of freedom, it may be tempting to use the endochronic models, owing to their simplicity. But there are at least two reasons why this may not be advisable. Firstly, it has been shown that increasing the number of degrees of freedom may introduce additional sources of nonphysical behavior. Secondly, it may be recalled that the W-B model may predict spurious instabilities. In a multi-degree-of-freedom system, the use of such models may cause a local instability in a member, leading to false prediction of the eventual collapse of the entire system.

| Response Quantity | The Wen-Bouc model | The Distributed Element model | Relative Error |
|---|---|---|---|
| $u_m$, Maximum displacement in m | 0.0865 | 0.0880 | -1.72% |
| $\mu$, Ductility | 3.93 | 3.995 | -1.72% |
| $(u_{max} - u_{min})$, Dynamic displacement in m | 0.1219 | 0.1218 | 0.08% |
| $t_{max}$, Time of maximum displacement in seconds | 3.12 | 5.54 | -43.68% |
| $\dot{u}_m$, Maximum velocity in m/sec | 0.359 | 0.362 | -0.83% |
| $C_b$, Base shear coeffecient | 0.0977 | 0.0966 | 1.13% |
| $u_{off}$, Final offset in m | 0.0342 | 0.0253 | 35.52% |
| $E(T)$, Hysteretic energy dissipated (normalized) in $m^2$ | 0.8403 E-02 | 0.7007 E-02 | 19.92% |

Table 5.1:    Comparison of eight characteristic quantities in the response of the Wen-Bouc and the Distributed Element models to the 1940 El Centro earthquake.

| | Post-yielding stiffness ratio $\alpha$ | Value of constant external force in % g $\bar{F}$ | Value of parameter in m⁻¹ $\beta$ | Comment |
|---|---|---|---|---|
| Case I | 0.0 | 0.0 | 7.67 | No post-yielding stiffness; zero mean loading; $\beta$ is such that mean ductility in the response of the DEL model is about 2.0 |
| Case II | 0.0 | 0.0 | 12.00 | No post-yielding stiffness; zero mean loading; $\beta$ is such that mean ductility in the response of the DEL model is about 4.0 |
| Case III | 0.0 | 0.0 | 17.53 | No post-yielding stiffness; zero mean loading; $\beta$ is such that mean ductility in the response of the DEL model is about 8.0 |
| Case IV | 0.05 | 0.0 | 12.00 | Effect of positive post-yielding stiffness on system in Case II |
| Case V | 0.0 | 2.0 | 12.00 | Effect of nonzero mean loading on system in Case II |
| Case VI | 0.05 | 2.0 | 12.00 | Combined effect of nonzero mean loading and postive post -yielding stiffness ratio on Case II |

Table 5.2: System parameters for the cases for which comparison is made of the response statistics of the two models when subjected to white noise excitation. In all cases, the following are kept constant: nominal natural frequency=1Hz, viscous damping as a fraction of critical=5%, $A$=1.0 and the ratio$\beta/\gamma$=-1.5

| Response quantity | The Wen-Bouc model | | | The Distributed Element model | | | Relative error (%) | | |
|---|---|---|---|---|---|---|---|---|---|
| | Mean | Standard deviation | Median | Mean | Standard deviation | Median | Mean | Standard deviation | Median |
| $u_m$ in cm | 18.65 | 5.92 | 17.57 | 16.03 | 3.54 | 15.53 | 17.47% | 30.96% | 13.54% |
| $\mu$ | 2.38 | 0.76 | 2.24 | 2.05 | 0.45 | 1.98 | 17.47% | 30.96% | 13.54% |
| $(u_{max} - u_{min})$ in cm | 27.04 | 6.27 | 25.87 | 27.72 | 4.97 | 27.26 | -1.81% | 17.70% | -4.65% |
| $t_{max}$ in secs | 13.52 | 5.59 | 14.59 | 10.81 | 5.84 | 10.96 | 93.06% | 244.96% | 191.78% |
| $\dot{u}_m$ in cm/sec | 64.49 | 7.45 | 63.88 | 69.76 | 8.80 | 69.08 | -7.09% | 7.77% | -6.69% |
| $C_b$ | 0.281 | 0.021 | 0.281 | 0.283 | 0.022 | 0.283 | -0.49% | 4.07% | -0.81% |
| $u_{off}$ in cm | 0.62 | 10.63 | 0.98 | 0.38 | 2.84 | 0.15 | - | - | - |
| $E(T)$ in cm$^2$ | 340.85 | 91.17 | 334.16 | 315.07 | 90.16 | 305.71 | 9.59% | 12.70% | 10.49% |

Table 5.3: Statistics of eight response quantities for the two hysteretic models subjected to white noise base excitation for Case I listed in Table 5.2

| Response quantity | The Wen-Bouc model | | | The Distributed Element model | | | Relative error (%) | | |
|---|---|---|---|---|---|---|---|---|---|
| | Mean | Standard deviation | Median | Mean | Standard deviation | Median | Mean | Standard deviation | Median |
| $u_m$ in cm | 24.56 | 9.39 | 23.48 | 19.60 | 5.57 | 18.57 | 27.06% | 37.83% | 24.65% |
| $\mu$ | 4.93 | 1.89 | 4.72 | 3.94 | 1.12 | 3.73 | 27.06% | 37.83% | 24.65% |
| $(u_{max} - u_{min})$ in cm | 33.10 | 9.37 | 31.67 | 31.03 | 6.61 | 30.49 | 7.26% | 22.42% | 3.31% |
| $t_{max}$ in secs | 13.99 | 5.40 | 14.91 | 11.78 | 5.81 | 12.50 | 75.68% | 221.59% | 4.89% |
| $\dot{u}_m$ in cm/sec | 59.91 | 7.23 | 59.42 | 65.08 | 8.26 | 64.78 | -7.59% | 7.18% | -8.17% |
| $C_b$ | 0.214 | 0.012 | 0.214 | 0.216 | 0.012 | 0.216 | -0.74% | 3.23% | -0.74% |
| $u_{off}$ in cm | 1.03 | 17.06 | 1.40 | 1.12 | 7.44 | 0.37 | - | - | - |
| $E(T)$ in cm$^2$ | 369.51 | 85.00 | 362.94 | 346.83 | 87.36 | 341.55 | 7.62% | 10.40% | 7.96% |

Table 5.4: Statistics of eight response quantities for the two hysteretic models subjected to white noise base excitation for Case II listed in Table 5.2

| Response quantity | The Wen-Bouc model | | | The Distributed Element model | | | Relative error (%) | | |
|---|---|---|---|---|---|---|---|---|---|
| | Mean | Standard deviation | Median | Mean | Standard deviation | Median | Mean | Standard deviation | Median |
| $u_m$ in cm | 34.03 | 14.65 | 31.05 | 28.04 | 11.16 | 25.56 | 23.99% | 36.06% | 21.66% |
| $\mu$ | 9.94 | 4.28 | 9.07 | 8.19 | 3.26 | 7.47 | 23.99% | 36.06& | 21.66% |
| $(u_{max} - u_{min})$ in cm | 43.61 | 13.99 | 40.79 | 39.52 | 11.29 | 37.36 | 11.80% | 23.39% | 8.65% |
| $t_{max}$ in secs | 14.47 | 5.28 | 15.82 | 13.18 | 5.55 | 13.94 | 44.78% | 161.47% | -4.29% |
| $\dot{u}_m$ in cm/sec | 58.29 | 7.71 | 57.65 | 62.89 | 8.28 | 62.18 | -7.05% | 6.89% | -7.51% |
| $C_b$ | 0.167 | 0.009 | 0.167 | 0.168 | 0.009 | 0.168 | -0.55% | 2.71% | -0.69% |
| $u_{off}$ in cm | -1.24 | 27.04 | -0.49 | -0.64 | 18.20 | -0.05 | - | - | - |
| $E(T)$ in cm$^2$ | 382.24 | 78.94 | 378.99 | 359.93 | 80.67 | 358.09 | 6.91% | 7.77% | 5.93% |

Table 5.5: Statistics of eight response quantities for the two hysteretic models subjected to white noise base excitation for Case III listed in Table 5.2

| Response quantity | The Wen-Bouc model | | | The Distributed Element model | | | Relative error (%) | | |
|---|---|---|---|---|---|---|---|---|---|
| | Mean | Standard deviation | Median | Mean | Standard deviation | Median | Mean | Standard deviation | Median |
| $u_m$ in cm | 17.97 | 4.46 | 17.70 | 18.07 | 4.44 | 17.41 | 1.00% | 18.78% | 0.05% |
| $\mu$ | 3.61 | 0.90 | 3.55 | 3.63 | 0.89 | 3.50 | 1.00% | 18.78% | 0.05% |
| $(u_{max} - u_{min})$ in cm | 28.54 | 6.08 | 28.13 | 30.14 | 5.96 | 29.53 | -4.68% | 12.79% | -5.17% |
| $t_{max}$ in secs | 11.56 | 5.53 | 11.57 | 11.39 | 5.69 | 11.78 | 31.86% | 139.93% | -9.58% |
| $\dot{u}_m$ in cm/sec | 60.96 | 7.37 | 60.43 | 66.53 | 8.55 | 66.13 | -8.02% | 6.83% | -8.57% |
| $C_b$ | 0.229 | 0.017 | 0.229 | 0.235 | 0.017 | 0.235 | -2.22% | 3.70% | -2.50% |
| $u_{off}$ in cm | 0.34 | 5.40 | 0.27 | 0.63 | 4.11 | 0.32 | - | - | - |
| $E(T)$ in cm$^2$ | 383.64 | 90.35 | 375.41 | 358.04 | 92.12 | 348.38 | 8.57% | 10.40% | 8.78% |

Table 5.6: Statistics of eight response quantities for the two hysteretic models subjected to white noise base excitation for Case IV listed in Table 5.2

| Response quantity | The Wen-Bouc model | | | The Distributed Element model | | | Relative error (%) | | |
|---|---|---|---|---|---|---|---|---|---|
| | Mean | Standard deviation | Median | Mean | Standard deviation | Median | Mean | Standard deviation | Median |
| $u_m$ in cm | 37.80 | 15.58 | 36.03 | 22.02 | 7.14 | 20.91 | 74.20% | 54.01% | 71.84% |
| $\mu$ | 7.59 | 3.13 | 7.24 | 4.42 | 1.43 | 4.20 | 74.20% | 54.01% | 71.84% |
| $(u_{max} - u_{min})$ in cm | 43.76 | 14.32 | 41.02 | 31.88 | 7.23 | 30.95 | 38.83% | 37.74% | 36.56% |
| $t_{max}$ in secs | 17.05 | 4.45 | 18.95 | 13.00 | 5.59 | 13.79 | 90.06% | 235.21% | 217.71% |
| $\dot{u}_m$ in cm/sec | 60.12 | 7.31 | 59.80 | 64.99 | 8.08 | 65.00 | -7.16% | 7.41% | -7.57% |
| $C_b$ | 0.215 | 0.012 | 0.216 | 0.218 | 0.012 | 0.219 | -1.32% | 2.97% | -1.33% |
| $u_{off}$ in cm | -29.32 | 17.58 | -28.61 | -7.39 | 8.44 | -6.62 | - | - | - |
| $E(T)$ in cm$^2$ | 383.52 | 88.59 | 379.85 | 351.21 | 88.74 | 341.29 | 10.31% | 10.79% | 10.41% |

Table 5.7: Statistics of eight response quantities for the two hysteretic models subjected to white noise base excitation for Case V listed in Table 5.2

| Response quantity | The Wen-Bouc model | | | The Distributed Element model | | | Relative error (%) | | |
|---|---|---|---|---|---|---|---|---|---|
| | Mean | Standard deviation | Median | Mean | Standard deviation | Median | Mean | Standard deviation | Median |
| $u_m$ in cm | 22.03 | 5.57 | 21.34 | 19.24 | 4.78 | 18.80 | 16.74% | 23.64% | 16.87% |
| $\mu$ | 4.42 | 1.12 | 4.29 | 3.86 | 0.96 | 3.78 | 16.74% | 23.64% | 16.87% |
| $(u_{max} - u_{min})$ in cm | 29.88 | 5.91 | 28.95 | 30.17 | 5.91 | 29.54 | 0.14% | 14.87% | -0.65% |
| $t_{max}$ in secs | 12.57 | 5.47 | 13.12 | 11.63 | 5.87 | 11.76 | 48.66% | 182.06% | -0.31% |
| $\dot{u}_m$ in cm/sec | 61.03 | 7.32 | 60.77 | 66.52 | 8.42 | 66.24 | -7.92% | 6.88% | -8.46% |
| $C_b$ | 0.236 | 0.018 | 0.235 | 0.238 | 0.018 | 0.240 | -1.03% | 3.59% | -1.09% |
| $u_{off}$ in cm | -7.34 | 5.38 | -7.36 | -3.41 | 4.18 | -3.45 | - | - | - |
| $E(T)$ in cm$^2$ | 387.14 | 90.58 | 380.36 | 359.48 | 93.31 | 352.95 | 8.82% | 10.38% | 8.87% |

Table 5.8: Statistics of eight response quantities for the two hysteretic models subjected to white noise base excitation for Case VI listed in Table 5.2

Figure 5.1:    Schematic representation of a restoring force system.
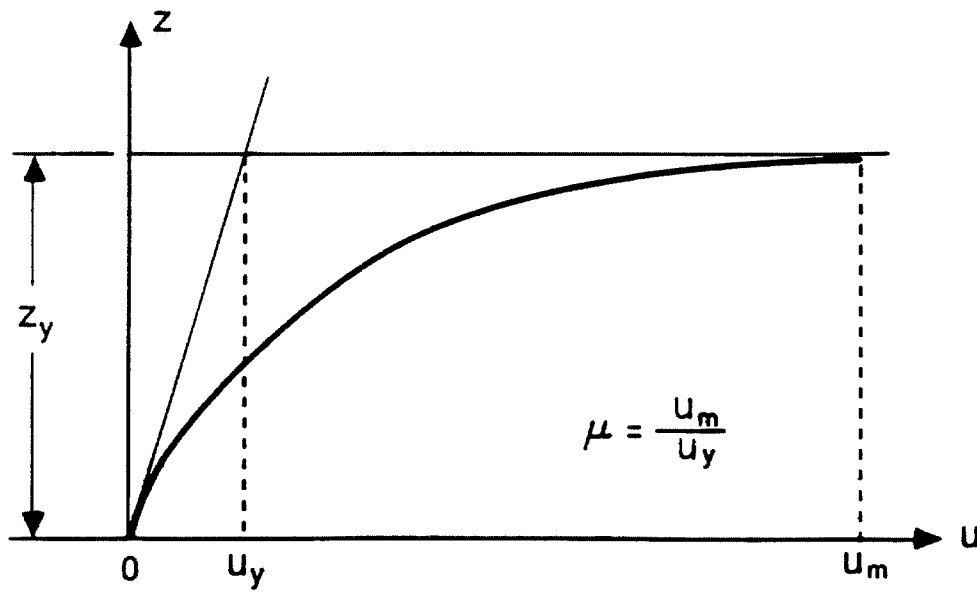


Figure 5.2:    Initial loading curve for the hysteretic models.
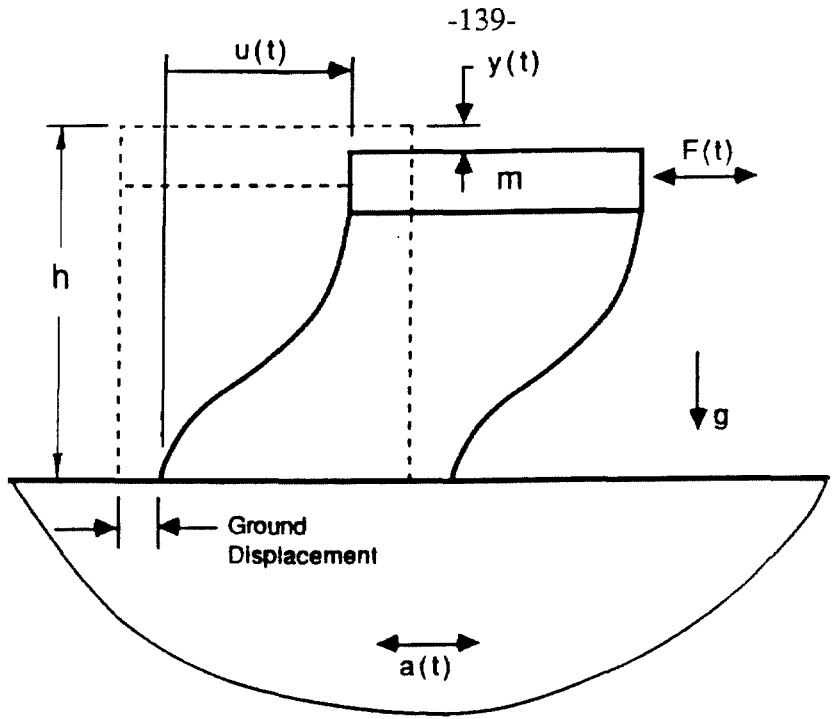
Figure 5.3:    Model for a single-degree-of-freedom structure in a gravitational field subjected to an earthquake ground motion and a horizontal external force.
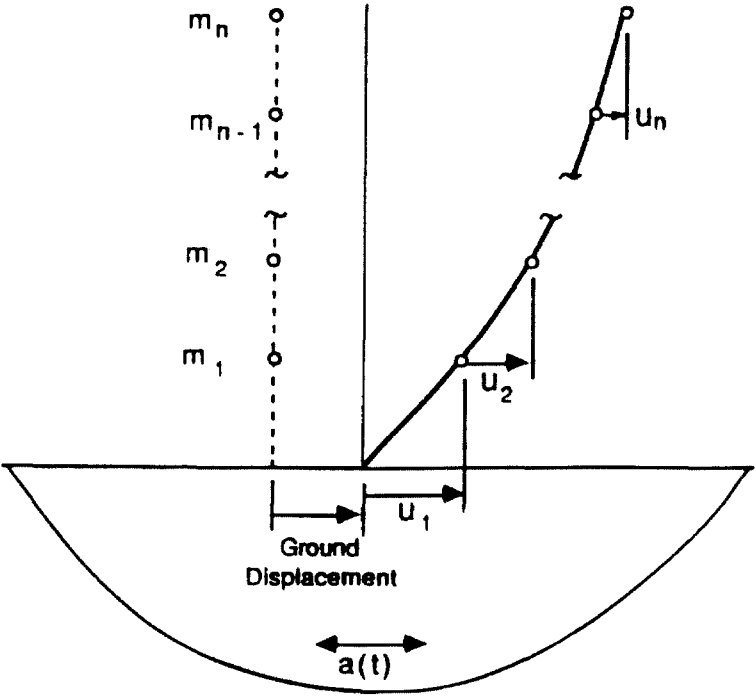


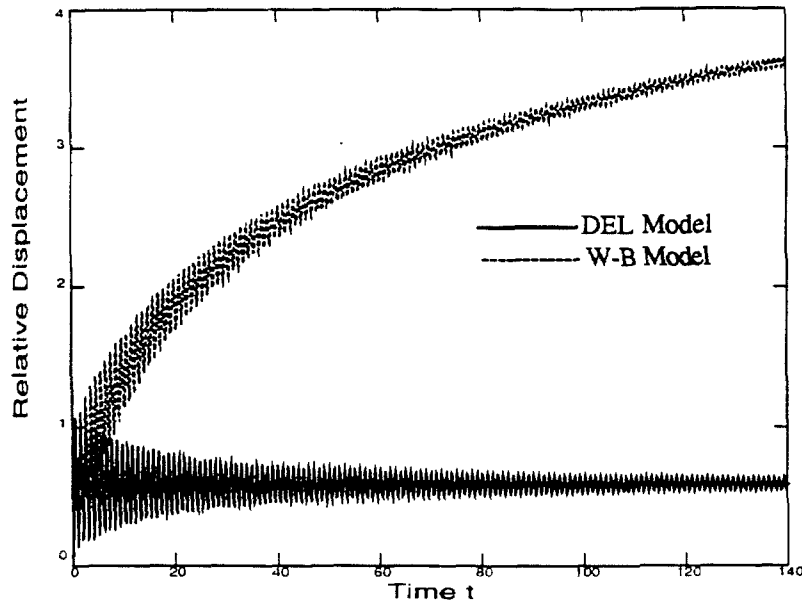Figure 5.4:    Model for a multi-degree-of-freedom structure subjected to earthquake ground motion.

Figure 5.5: The displacement response of the two hysteretic models when subjected to a sudden external load. The post-yielding stiffness ratio is 0.05 and gravitational effects are neglected.
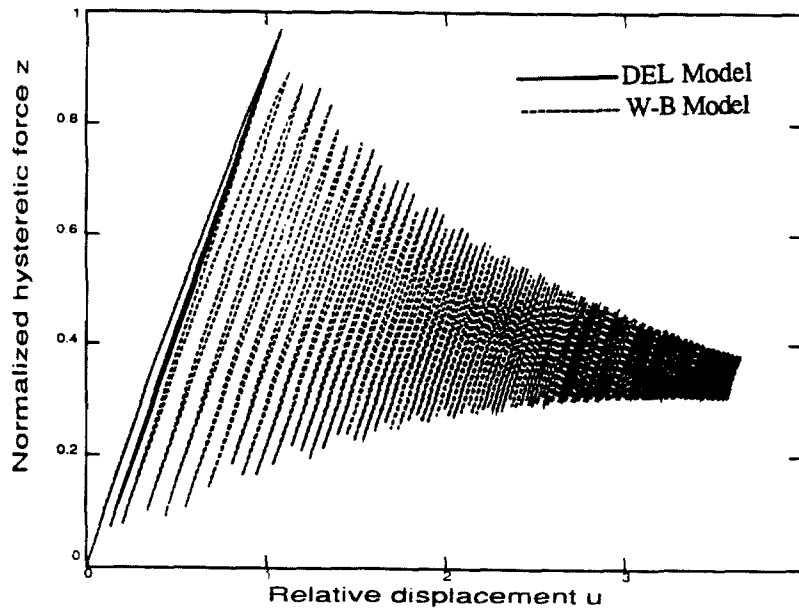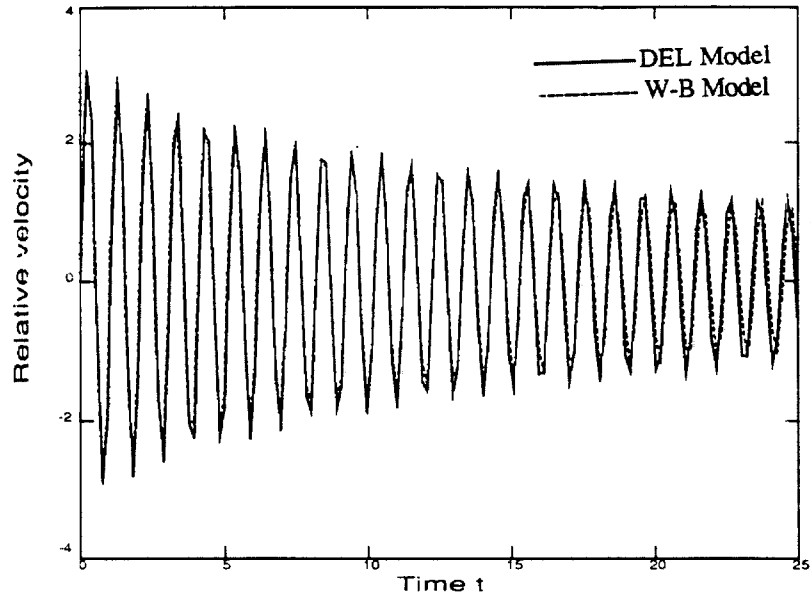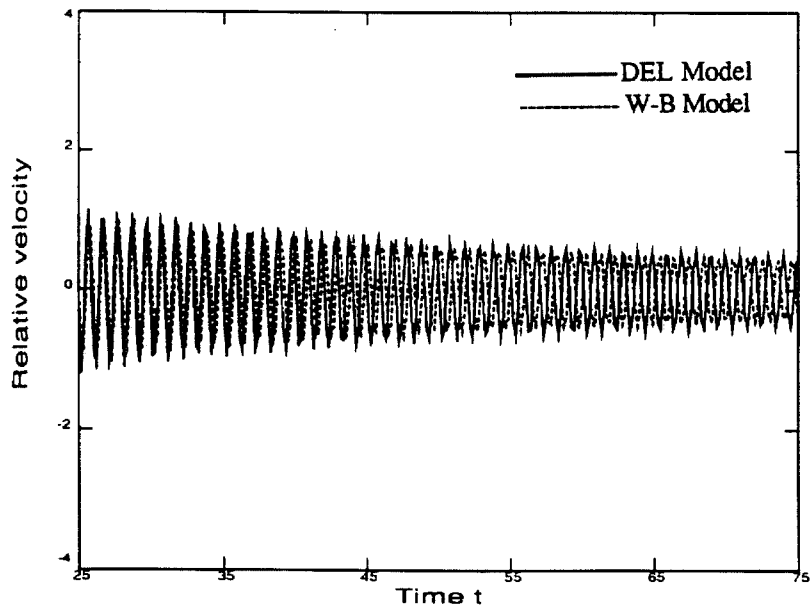


Figure 5.6: The hysteretic restoring force-displacement diagrams for the two hysteretic models when subjected to a sudden external load. The post-yielding stiffness ratio is 0.05 and gravitational effects are neglected.

(a)



(b)

Figure 5.7:   The velocity response of the two hysteretic models when subjected to a sudden external load for (a) the first 25 seconds after first application of the load (b) the next 50 seconds. The post-yielding stiffness ratio is 0.05 and gravitational effects are neglected.
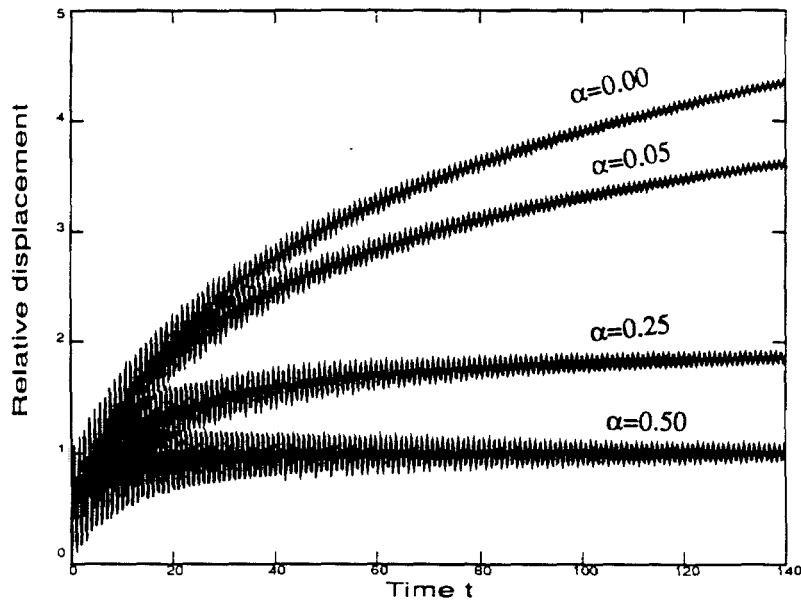
Figure 5.8:    The displacement response of the W-B model when subjected to a sudden external load for different values of α, the post-yielding stiffness ratio.



Figure 5.9:    The displacement response of the two hysteretic models when subjected to a sudden external load. The post-yielding stiffness ratio is 0.05 and gravitational effects are included ($\eta$=0.071).

Figure 5.10:   The hysteretic restoring force-displacement diagrams for the two hysteretic models when subjected to a sudden external load. The post-yielding stiffness ratio is 0.05 and gravitational effects are included ($\eta$=0.071).
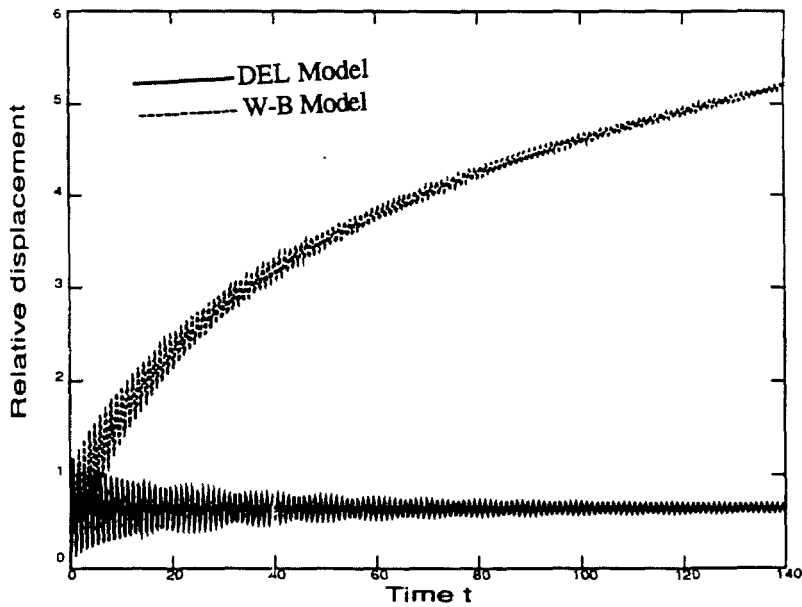


Figure 5.11:   The displacement response of the two hysteretic models when subjected to a sudden external load. The post-yielding stiffness ratio is 0.05 and gravitational effects are included ($\eta$=0.250).
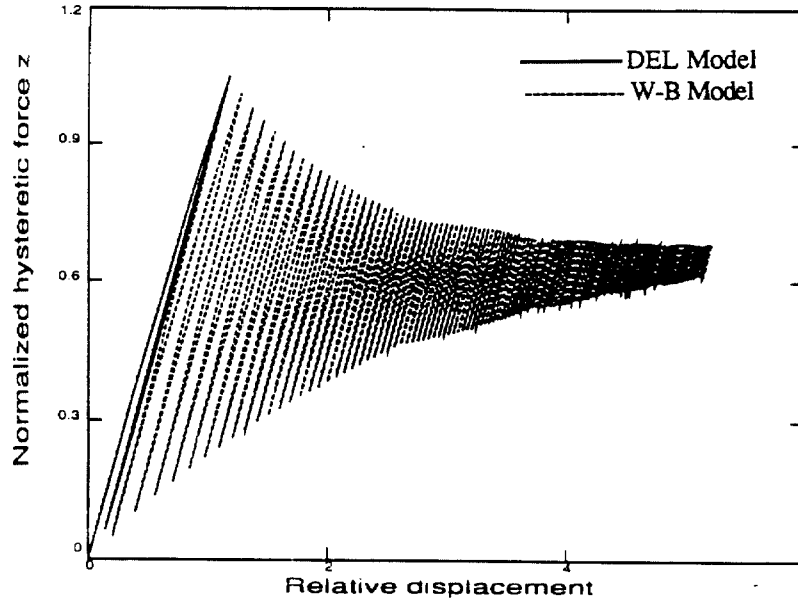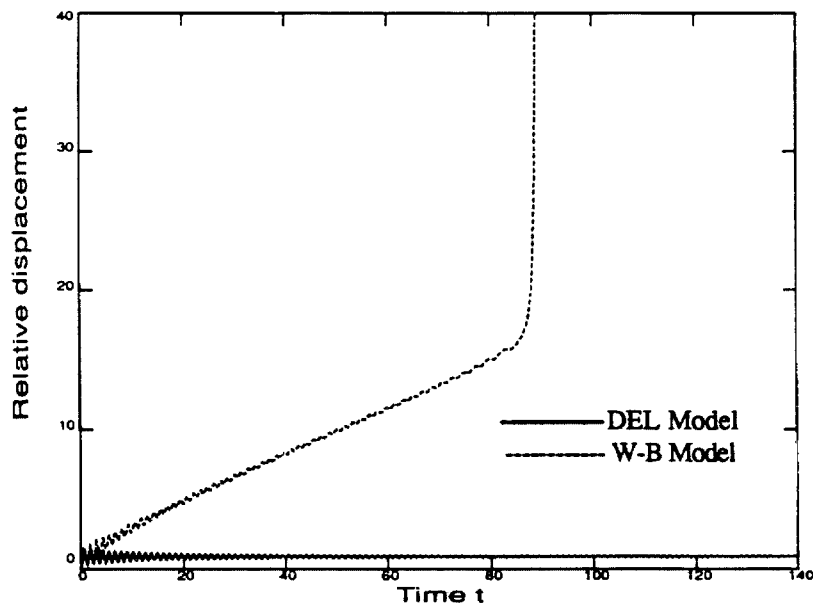
Figure 5.12: The hysteretic restoring force-displacement diagrams for the two hysteretic models when subjected to a sudden external load. The post-yielding stiffness ratio is 0.05 and gravitational effects are included ($\eta=0.250$).


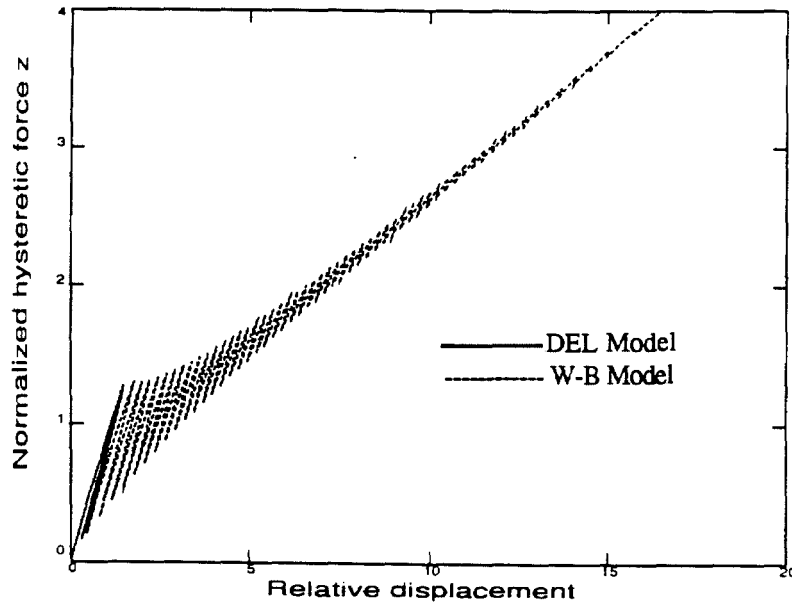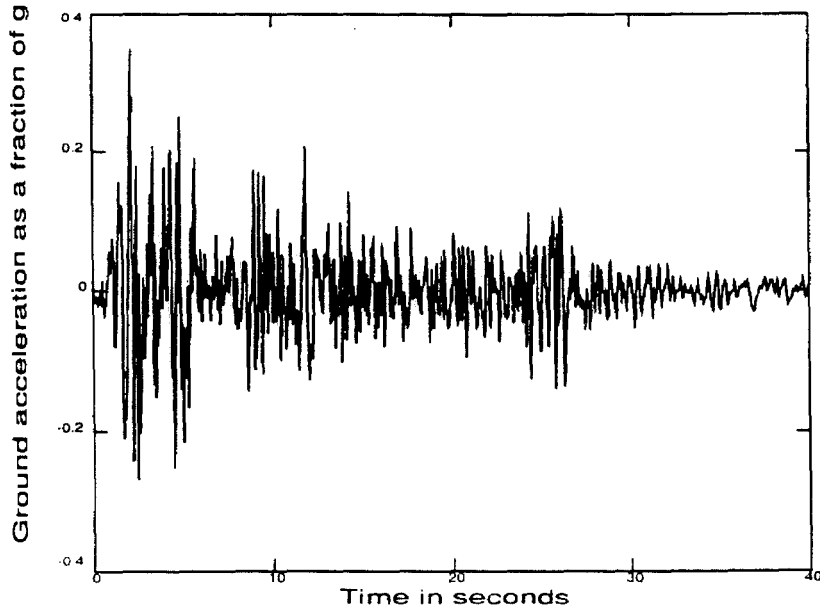
Figure 5.13: The N-S component of the 1940 El Centro earthquake .
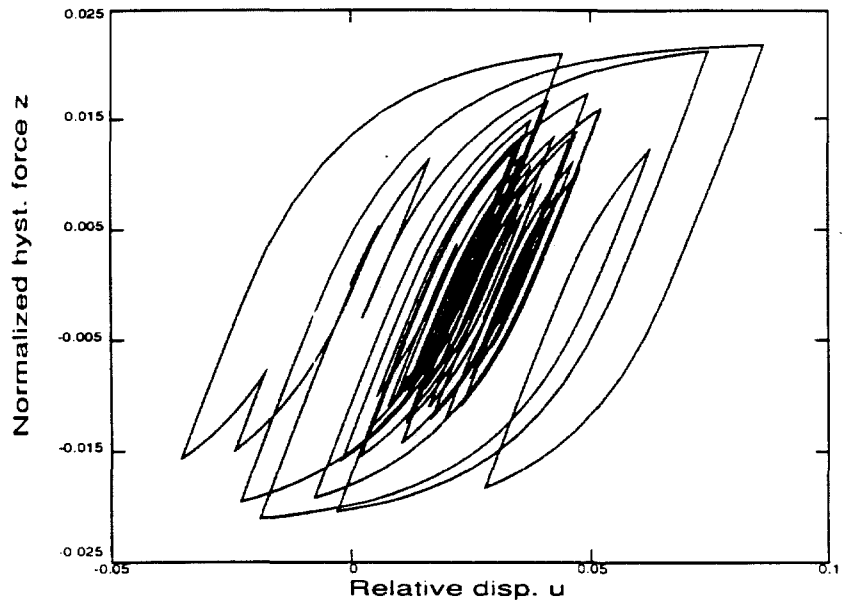
(a)
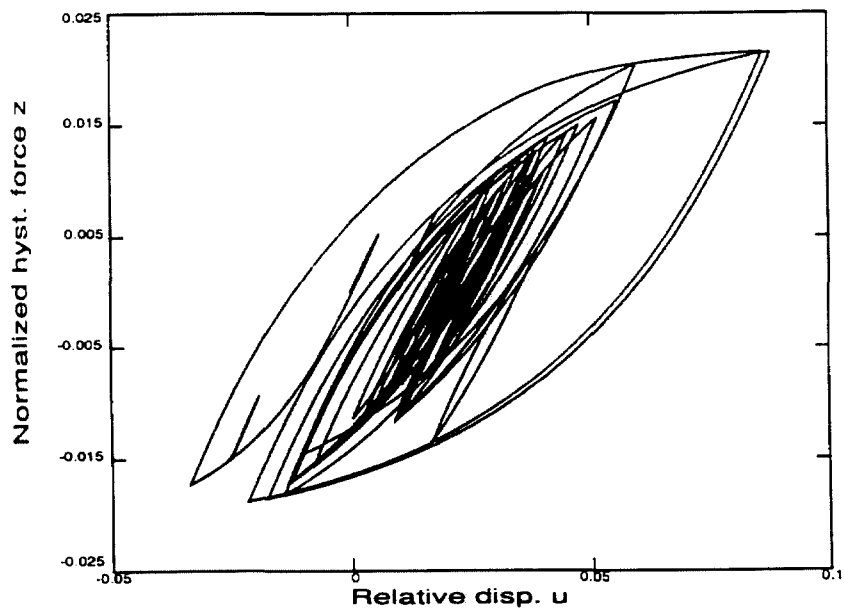


(b)

Figure 5.14:    The hysteretic restoring force-displacement behavior of the (a) W-B model
(b) DEL model when subjected to the El Centro earthquake.
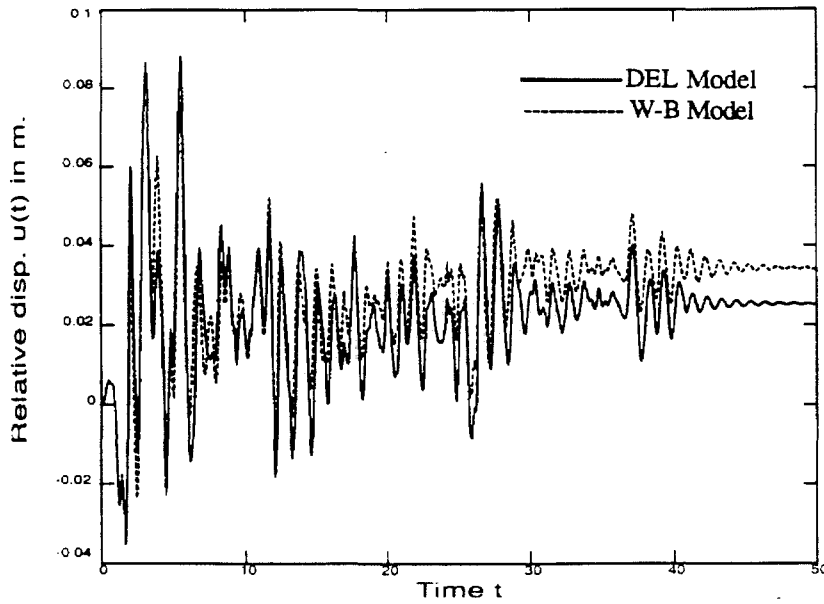
Figure 5.15:   The displacement response of the two hysteretic models when subjected to the El Centro earthquake.
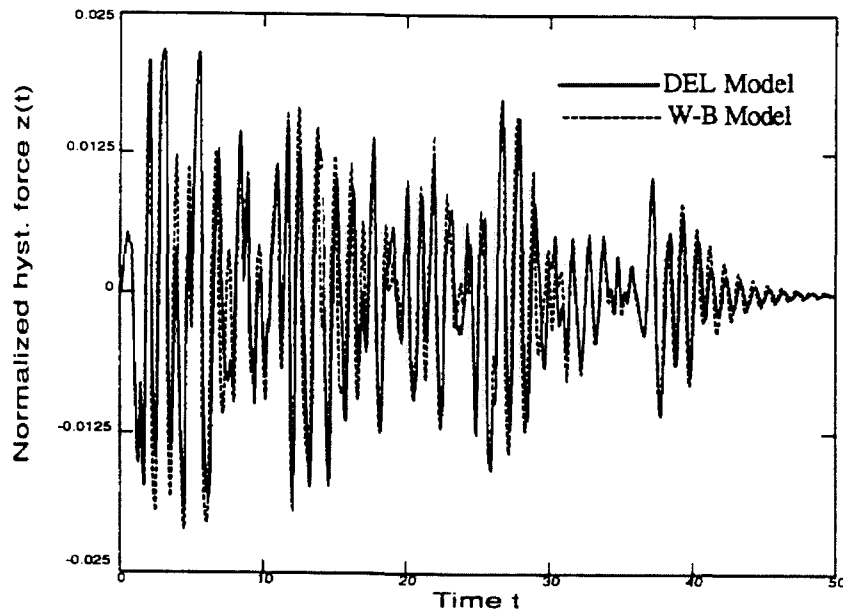


Figure 5.16:   The hysteretic restoring force response time history of the two models when subjected to the El Centro earthquake.
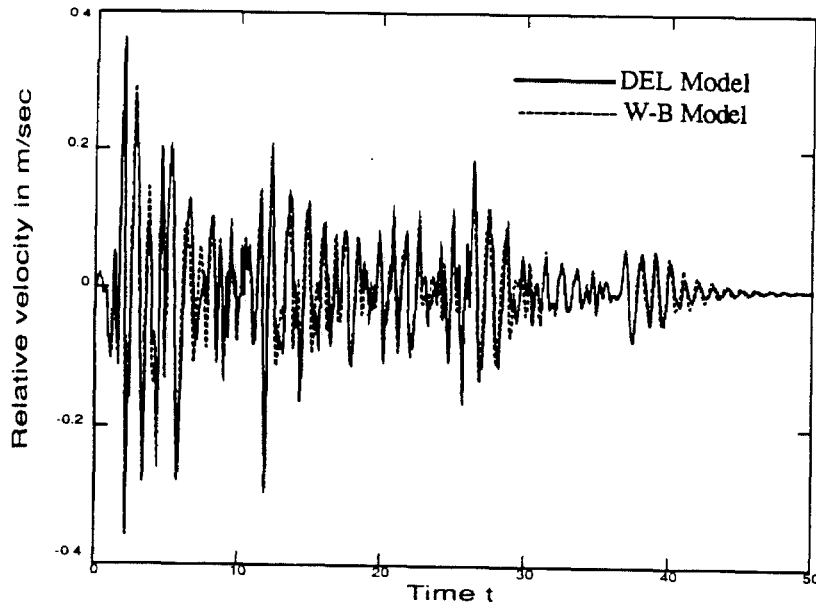
Figure 5.17:   The velocity response of the two models when subjected to the El Centro earthquake.



Figure 5.18:   The maximum relative displacement, $u_m$, of the two models when subjected to the El Centro earthquake, for a range of yield levels.
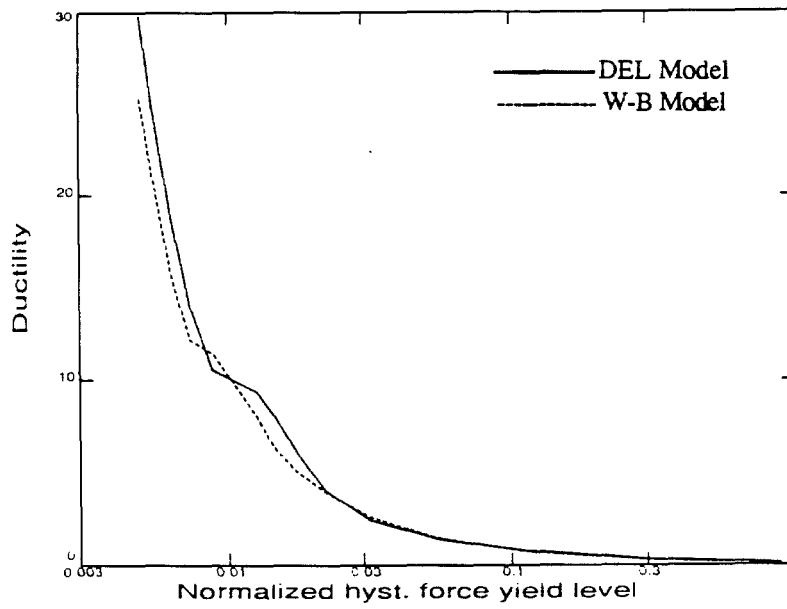
Figure 5.19:  The ductility factor, $\mu$, of the two models when subjected to the El
Centro earthquake, for a range of yield levels.
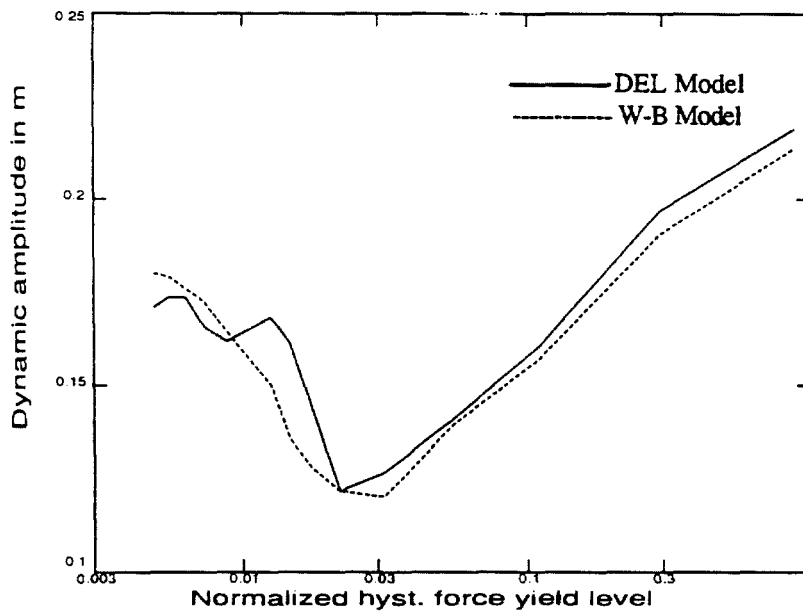


Figure 5.20:  The dynamic amplitude, $(u_{max} - u_{min})$, of the two models when subjected
to the El Centro earthquake, for a range of yield levels.

Figure 5.21:   The maximum relative velocity, $\dot{u}_m$, of the two models when subjected to the El Centro earthquake, for a range of yield levels.
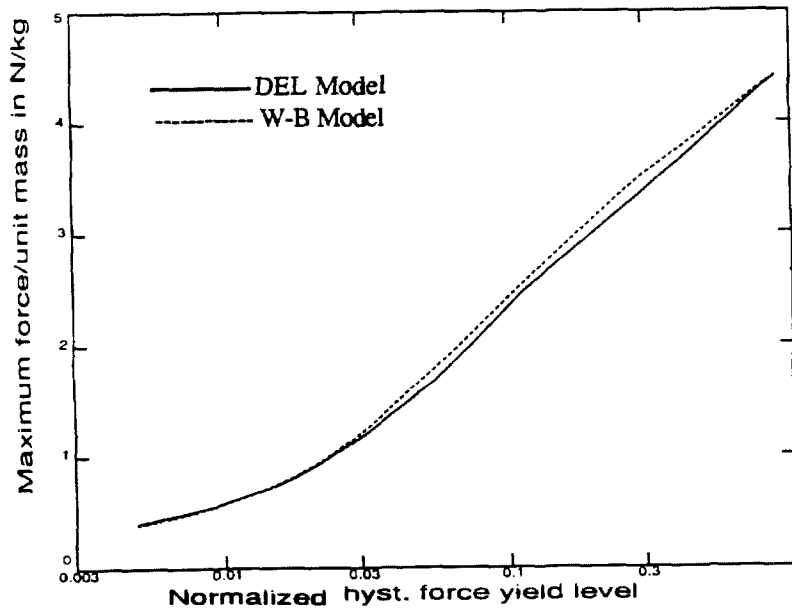


Figure 5.22:   The base shear coefficient, $C_b$, of the two models when subjected to the El Centro earthquake, for a range of yield levels.
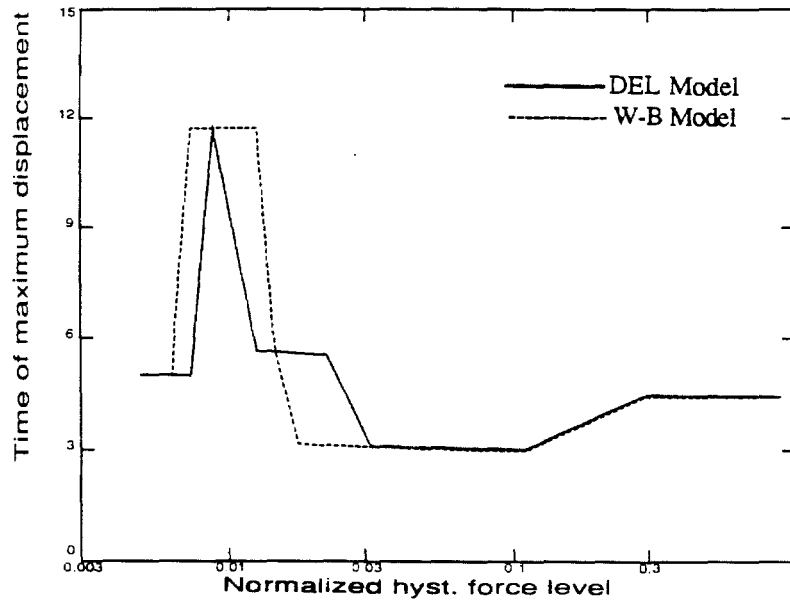
Figure 5.23: The instant in time at which $u_m$ occurs, $t_{max}$, of the two models when subjected to the El Centro earthquake, for a range of yield levels.
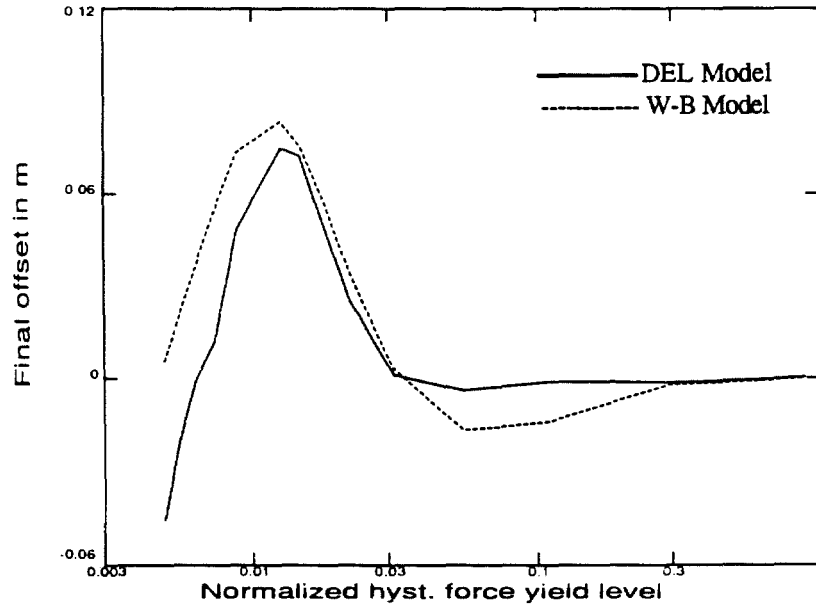


Figure 5.24: The final offset, $u_{off}$, of the two models when subjected to the El Centro earthquake, for a range of yield levels.

Figure 5.25: The hysteretic energy dissipated, $E(T)$, by the two models when subjected to the El Centro earthquake, for a range of yield levels.
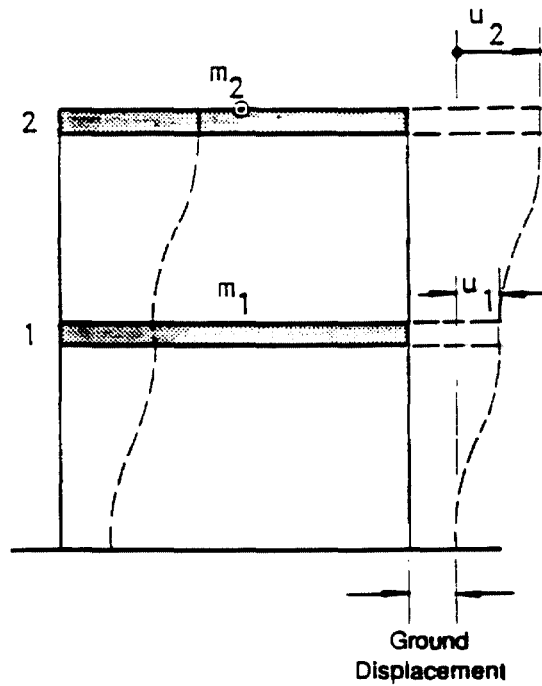


Figure 5.26: A two-story building structure subjected to earthquake ground motion.
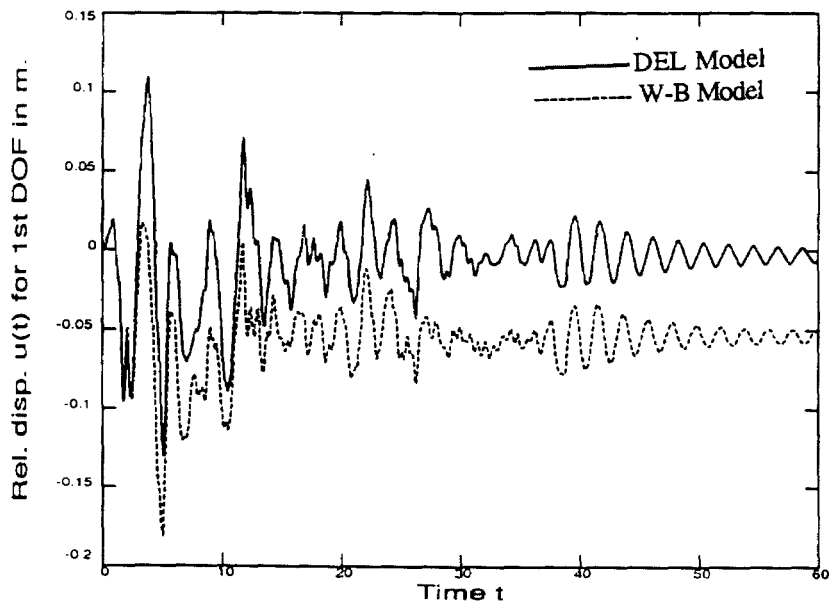
Figure 5.27:   The displacement response of the first story of a two-story structure for the two models when subjected to the El Centro earthquake.
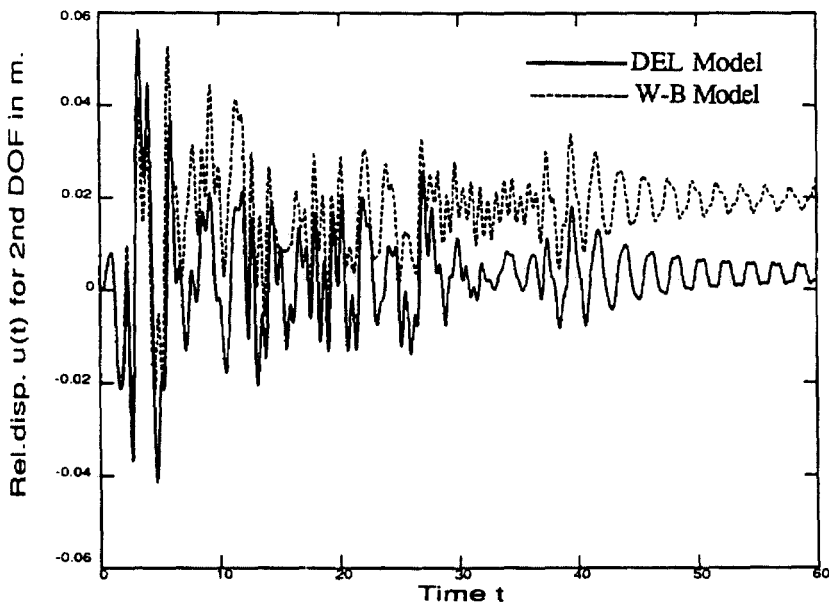


Figure 5.28:   The displacement response of the second story of a two-story structure for the two models when subjected to the El Centro earthquake.
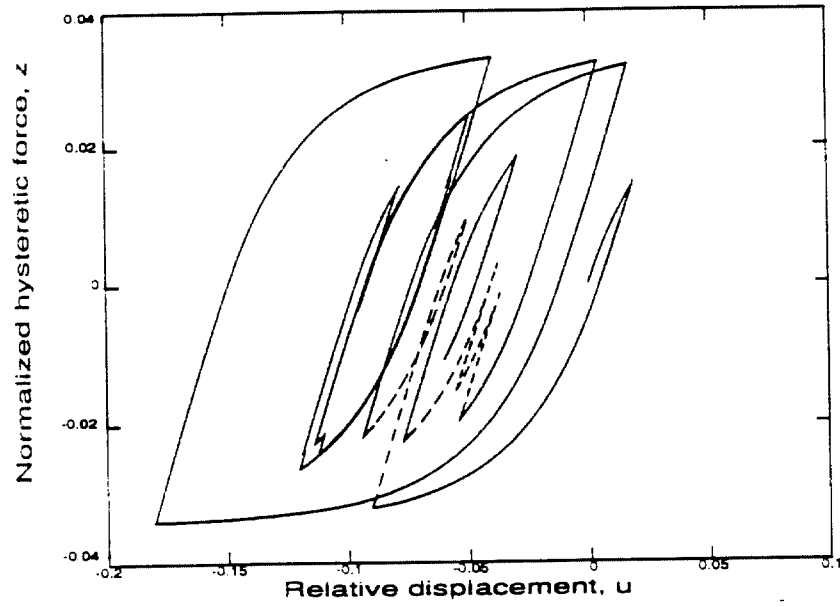
(a)
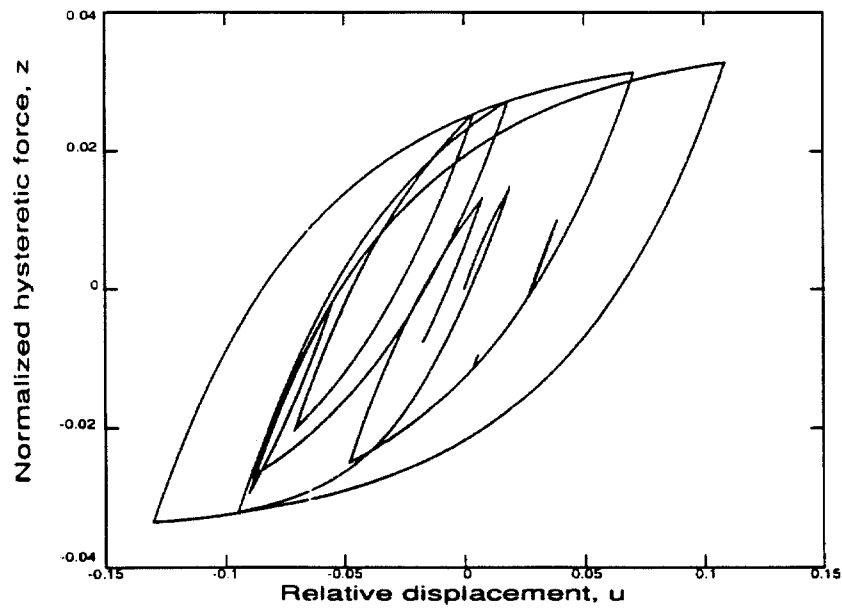


(b)

Figure 5.29:   The hysteretic restoring force-displacement behavior of the first story of a
two-story structure for (a) the W-B model (b) the DEL model when
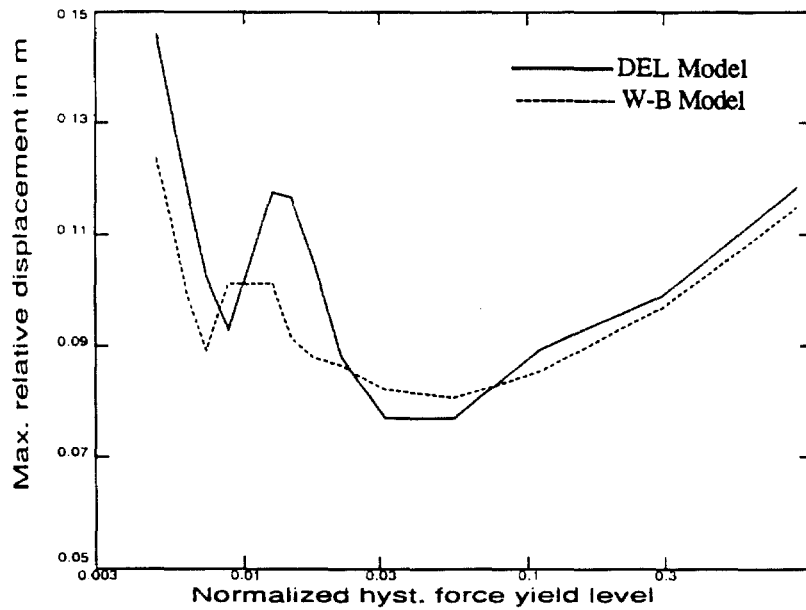subjected to the El Centro earthquake.
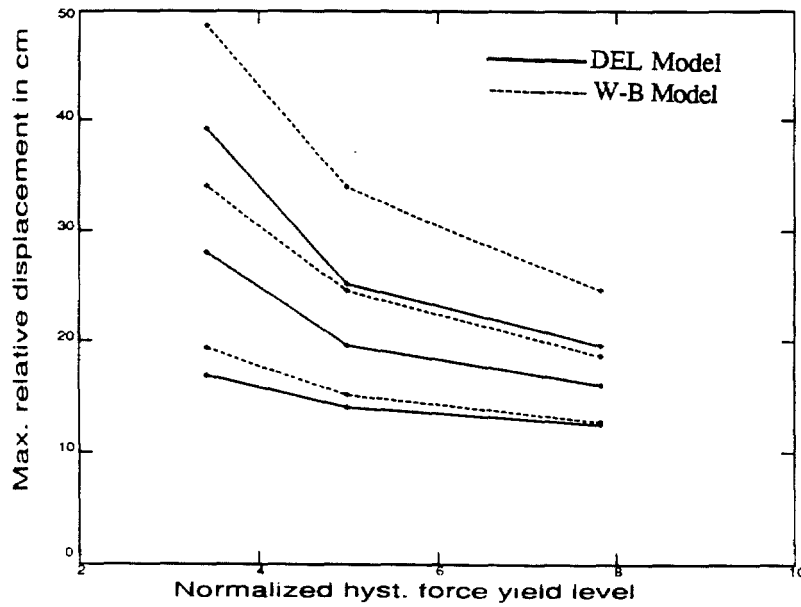
Figure 5.30: The maximum relative displacement, $u_m$, of the two models when subjected to white noise base excitation, for a range of yield levels. The three curves shown for each model correspond to values of the mean minus one standard deviation, the mean, and the mean plus one standard deviation.
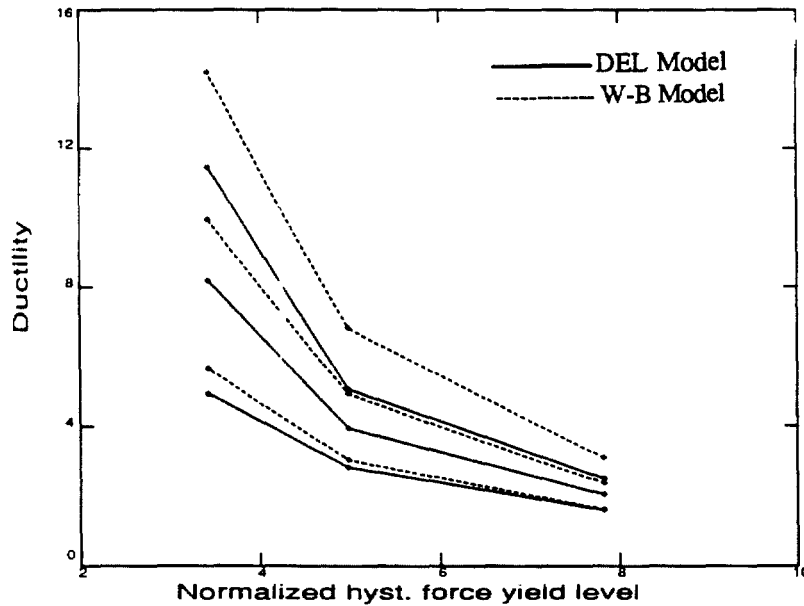


Figure 5.31: The ductility factor, $\mu$, of the two models when subjected to white noise base excitation, for a range of yield levels. The three curves shown for each model correspond to the values of the mean minus one standard deviation, the mean, and the mean plus one standard deviation.
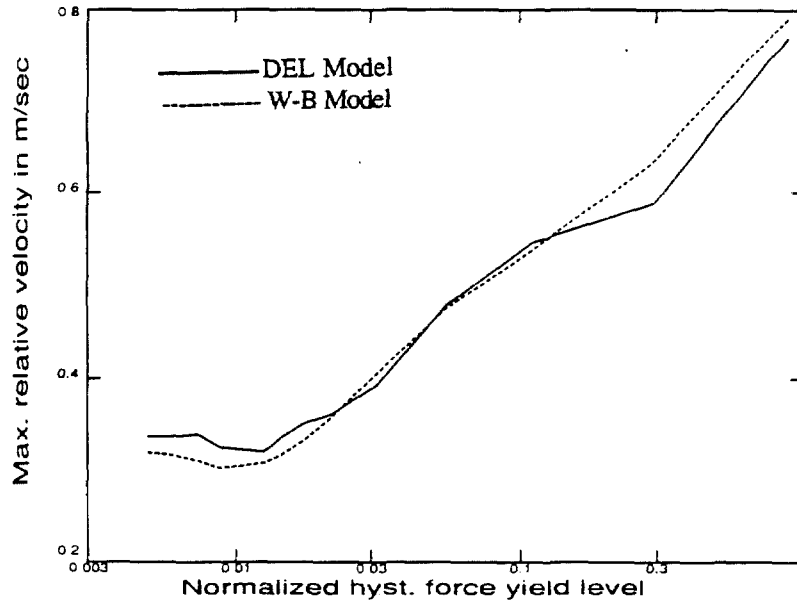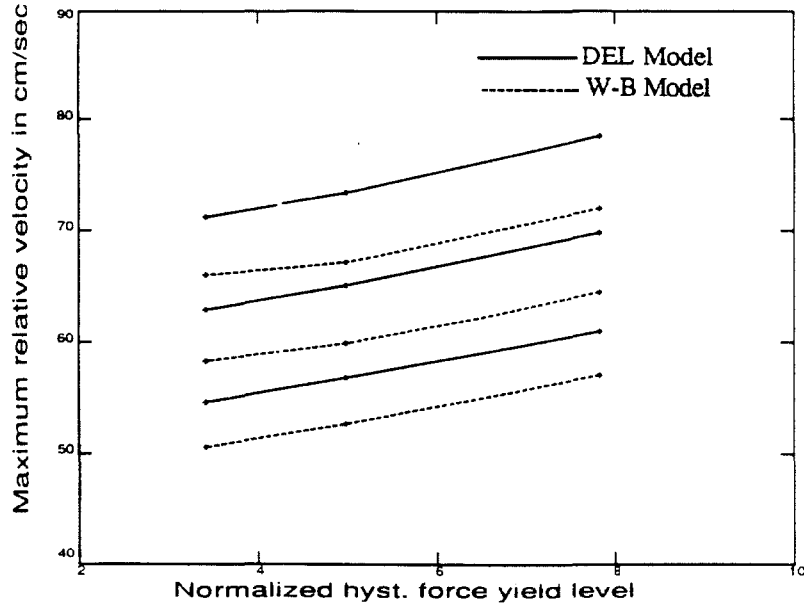
Figure 5.32:   The maximum relative velocity, $\dot{u}_m$, of the two models when subjected to white noise base excitation, for a range of yield levels. The three curves shown for each model correspond to the values of the mean minus one standard deviation, the mean, and the mean plus one standard deviation.
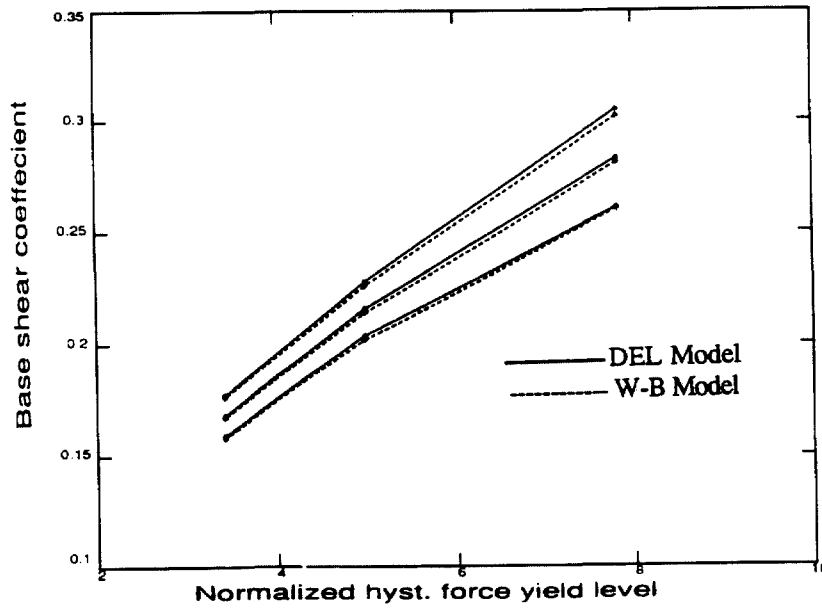


Figure 5.33:   The base shear coefficient, $C_b$, of the two models when subjected to white noise base excitation, for a range of yield levels. The three curves shown for each model correspond to the values of the mean minus one standard deviation, the mean, and the mean plus one standard deviation.
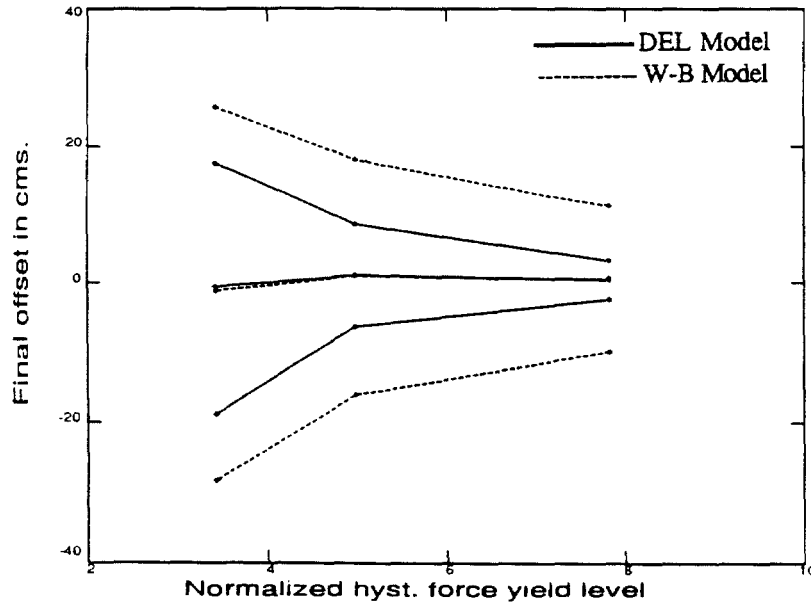
Figure 5.34:   The final offset, $u_{off}$, of the two models when subjected to white noise base excitation, for a range of yield levels. The three curves shown for each model correspond to the values of the mean minus one standard deviation, the mean, and the mean plus one standard deviation.
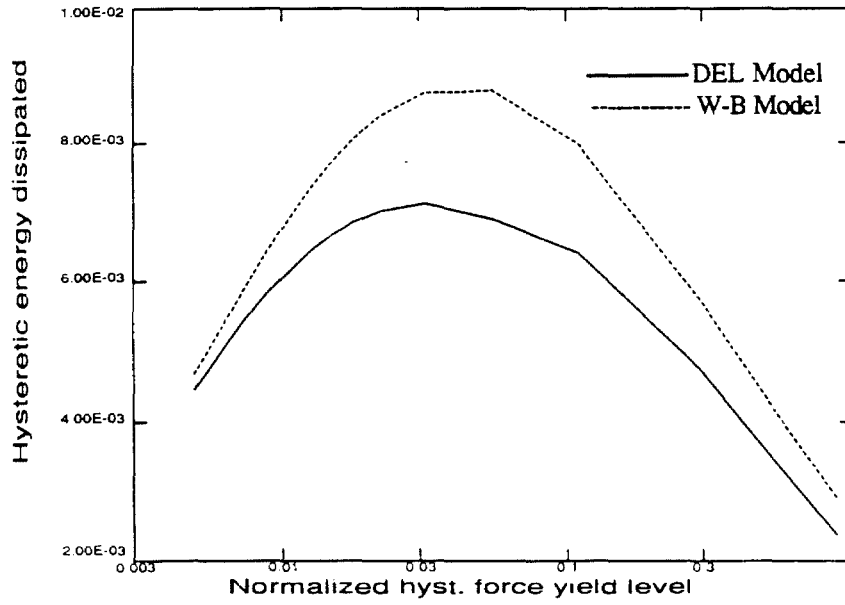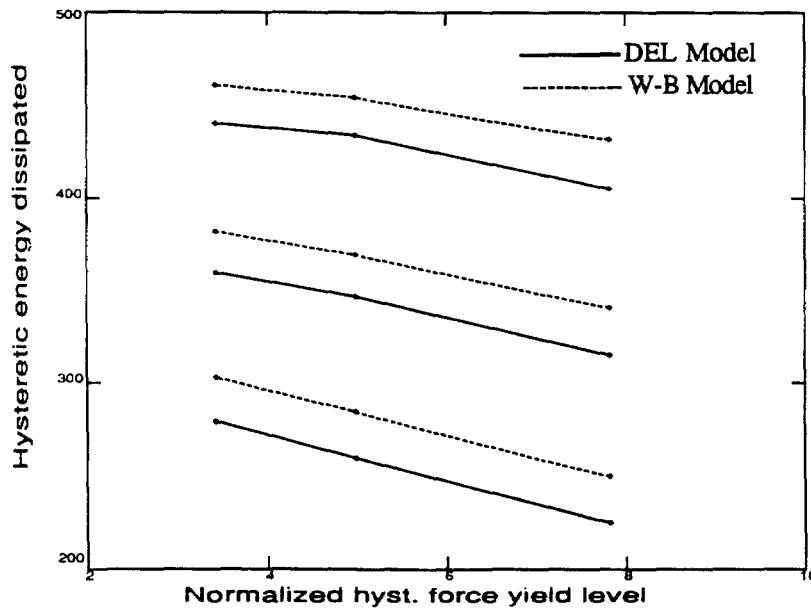


Figure 5.35:   The hysteretic energy dissipated, $E(T)$, by the two models when subjected to white noise base excitation, for a range of yield levels. The three curves shown for each model correspond to the values of the mean minus one standard deviation, the mean, and the mean plus one standard deviation.
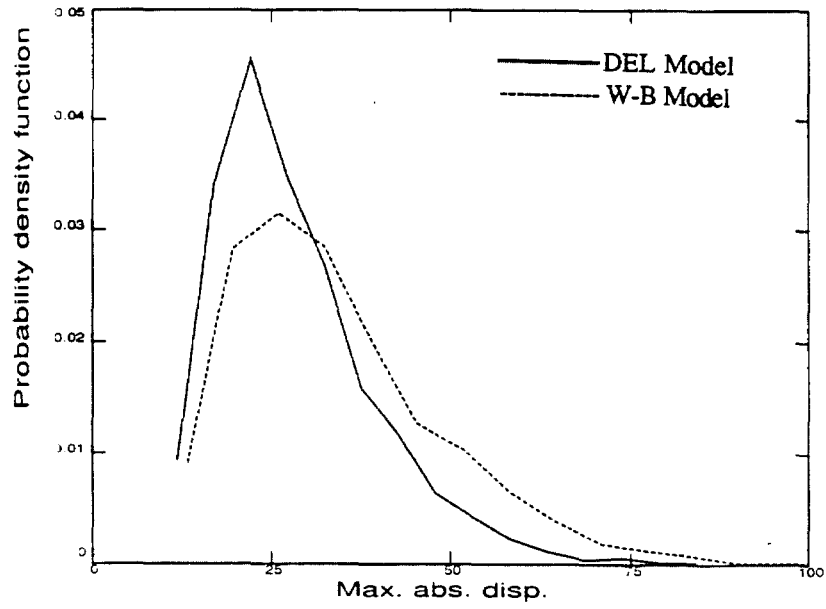
Figure 5.36:   The probability density function of $u_m$, the maximum relative displacement of the two models for Case III listed in Table 5.2.
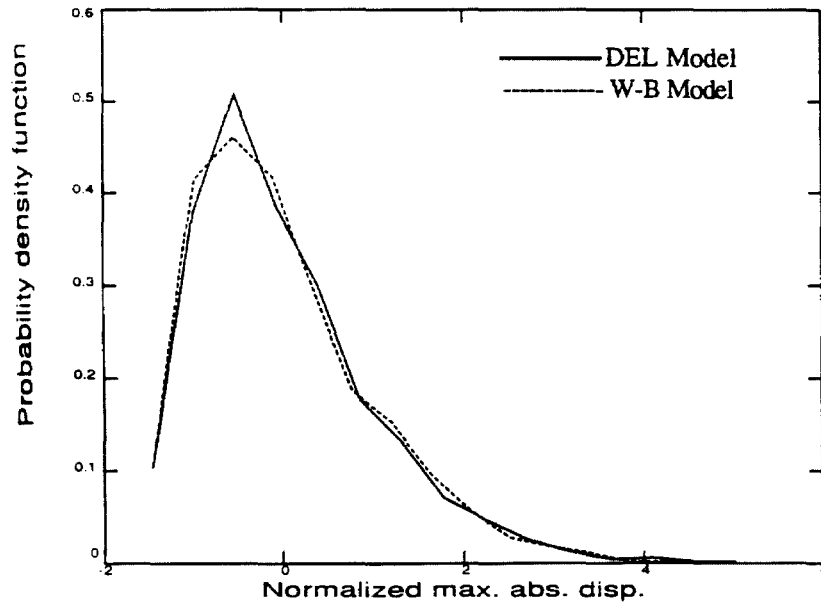


Figure 5.37:   The probability density function of the normalized value of $u_m$, the maximum relative displacement of the two models for Case III listed in Table 5.2.
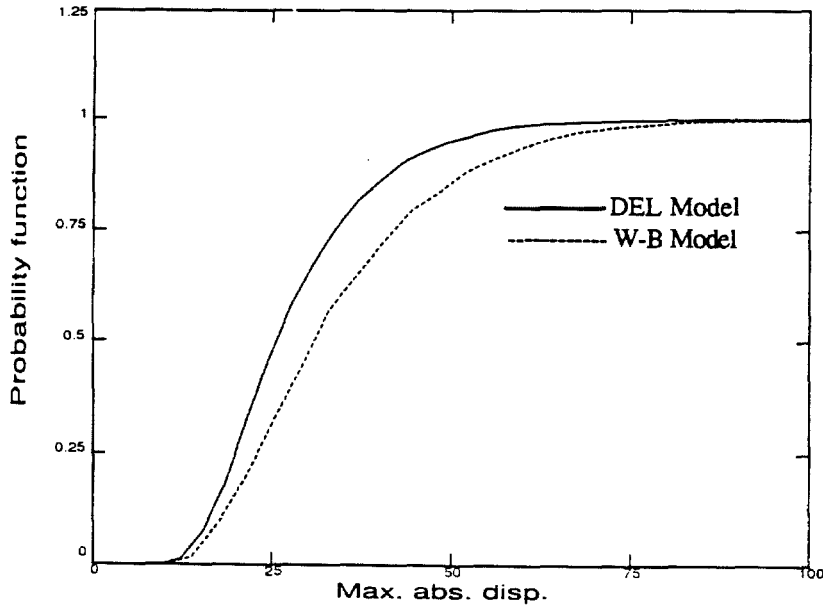
Figure 5.38:   The cumulative probability function of $u_m$, the maximum relative displacement of the two models for Case III listed in Table 5.2.
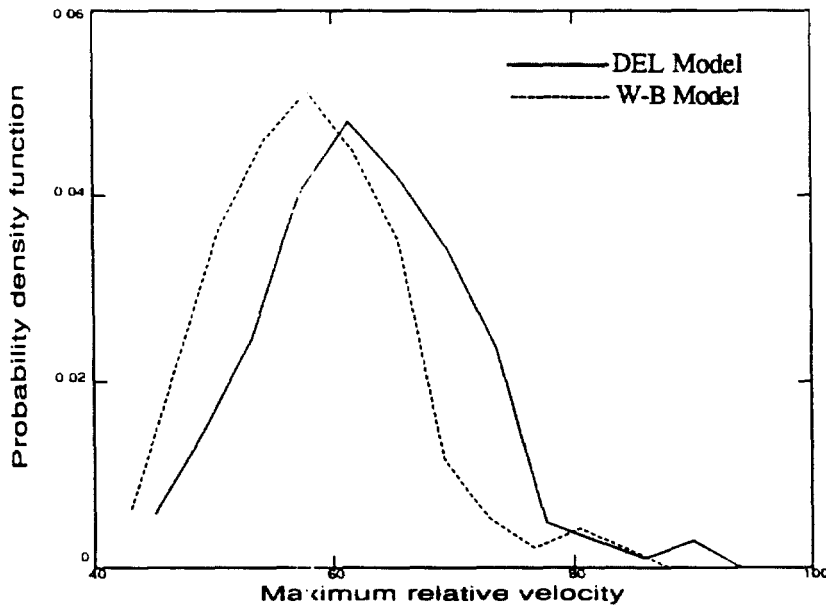


Figure 5.39:   The probability density function of $\dot{u}_m$, the maximum relative velocity of the two models for Case III listed in Table 5.2.
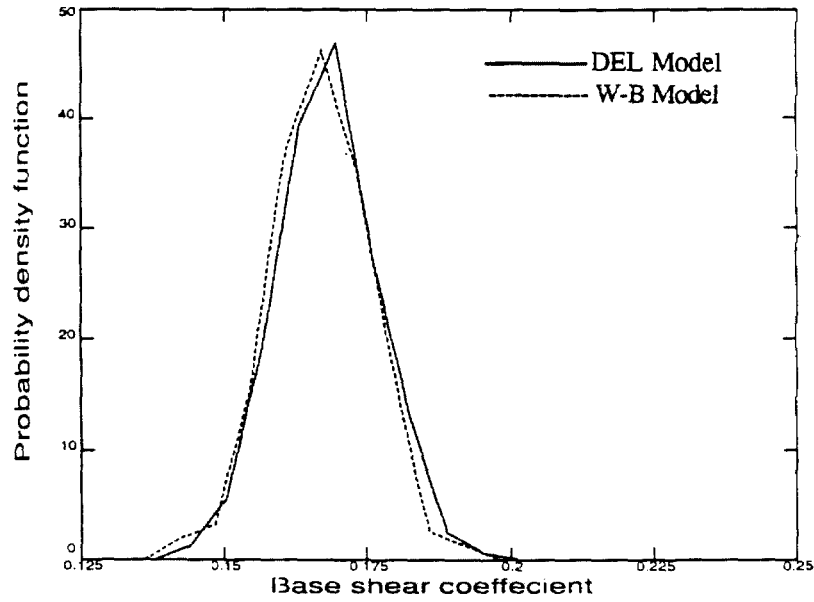
Figure 5.40: The probability density function of $C_b$, the base shear coefficient of the two models for Case III listed in Table 5.2.
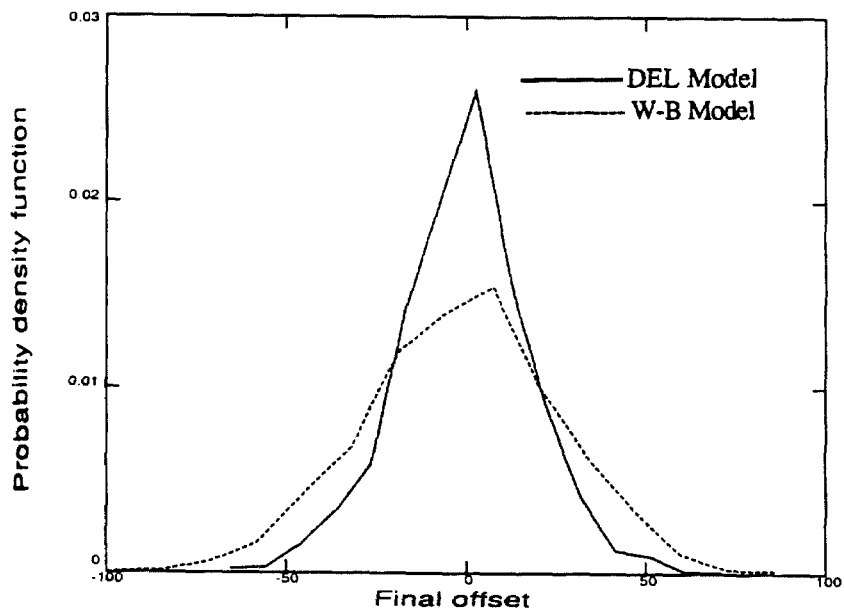


Figure 5.41: The probability density function of $u_{off}$, the final offset of the two models for Case III listed in Table 5.2.
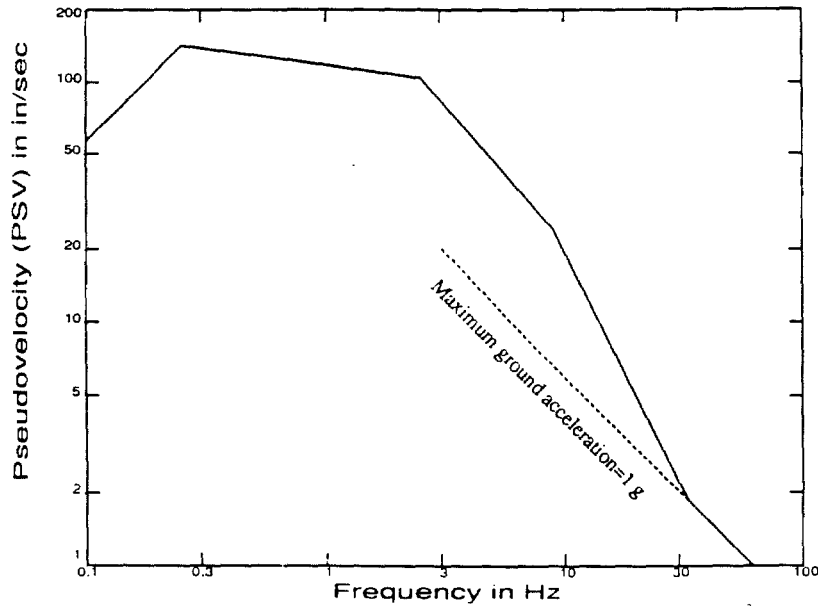
Figure 5.42: The NRC Reg. Guide 1.60 Horizontal mean design response spectrum for a viscous damping ratio of 2%.
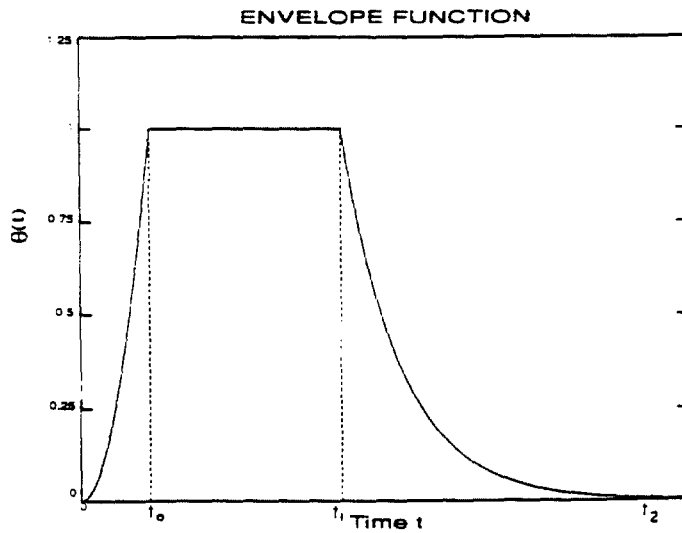


$$\theta(t) = \begin{cases} (t/t_0)^2 & \text{for } 0 \le t \le t_0 \\ 1.0 & \text{for } t_0 \le t \le t_1 \\ e^{-\gamma(t-t_1)} & \text{for } t_1 \le t \le t_2 \\ 0.0 & \text{for } t > t_2 \end{cases}$$

Figure 5.43: Envelope function used to modulate stationary,Gaussian noise to obtain earthquake-like excitations.
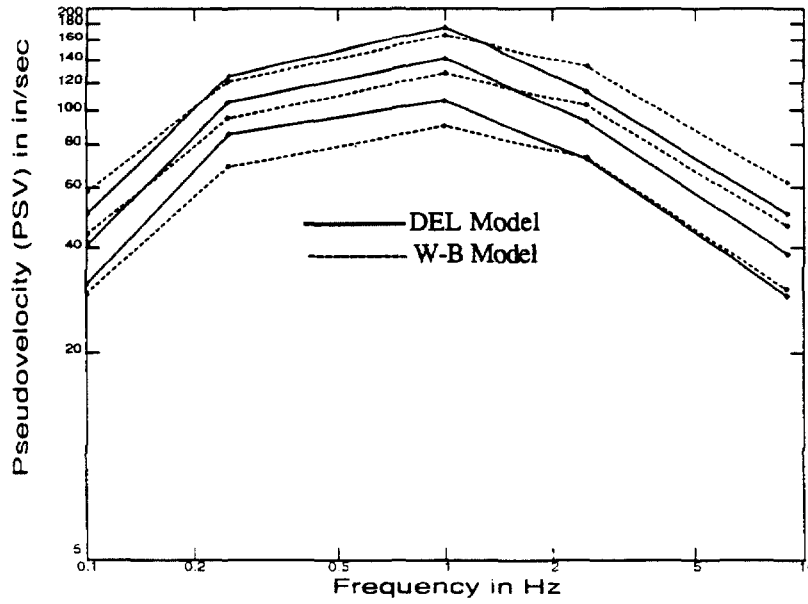
Figure 5.44:   The inelastic pseudovelocity (PSV) response spectrum of the two
hysteretic models corresponding to the Reg. Guide 1.60 elastic spectrum
shown in Fig. 5.42. These spectra correspond to a mean value of about 4
in the response of the DEL model.
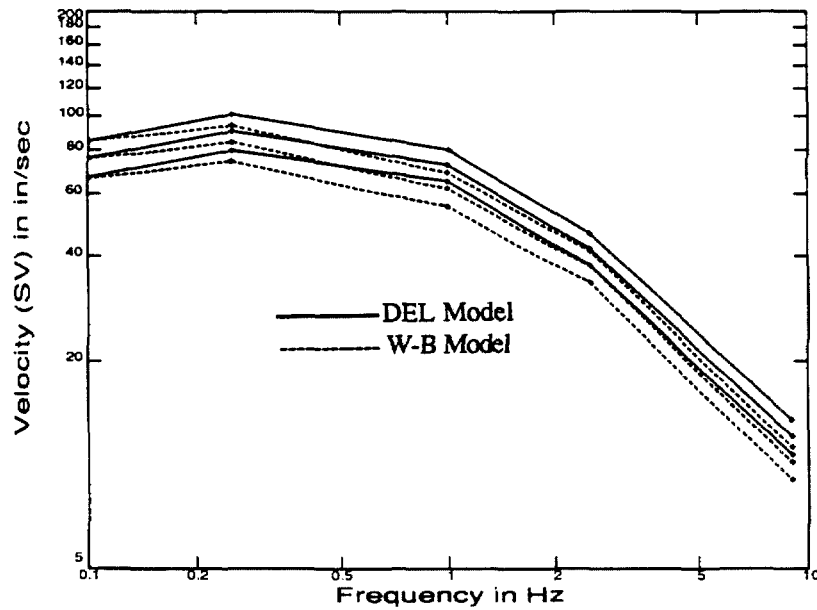


Figure 5.45:   The inelastic spectral velocity (SV) response spectrum of the two
hysteretic models corresponding to the Reg. Guide 1.60 elastic spectrum
shown in Fig. 5.42. These spectra correspond to a mean value of about 4
in the response of the DEL model.
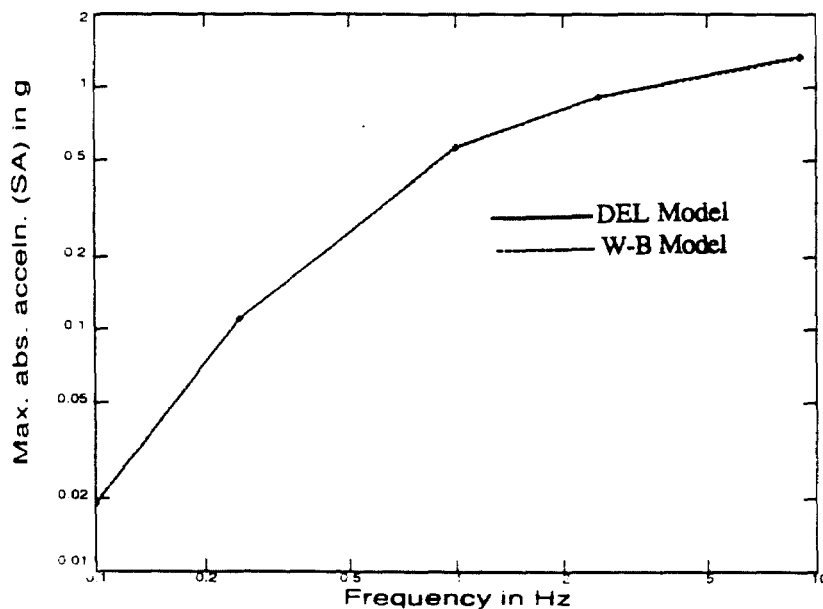
Figure 5.46:   The inelastic spectral acceleration (SA) response spectrum of the two
hysteretic models corresponding to the Reg. Guide 1.60 elastic spectrum
shown in Fig. 5.42. These spectra correspond to a mean value of about 4
in the response of the DEL model.
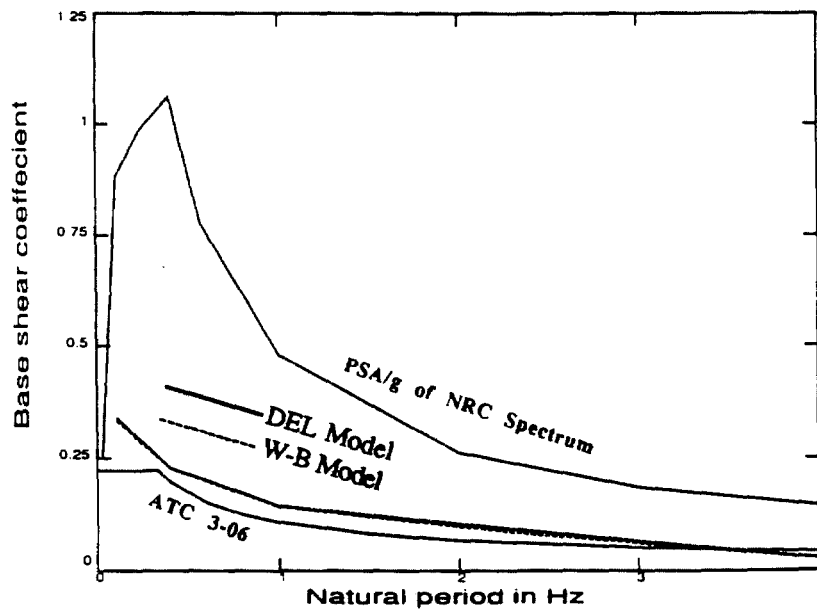


Figure 5.47:   Comparison of the design base shear coefficient as per the elastic NRC
spectrum, the DEL model, the W-B model and the ATC-3.06 lateral force
procedure.
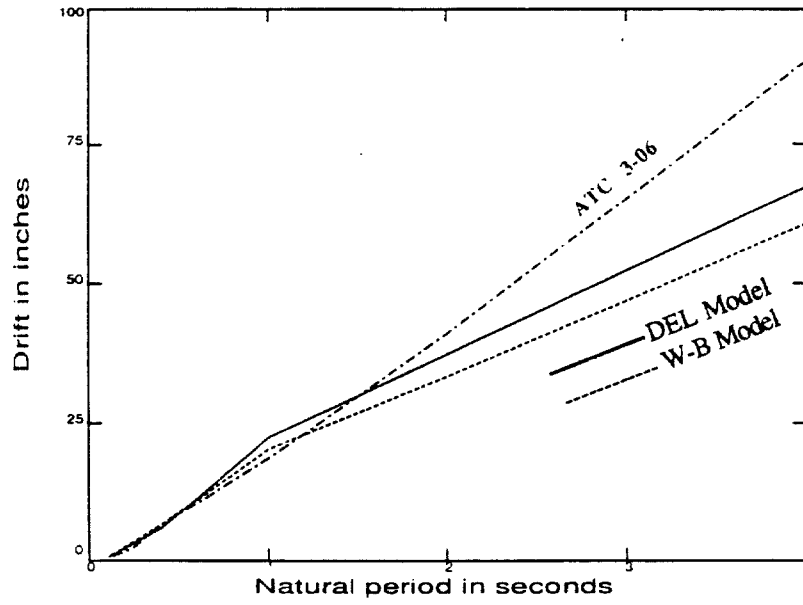
Figure 5.48: Comparison of design displacement drifts as per the two hysteretic models and the ATC-3.06 code.

# CHAPTER 6
# SUMMARY AND CONCLUSIONS

Based on the first five chapters of this thesis, a concluding summary on the analysis carried out and the results obtained may be presented as follows:

(1) Recently proposed mathematical representations for certain piecewise-linear hysteretic models have been beneficial in the sense that they have helped cast the models in a history-independent framework, thus enabling a stochastic linearization to determine the approximate response statistics. Such representations are available for the elastoplastic and bilinear models, the polylinear model, the double-bilinear model, the Clough-Johnston model, the slip model, the origin-oriented model, the peak-oriented model, etc. Unfortunately, there are no curvilinear hysteretic models for which these representations are currently available; as a matter of fact, it is not clear whether such representations involving only a small number of additional state variables exist at all for curvilinear models.

(2) When subjected to transient loading, the models belonging to the Distributed Element class of curvilinear hysteretic models satisfy an extended version of the Massing's hypothesis [24], which was originally proposed by Massing for steady-state behavior. This fact does not help in the equivalent linearization of the hysteretic models. However, it does simplify significantly the numerical implementation of the models when they are used to describe the hysteretic behavior of a system subjected to an arbitrary transient loading. This simplification, combined with the ability of these models to reproduce a wide range of hysteretic behavior, including both degrading and nondegrading systems, makes the Distributed Element class of models an excellent choice for the mathematical modeling of physical systems.

(3) A relatively simple identification procedure for nonlinear systems has been proposed in Chapter 3, which is based on matching the slopes of the hysteretic branches of the restoring force diagram rather than on the time history of the response. This procedure can be applied to hysteretic as well as to nonhysteretic systems. Examples shown in the same chapter indicate that the method is satisfactory for systems whose hysteretic behavior is governed by the bilinear model or by the endochronic model, for instance, the Wen-Bouc model.

(4) The response behavior of endochronic models, such as that of the Wen-Bouc model examined in Chapters 4 and 5, raises serious questions about the applicability of these models to represent physical hysteretic structures. The Wen-Bouc model, when subjected to certain quasi-static loading sequences, exhibits some inconsistent response behavior, for instance, displacement drift, loop nonclosure, stiffening, force relaxation to a zero mean value, etc. Also, these models violate the Drucker's and Ilyushin's stability postulates, calling to attention the possibility of inaccurate numerical solutions and/or nonunique solutions.

The instability of the endochronic models becomes quite apparent in Chapter 5 when the Wen-Bouc model is used to model a structure exhibiting the $P\text{-}\delta$ phenomenon. In this case, a suddenly applied external load on a structure causes very large response deformations, leading to its eventual collapse. This tendency to predict unusually large displacements is especially pronounced for very small values of the post-yielding system stiffness, and/or when the external load has a nonzero mean value. The possibility of the spurious instability predictions by these models raises the concern that it may not be possible to determine whether a failure predicted during analysis is due to the mathematical modeling, or to the actual failure of the structure to withstand excessive loading.

It may be recalled that one of the most prominent applications of the endochronic models has been in the estimation of the approximate response statistics of hysteretic systems subjected to stochastic excitation. With this in mind, a simulation analysis was performed with the Wen-Bouc model and the physically based Distributed Element model with identical initial loading behavior, in order to evaluate the ability of the endochronic model to predict satisfactorily the stochastic response of physical systems. The difference in the response statistics of the two models varies widely depending on the response quantity being extracted and the type of system (value of post-yielding stiffness, number of degrees of freedom, etc.). In one case with nonzero mean, white noise base excitation, the mean of the absolute value of the response displacement predicted by the W-B model is about 1.72 times the corresponding value provided by the Distributed Element model. In this context, a remark needs to be made. Generally speaking, it is observed that velocity predictions by the Wen-Bouc model are better than displacement and displacement-related quantities like ductility and final offset. By the same token, estimates of the acceleration-related quantities like the base shear coefficient seem to be even better than those of the velocity.

In view of the observed differences in the predicted values of certain response quantities in the simulation analysis, the following observation may be made. Even though the mathematical structure of the endochronic models is quite elegant and rather readily affords a direct stochastic linearization, it is a moot point as to how relevant the approximate response statistics obtained by the use of such models are in the analysis of physical hysteretic systems, because, simply put, these models are capable of behaving in a fashion quite inconsistent with realistic structural behavior. Caution must therefore be exercised in interpreting the estimates of response statistics obtained with the use of these models in the description of hysteretic behavior of nonlinear systems.

In light of the above conclusions, a few suggestions for continued research in the analysis of hysteretic structures may be made here. There are basically two broad avenues where further study would be profitable. The first is in improved mathematical modeling of hysteretic systems. An ideal mathematical model should satisfy the following properties:

(a) the model should be able to capture most of the important attributes of the response behavior of physical systems,

(b) the model should not exhibit abnormal characteristics that are not usually observed in physical systems, and

(c) the model representation should be simple enough to readily facilitate deterministic and stochastic analysis, including linearization.

It is clear that the piecewise-linear models satisfy (b) and (c) but not (a), the endochronic models satisfies (a) and (c) but not (b), and the Distributed Element models satisfy (a) and (b) but not (c), since they cannot be easily linearized in order to obtain approximate response statistics. Whether or not a model satisfying (a), (b) and (c) exists remains to be seen.

One possible model for hysteresis, containing some features of both the endochronic and the Distributed Element models, may be proposed as follows. It may be recalled that in the case of the endochronic models, the slopes of the restoring force diagram depend only on the instantaneous value of the restoring force, while in the case of the Distributed Element models, they depend not only on the instantaneous value of the restoring force, but also on all of the nested turning points. As in the case of the bounding-surface model proposed by Dafalias [16], the slopes of the restoring force diagram for the suggested model depend only on the most recent turning point in addition to the usual dependence on the instantaneous value of the restoring force. The slope of any loading/reloading /unloading path is assumed to vary linearly from the value of the initial system stiffness at the point of load reversal to an asymptotic value of zero at the maximum or yielding value

of the force. By its very formulation, the hysteresis loops are guaranteed to close at least partially. The hysteretic behavior of this model is similar to that reported by Jennings in [25].

In the search for improved mathematical models, one interesting field of investigation may lie in the possibility of extending the Massing's hypothesis to two and three dimensions. Iwan [21] has extended the hysteretic restoring force behavior of the one-dimensional class of Distributed Element models to three dimensions by introducing the concept of nested yield surfaces. It will be instructive to determine whether the Massing's hypothesis can in some way be extended to this three-dimensional class of models.

The second area of considerable research potential is in the possible generalization of the theory of equivalent linearization so as to include the class of Distributed Element models. For this purpose, it may be helpful to start with the history-independent representation for the parallel-series model indicated by Eqn. (2.42). Investigations may also be undertaken to examine the feasibility of linearizing the Dafalias-like model suggested earlier.

It is evident that the modeling and analysis of hysteretic systems is an area of immense research potential and challenge. Every effort must be made to facilitate clear understanding of the hysteretic nature of nonlinear response behavior, considering its crucial importance in structural dynamics.

# REFERENCES

[1] **American Standards Institute, New York,** "American National Standards and Building Code Requirements For Minimum Design Loads in Buildings and Other Structures," ANSI A 58.1-1972.

[2] **Applied Technology Council,** "Tentative Provisions for the Development of Seismic Regulations for Buildings (Including Proposed Amendments)," ATC 3-06 (Amended), Second printing, April 1984.

[3] **Asano, K.** and **Iwan, W.D.,** "An Alternative Approach to The Random Response of Bilinear Hysteretic Systems," *Earthquake Engineering and Structural Dynamics,* Vol. 12, 229-236, 1984.

[4] **Atalik, T.S.** and **Utku, S.,** "Stochastic Linearization of Multi Degree-Of-Freedom Nonlinear Systems," *Earthquake Engineering and Structural Dynamics,* Vol.4, 411-420, 1974.

[5] **Baber, T.T.,** "Nonzero Mean Random Vibration of Hysteretic Systems," *Journal of Applied Mechanics,* Vol. 110, No. 3, 1036-1049, 1984.

[6] **Bardet, J.P,** "Application of Plasticity Theory to Soil Behavior: A New Sand Model," *Ph. D. Dissertation,* California Institute of Technology, Pasadena, 1983.

[7] **Bazant, Z.P.** and **Bhat, P.,** "Endochronic Theory of Inelasticity and Failure of Concrete," *Journal of the Engineering Mechanics Division,* ASCE, Vol. 12, No. EM4, 701-722, August 1976.

[8] **Beck, J.L,** "Determining Models of Structures from Earthquake Records," *Ph. D Dissertation,* California Institute of Technology, Pasadena, 1978.

[9] **Bycroft, G.N.,** "White Noise Representation of Earthquakes," *Journal of the Engineering Mechanics Division,* Transactions of the ASCE, Vol. 86, No. EM2, 1-16, April 1960.

[10] **Casciyati,** "Nonlinear Stochastic Dynamics of Large Structural Systems By Equivalent Linearization," *Proceedings of the ICASP5, the Fifth International Conference on Application of Statistics and Probability in Soil and Structural Engineering,* University of British Columbia, Vancouver, 1987.

[11] **Caughey, T.K.,** "Random Excitation of a System with Bilinear Hysteresis," *Journal of Applied Mechanics,* ASME, Vol. 27, 649-652, December 1960.

[12] Caughey, T.K., "Equivalent Linearization Techniques," *Journal of Acoustical Society of America*, Vol. 35, 1706-1711, 1963.

[13] Cifuentes, A.O., "System Identification of Hysteretic Systems," *Ph. D. Dissertation*, California Institute of Technology, Pasadena, 1984.

[14] Clough, W. and Johnston, S.B., "Effects of Stiffness Degradation on Earthquake Ductility Requirements," *Proceedings of the Second Japan Earthquake Engineering Symposium*, Tokyo, 227-232, October 1966.

[15] Clough, R.W. and Penzien, J., *Dynamics Of Structures*, McGraw-Hill Publications: New York, 1975.

[16] Dafalias, Y., "On Cyclic and Anisotropic Plasticity," *Ph. D. Dissertation in Engineering Science*, University of California, Berkeley, 1975.

[17] Hildebrand, F.B., *Introduction to Numerical Analysis*, Dover Publications: New York, pp. 290-292, 1974.

[18] Housner, G.W., "Characteristics of Strong-Motion Earthquakes," *Bulletin of the Seismological Society of America*, Vol. 37, 19-31, 1947.

[19] Iemura, H. and Jennings, P.C., "Hysteretic Response of a Nine-Story Reinforced Concrete Building," *International Journal of Earthquake Engineering and Structural Dynamics*, Vol. 3, 183-201, 1974.

[20] Iwan, W.D., " A Distributed-Element Model for Hysteresis and its Steady-State Dynamic Response," *Journal of Applied Mechanics*, ASME, Vol. 33, No. 4, 893-900, 1966.

[21] Iwan, W.D., "On a Class of Models for the Yielding Behavior of Continuous And Composite Systems," *Journal of Applied Mechanics*, ASME, Vol. 34, No. 3, 612-617, 1967.

[22] Iwan, W.D., "A Generalization of the Concept of Equivalent Linearization," *International Journal of Nonlinear Mechanics*, Vol. 8, 279-287, 1973.

[23] Iwan, W.D., "Estimating Inelastic Response Spectra from Elastic Spectra," *Earthquake Engineering and Structural Dynamics*, Vol. 8, 375-388, 1980.

[24] Jayakumar, P., "Modeling and Identification in Structural Dynamics," *Ph. D. Dissertation*, California Institute of Technology, Pasadena, 1987.

[25] Jennings, P.C., "Response of Simple Yielding Structures to Earthquake Excitation," *Ph. D. Dissertation*, California Institute of Technology, Pasadena, 1963.

[26] Jennings, P.C., Housner, G.W. and Tsai, N.C., "Simulated Earthquake Motions," *Earthquake Engineering Research Laboratory Report*, California Institute of Technology, Pasadena, 1968.

[27] Jeong, G.D., "Cumulative Damage of Structures Subjected to Response Spectrum-Consistent Random Processes," *Ph. D. Dissertation*, California Institute of Technology, Pasadena, 1985.

[28] Masing, G., "Eigenspannungen Und Verfestigung Beim Messing," *Proceedings of the Second International Congress for Applied Mechanics*, Zurich, Switzerland, 332-335, 1926 (in German).

[29] Mason, A.B., Jr., "Some Observations on the Random Response of Linear and Nonlinear Dynamical Systems," *Ph. D. Dissertation*, California Institute of Technology, Pasadena, 1979.

[30] Mason, A.B., Jr., and Iwan, W.D., "An Approach to the First Passage Problem in Random Vibration," *Journal of Applied Mechanics*, Vol. 50, 641-646, September 1983.

[31] Masri, S.F. and Caughey, T.K., "A Nonparametric Identification Technique for Nonlinear Dynamic Problems," *Journal of Applied Mechanics*, Vol. 46, 433-447, June 1979.

[32] McVerry, G.H., "Frequency Domain Identification of Structural Models from Earthquake Records," *Ph. D. Dissertation*, California Institute of Technology, Pasadena, 1979.

[33] Morrow, J. and Sinclair G., "Cyclic Stress Relaxation," *ASTM Symposium on Basic Mechanics of Fatigue*, ASTM, Special Technical Publication 237, Boston, 1958.

[34] Nuclear Regulatory Commission, "Design Response Spectra for Seismic Design," Reg. Guide 1.60, Revision 1, December 1973.

[35] Özdemir, H., "Nonlinear Transient Dynamic Analysis of Yielding Structures," *Ph. D. Dissertation*, University of California, Berkeley, June 1976.

[36] Paparizos, L.G., "Some Observations on the Random Response of Hysteretic Systems," *Ph. D. Dissertation*, California Institute of Technology, Pasadena, 1986.

[37] Park, Y.J., Wen, Y.K. and Ang, A. H-S, "Random Vibration of Hysteretic Systems under Bi-directional Ground Motions," *Earthquake Engineering and Structural Dynamics*, Vol. 14, 543-557, 1986.

[38] Picard, E., "La Mécanique Classique et Ses Approximations Successive," *Revista di Scienza*, Vol. 1, 4-15, 1907 (In French).

[39] Popov, E.P., "Seismic Behavior of Structural Assemblages," *Journal of the Structural Division*, Proceedings of the ASCE, Vol. 106, 1451-1474, July 1980.

[40] Rice, J.R., "On the Structure of Stress-Strain Relations for Time-Dependent Plastic Deformation in Metals," *Journal of Applied Mechanics*, Vol. 37, 728-737, 1970.

[41] Rice, J.R., "Continuum Mechanics and Thermodynamics of Plasticity in Relation to Microscale Deformation Mechanisms," *Constitutive equations in Plasticity*, pp. 23-79, MIT Press, Cambridge, Massachusetts.

[42] Rosenblueth, E. and Bustamente, J.E., "Distribution of Structural Response to Earthquakes," *Journal of the Engineering Mechanics Division*, No. EM3, 75-106, June 1962.

[43] Salmon, C.G. and Johnson, J.E., *Steel Structures - Design And Behavior*, Second Edition, Harper and Row: New York, 1980.

[44] Sandler, I.S., "On the Uniqueness and Stability of Endochronic Theories Of Material Behavior," *Journal of Applied Mechanics*, Vol. 45, 263-266, 1978.

[45] Spanos, P.D. and Iwan, W.D., "On the Existence and Uniqueness of Solutions Generated by Equivalent Linearization," *International Journal of Nonlinear Mechanics*, Vol. 13, 71-78, 1978.

[46] Sues, R.H., Wen, Y.K. and Ang, A. H-S., "Stochastic Seismic Performance Evaluation of Buildings," *Civil Engineering Studies, Structural Series No. 506*, University of Illinois at Urbana-Champaign, Urbana, Illinois, May 1973; also, *Journal of Applied Mechanics*, Vol. 114, No. 5, 833-846, May 1988.

[47] Suzuki, Y. and Minai, R., " A Method of Seismic Response Analysis of Hysteretic Structures Based on Stochastic Differential Equations," *Proceedings of the Eighth World Conference in Earthquake Engineering*, Vol. 4, 459-466, 1984.

[48] Suzuki, Y. and Minai, R., "Seismic Reliability Analysis of Hysteretic Structures Based on Stochastic Differential Equations," *Proceedings of the Fourth ICOSSAR*, Vol. 2, 177-186, 1985.

[49] Takeda, T., Sozen, M.A. and Nielsen, N.N., "Reinforced Concrete Response to Simulated Earthquakes," *Journal of the Structural Division*, Transactions of the ASCE, Vol. 96, 2557-2573, December 1970.

[50] Valanis, K.C., "On The Foundations of the Endochronic Theory of Viscoplasticity," *Archiwum Mechaniki Stosowanej*, Vol. 27, No. 5-6, 857-868, 1975.

[51] Veletsos, A.S. and Newmark, N.M., "Effects of Inelastic Behavior on the Response of Simple Systems to Earthquake Motions," *Proceedings of the Second World Conference on Earthquake Engineering*, Tokyo, Japan, Vol. 2, 895-912, 1960.

[52] **Volterra, V.,** *Theory of Functionals and Integro-differential Equations,* Dover Publications: New York, 1959.

[53] **Wen, Y.K.,** "Equivalent Linearization for Hysteretic Systems under Random Excitations," *Journal of Applied Mechanics,* ASME, Vol. 47, No. 1, 150-154, March 1980.

[54] **Wen, Y.K.,** "Stochastic Response and Damage Analysis of Inelastic Structures," *Probabilistic Engineering Mechanics,* Vol.1, No. 1, 49-57, 1986.

[55] **Yang, J.N.,** "On the Normality and Accuracy of Simulated Random Processes," *Journal of Sound and Vibration,* Vol. 26, 417-428, 1973.

# CALIFORNIA INSTITUTE OF TECHNOLOGY

Reports Published

by

Earthquake Engineering Research Laboratory*
Dynamic Laboratory
Disaster Research Center

*Note*: Numbers in parenthesis are Accession Numbers assigned by the National Technical Information Service; these reports may be ordered from the National Technical Information Service, 5285 Port Royal Road, Springfield, Virginia, 22161. Accession Numbers should be quoted on orders for reports (PB — —). Reports without this information either have not been submitted to NTIS or the information was not available at the time of printing. An N/A in parenthesis indicates that the report is no longer available at Caltech.

1. Alford, J.L., G.W. Housner and R.R. Martel, "Spectrum Analysis of Strong-Motion Earthquake," 1951. (Revised August 1964). (N/A)

2. Housner, G.W., "Intensity of Ground Motion During Strong Earthquakes," 1952. (N/A)

3. Hudson, D.E., J.L. Alford and G.W. Housner, "Response of a Structure to an Explosive Generated Ground Shock," 1952. (N/A)

4. Housner, G.W., "Analysis of the Taft Accelerogram of the Earthquake of 21 July 1952." (N/A)

5. Housner, G.W., "A Dislocation Theory of Earthquakes," 1953. (N/A)

6. Caughey, T.K. and D.E. Hudson, "An Electric Analog Type Response Spectrum," 1954. (N/A)

7. Hudson, D.E. and G.W. Housner, "Vibration Tests of a Steel-Frame Building," 1954. (N/A)

8. Housner, G.W., "Earthquake Pressures on Fluid Containers," 1954. (N/A)

9. Hudson, D.E., "The Wilmot Survey Type Strong-Motion Earthquake Recorder," 1958. (N/A)

10. Hudson, D.E. and W.D. Iwan, "The Wilmot Survey Type Strong-Motion Earthquake Recorder, Part II," 1960. (N/A)

11. Caughey, T.K., D.E. Hudson and R.V. Powell, "The CIT Mark II Electric Analog Type Response Spectrum Analyzer for Earthquake Excitation Studies," 1960. (N/A)

12. Keightley, W.O., G.W. Housner and D.E. Hudson, "Vibration Tests of the Encino Dam Intake Tower," 1961. (N/A)

---

* To order directly by phone, the number is (703) 487-4650.

13. Merchant, H.C., "Mode Superposition Methods Applied to Linear Mechanical Systems Under Earthquake Type Excitation," 1961. (N/A)

14. Iwan, W.D., "The Dynamic Response of Bilinear Hysteretic Systems," 1961. (N/A)

15. Hudson, D.E., "A New Vibration Exciter for Dynamic Test of Full-Scale Structures," 1961. (N/A)

16. Hudson, D.E., "Synchronized Vibration Generators for Dynamic Tests of Full-Scale Structures," 1962. (N/A)

17. Jennings, P.C., "Velocity Spectra of the Mexican Earthquakes of 11 May and 19 May 1962," 1962. (N/A)

18. Jennings, P.C., "Response of Simple Yielding Structures to Earthquake Excitation," 1963. (N/A)

19. Keightley, W.O., "Vibration Tests of Structures," 1963. (N/A)

20. Caughey, T.K. and M.E.J. O'Kelly, "General Theory of Vibration of Damped Linear Dynamic Systems," 1963. (N/A)

21. O'Kelly, M.E.J., "Vibration of Viscously Damped Linear Dynamic Systems," 1964. (N/A)

22. Nielsen, N.N., "Dynamic Response of Multistory Buildings," 1964. (N/A)

23. Tso, W.K., "Dynamics of Thin-Walled Beams of Open Section," 1964. (N/A)

24. Keightley, W.O., "A Dynamic Investigation of Bouquet Canyon Dam," 1964. (N/A)

25. Malhotra, R.K., "Free and Forced Oscillations of a Class of Self-Excited Oscillators," 1964.

26. Hanson, R.D., "Post-Elastic Response of Mild Steel Structures," 1965.

27. Masri, S.F., "Analytical and Experimental Studies of Impact Dampers," 1965.

28. Hanson, R.D., "Static and Dynamic Tests of a Full-Scale Steel-Frame Structures," 1965.

29. Cronin, D.L., "Response of Linear, Viscous Damped Systems to Excitations Having Time-Varying Frequency," 1965.

30. Hu, P.Y.-F., "Analytical and Experimental Studies of Random Vibration," 1965.

31. Crede, C.E., "Research on Failure of Equipment when Subject to Vibration," 1965.

32. Lutes, L.D., "Numerical Response Characteristics of a Uniform Beam Carrying One Discrete Load," 1965. (N/A)

33. Rocke, R.D., "Transmission Matrices and Lumped Parameter Models for Continuous Systems," 1966. (N/A)

34. Brady, A.G., "Studies of Response to Earthquake Ground Motion," 1966. (N/A)

35. Atkinson, J.D., "Spectral Density of First Order Piecewise Linear Systems Excited by White Noise," 1967. (N/A)

36. Dickerson, J.R., "Stability of Parametrically Excited Differential Equations," 1967. (N/A)

37. Giberson, M.F., "The Response of Nonlinear Multi-Story Structures Subjected to Earthquake Excitation," 1967. (N/A)

38. Hallanger, L.W., "The Dynamic Stability of an Unbalanced Mass Exciter," 1967.

39. Husid, R., "Gravity Effects on the Earthquake Response of Yielding Structures," 1967. (N/A)

40. Kuroiwa, J.H., "Vibration Test of a Multistory Building," 1967. (N/A)

41. Lutes, L.D., "Stationary Random Response of Bilinear Hysteretic Systems," 1967.

42. Nigam, N.C., "Inelastic Interactions in the Dynamic Response of Structures," 1967.

43. Nigam, N.C. and P.C. Jennings, "Digital Calculation of Response Spectra from Strong-Motion Earthquake Records," 1968.

44. Spencer, R.A., "The Nonlinear Response of Some Multistory Reinforced and Prestressed Concrete Structures Subjected to Earthquake Excitation," 1968. (N/A)

45. Jennings, P.C., G.W. Housner and N.C. Tsai, "Simulated Earthquake Motions," 1968.

46. "Strong-Motion Instrumental Data on the Borrego Mountain Earthquake of 9 April 1968," (USGS and EERL Joint Report), 1968.

47. Peters, R.B., "Strong Motion Accelerograph Evaluation," 1969.

48. Heitner, K.L., "A Mathematical Model for Calculation of the Run-Up of Tsunamis," 1969.

49. Trifunac, M.D., "Investigation of Strong Earthquake Ground Motion," 1969. (N/A)

50. Tsai, N.C., "Influence of Local Geology on Earthquake Ground Motion," 1969. (N/A)

51. Trifunac, M.D., "Wind and Microtremor Induced Vibrations of a Twenty-Two Steel Frame Building," EERL 70-01, 1970.

52. Yang, I-M., "Stationary Random Response of Multidegree-of-Freedom Systems," DYNL-100, June 1970. (N/A)

53. Patula, E.J., "Equivalent Differential Equations for Non-linear Dynamic Systems," DYNL-101, June 1970.

54. Prelewicz, D.A., "Range of Validity of the Method of Averaging," DYNL-102, 1970.

55. Trifunac, M.D., "On the Statistics and Possible Triggering Mechanism of Earthquakes in Southern California," EERL 70-03, July 1970.

56. Heitner, K.L., "Additional Investigations on a Mathematical Model for Calculation of Run-Up of Tsunamis," July 1970.

57. Trifunac, M.D., "Ambient Vibration Tests of a Thirty-Nine Story Steel Frame Building," EERL 70-02, July 1970.

58. Trifunac, M.D. and D.E. Hudson, "Laboratory Evaluations and Instrument Corrections of Strong-Motion Accelerographs," EERL 70-04, August 1970. (N/A)

59. Trifunac, M.D., "Response Envelope Spectrum and Interpretation of Strong Earthquake Ground Motion," EERL 70-06, August 1970.

60. Keightley, W.O., "A Strong-Motion Accelerograph Array with Telephone Line Interconnections," EERL 70-05, September 1970.

61. Trifunac, M.D., "Low Frequency Digitization Errors and a New Method for Zero Baseline Correction of Strong-Motion Accelerograms," EERL 70-07, September 1970.

62. Vijayaraghavan, A., "Free and Forced Oscillations in a Class of Piecewise-Linear Dynamic Systems," DYNL-103, January 1971.

63. Jennings, P.C., R.B. Mathiesen and J.B. Hoerner, "Forced Vibrations of a 22-Story Steel Frame Building," EERL 71-01, February 1971. (N/A) (PB 205 161)

64. Jennings, P.C., "Engineering Features of the San Fernando Earthquake of February 9, 1971," EERL 71-02, June 1971. (PB 202 550)

65. Bielak, J., "Earthquake Response of Building-Foundation Systems," EERL 71-04, June 1971. (N/A) (PB 205 305)

66. Adu, R.A., "Response and Failure of Structures Under Stationary Random Excitation," EERL 71-03, June 1971. (N/A) (PB 205 304)

67. Skattum, K.S., "Dynamic Analysis of Coupled Shear Walls and Sandwich Beams," EERL 71-06, June 1971. (N/A) (PB 205 267)

68. Hoerner, J.B., "Model Coupling and Earthquake Response of Tall Buildings," EERL 71-07, June 1971. (N/A) (PB 207 635)

69. Stahl, K.J., "Dynamic Response of Circular Plates Subjected to Moving Massive Loads," DYNL-104, June 1971. (N/A)

70. Trifunac, M.D., F.E. Udwadia and A.G. Brady, "High Frequency Errors and Instrument Corrections of Strong-Motion Accelerograms," EERL 71-05, 1971. (PB 205 369)

71. Furuike, D.M., "Dynamic Response of Hysteretic Systems With Application to a System Containing Limited Slip," DYNL-105, September 1971. (N/A)

72. Hudson, D.E. (Editor), "Strong-Motion Instrumental Data on the San Fernando Earthquake of February 9, 1971," (Seismological Field Survey, NOAA, C.I.T. Joint Report), September 1971. (PB 204 198)

73. Jennings, P.C. and J. Bielak, "Dynamics of Building-Soil Interaction," EERL 72-01, April 1972. (PB 209 666)

74. Kim, B.-K., "Piecewise Linear Dynamic Systems with Time Delays," DYNL-106, April 1972.

75. Viano, D.C., "Wave Propagation in a Symmetrically Layered Elastic Plate," DYNL-107, May 1972.

76. Whitney, A.W., "On Insurance Settlements Incident to the 1906 San Francisco Fire," DRC 72-01, August 1972. (PB 213 256)

77. Udwadia, F.E., "Investigation of Earthquake and Microtremor Ground Motions," EERL 72-02, September 1972. (PB 212 853)

78. Wood, J.H., "Analysis of the Earthquake Response of a Nine-Story Steel Frame Building During the San Fernando Earthquake," EERL 72-04, October 1972. (PB 215 823)

79. Jennings, P.C., "Rapid Calculation of Selected Fourier Spectrum Ordinates," EERL 72-05, November 1972.

80. "Research Papers Submitted to Fifth World Conference on Earthquake Engineering, Rome, Italy, 25–29 June 1973," EERL 73-02, March 1973. (PB 220 431)

81. Udwadia, F.E. and M.D. Trifunac, "The Fourier Transform, Response Spectra and Their Relationship Through the Statistics of Oscillator Response," EERL 73-01, April 1973. (PB 220 458)

82. Housner, G.W., "Earthquake-Resistant Design of High-Rise Buildings," DRC 73-01, July 1973. (N/A)

83. "Earthquake and Insurance," Earthquake Research Affiliates Conference, 2-3 April, 1973, DRC 73-02, July 1973. (PB 223 033)

84. Wood, J.H., "Earthquake-Induced Soil Pressures on Structures," EERL 73-05, August 1973. (N/A)

85. Crouse, C.B., "Engineering Studies of the San Fernando Earthquake," EERL 73-04, March 1973. (N/A)

86. Irvine, H.M., "The Veracruz Earthquake of 28 August 1973," EERL 73-06, October 1973.

87. Iemura, H. and P.C. Jennings, "Hysteretic Response of a Nine-Story Reinforced Concrete Building During the San Fernando Earthquake," EERL 73-07, October 1973.

88. Trifunac, M.D. and V. Lee, "Routine Computer Processing of Strong-Motion Accelerograms," EERL 73-03, October 1973. (N/A) (PB 226 047/AS)

89. Moeller, T.L., "The Dynamics of a Spinning Elastic Disk with Massive Load," DYNL 73-01, October 1973.

90. Blevins, R.D., "Flow Induced Vibration of Bluff Structures," DYNL 74-01, February 1974.

91. Irvine, H.M., "Studies in the Statics and Dynamics of Simple Cable Systems," DYNL-108, January 1974.

92. Jephcott, D.K. and D.E. Hudson, "The Performance of Public School Plants During the San Fernando Earthquake," EERL 74-01, September 1974. (PB 240 000/AS)

93. Wong, H.L., "Dynamic Soil-Structure Interaction," EERL 75-01, May 1975. (N/A) (PB 247 233/AS)

94. Foutch, D.A., G.W. Housner and P.C. Jennings, "Dynamic Responses of Six Multistory Buildings During the San Fernando Earthquake," EERL 75-02, October 1975. (PB 248 144/AS)

95.  Miller, R.K., "The Steady-State Response of Multidegree-of-Freedom Systems with a Spatially Localized Nonlinearity," EERL 75-03, October 1975. (PB 252 459/AS)

96.  Abdel-Ghaffar, A.M., "Dynamic Analyses of Suspension Bridge Structures," EERL 76-01, May 1976. (PB 258 744/AS)

97.  Foutch, D.A., "A Study of the Vibrational Characteristics of Two Multistory Buildings," EERL 76-03, September 1976. (PB 260 874/AS)

98.  "Strong Motion Earthquake Accelerograms Index Volume," Earthquake Engineering Research Laboratory, EERL 76-02, August 1976. (PB 260 929/AS)

99.  Spanos, P-T.D., "Linearization Techniques for Non-Linear Dynamical Systems," EERL 76-04, September 1976. (PB 266 083/AS)

100. Edwards, D.B., "Time Domain Analysis of Switching Regulators," DYNL 77-01, March 1977.

101. Abdel-Ghaffar, A.M., "Studies of the Effect of Differential Motions of Two Foundations upon the Response of the Superstructure of a Bridge," EERL 77-02, January 1977. (PB 271 095/AS)

102. Gates, N.C., "The Earthquake Response of Deteriorating Systems," EERL 77-03, March 1977. (PB 271 090/AS)

103. Daly, W., W. Judd and R. Meade, "Evaluation of Seismicity at U.S. Reservoirs," USCOLD, Committee on Earthquakes, May 1. (PB 270 036/AS)

104. Abdel-Ghaffer, A.M. and G.W. Housner, "An Analysis of the Dynamic Characteristics of a Suspension Bridge by Ambient Vibration Measurements," EERL 77-01, January 1977. (PB 275 063/AS)

105. Housner, G.W. and P.C. Jennings, "Earthquake Design Criteria for Structures," EERL 77-06, November 1977 (PB 276 502/AS)

106. Morrison, P., R. Maley, G. Brady and R. Porcella, "Earthquake Recordings on or Near Dams," USCOLD, Committee on Earthquakes, November 1977. (PB 285 867/AS)

107. Abdel-Ghaffar, A.M., "Engineering Data and Analyses of the Whittier, California Earthquake of January 1, 1976," EERL 77-05, November 1977. (PB 283 750/AS)

108. Beck, J.L., "Determining Models of Structures from Earthquake Records," EERL 78-01, June 1978 (PB 288 806/AS)

109. Psycharis, I., "The Salonica (Thessaloniki) Earthquake of June 20, 1978," EERL 78-03, October 1978. (PB 290 120/AS)

110. Abdel-Ghaffar, A.M. and R.F. Scott, "An Investigation of the Dynamic Characteristics of an Earth Dam," EERL 78-02, August 1978. (PB 288 878/AS)

111. Mason, A.B., Jr., "Some Observations on the Random Response of Linear and Nonlinear Dynamical Systems," EERL 79-01, January 1979. (PB 290 808/AS)

112. Helmberger, D.V. and P.C. Jennings (Organizers), "Strong Ground Motion: N.S.F. Seminar-Workshop," SL-EERL 79-02, February 1978.

113. Lee, D.M., P.C. Jennings and G.W. Housner, "A Selection of Important Strong Motion Earthquake Records," EERL 80-01, January 1980. (PB 80 169196)

114. McVerry, G.H., "Frequency Domain Identification of Structural Models from Earthquake Records," EERL 79-02, October 1979. (PB-80-194301)

115. Abdel-Ghaffar A.M., R.F.Scott and M.J.Craig, "Full-Scale Experimental Investigation of a Modern Earth Dam," EERL 80-02, February 1980. (PB-81-123788)

116. Rutenberg, A., P.C. Jennings and G.W. Housner, "The Response of Veterans Hospital Building 41 in the San Fernando Earthquake," EERL 80-03, May 1980. (PB-82-201377)

117. Haroun, M.A., "Dynamic Analyses of Liquid Storage Tanks," EERL 80-04, February 1980. (PB-81-123275)

118. Liu, W.K., "Development of Finite Element Procedures for Fluid-Structure Interaction," EERL 80-06, August 1980. (PB 184078)

119. Yoder, P.J., "A Strain-Space Plasticity Theory and Numerical Implementation," EERL 80-07, August 1980. (PB-82-201682)

120. Krousgrill, C.M., Jr., "A Linearization Technique for the Dynamic Response of Nonlinear Continua," EERL 80-08, September 1980. (PB-82-201823)

121. Cohen, M., "Silent Boundary Methods for Transient Wave Analysis," EERL 80-09, September 1980. (PB-82-201831)

122. Hall, S.A., "Vortex-Induced Vibrations of Structures," EERL 81-01, January 1981. (PB-82-201849)

123. Psycharis, I.N., "Dynamic Behavior of Rocking Structures Allowed to Uplift," EERL 81-02, August 1981. (PB-82-212945)

124. Shih, C.-F., "Failure of Liquid Storage Tanks Due to Earthquake Excitation," EERL 81-04, May 1981. (PB-82-215013)

125. Lin, A.N., "Experimental Observations of the Effect of Foundation Embedment on Structural Response," EERL 82-01, May 1982. (PB-84-163252)

126. Botelho, D.L.R., "An Empirical Model for Vortex-Induced Vibrations," EERL 82-02, August 1982. (PB-84-161157)

127. Ortiz, L.A., "Dynamic Centrifuge Testing of Cantilever Retaining Walls," SML 82-02, August 1982. (PB-84-162312)

128. Iwan, W.D. (Editor) "Proceedings of the U.S. National Workshop on Strong-Motion Earthquake Instrumentation, April 12-14, 1981, Santa Barbara, California," California Institute of Technology, Pasadena, California, 1981.

129. Rashed, A., "Dynamic Analysis of Fluid-Structure Systems, " EERL 82-03, July 1982. (PB-84-162916)

130. National Academy Press, "Earthquake Engineering Research—1982."

131. National Academy Press, "Earthquake Engineering Research—1982, Overview and Recommendations."

132. Jain, S.K., "Analytical Models for the Dynamics of Buildings," EERL 83-02, May 1983. (PB-84-161009)

133. Huang, M.-J., "Investigation of Local Geology Effects on Strong Earthquake Ground Motions," EERL 83-03, July 1983. (PB-84-161488)

134. McVerry, G.H. and J.L. Beck, "Structural Identification of JPL Building 180 Using Optimally Synchronized Earthquake Records." EERL 83-01, August 1983. (PB-84-162833)

135. Bardet, J.P., "Application of Plasticity Theory to Soil Behavior: A New Sand Model," SML 83-01, September 1983. (PB-84-162304)

136. Wilson, J.C., "Analysis of the Observed Earthquake Response of a Multiple Span Bridge," EERL 84-01, May 1984. (PB-85-240505/AS)

137. Hushmand, B., "Experimental Studies of Dynamic Response of Foundations," SML 83-02, November 1983. (PB-86-115383/A)

138. Cifuentes, A.O., "System Identification of Hysteretic Structures," EERL 84-04, 1984. (PB-240489/AS14)

139. Smith, K.S., "Stochastic Analysis of the Seismic Response of Secondary Systems," EERL 85-01, November 1984. (PB-85-240497/AS)

140. Maragakis, E., "A Model for the Rigid Body Motions of Skew Bridges," EERL 85-02, December 1984. (PB-85-248433/AS)

141. Jeong, G.D., "Cumulative Damage of Structures Subjected to Response Spectrum Consistent Random Process," EERL 85-03, January 1985. (PB-86-100807)

142. Chelvakumar, K., "A Simple Strain-Space Plasticity Model for Clays," EERL 85-05, 1985. (PB-87-234308/CC)

143. Pak, R.Y.S., "Dynamic Response of a Partially Embedded Bar Under Transverse Excitations," EERL 85-04, May 1985. (PB-87-232856/A06)

144. Tan, T.-S., "Two Phase Soil Study: A. Finite Strain Consolidation, B. Centrifuge Scaling Considerations," SML 85-01, August 1985. (PB-87-232864/CC)

145. Iwan, W.D., M.A. Moser and C.-Y. Peng, "Strong-Motion Earthquake Measurement Using a Digital Accelerograph," EERL 84-02, April 1984.

146. Beck, R.T. and J.L. Beck, "Comparison Between Transfer Function and Modal Minimization Methods for System Identification," EERL 85-06, November 1985. (PB-87-234688/A04)

147. Jones, N.P., "Flow-Induced Vibration of Long Structures," DYNL 86-01, May 1986. (PB-88-106646/A08)

148. Peek, R., "Analysis of Unanchored Liquid Storage Tanks Under Seismic Loads," EERL 86-01, April 1986. (PB-87-232872/A12)

149. Paparizos, L.G., "Some Observations on the Random Response of Hysteretic Systems," EERL 86-02. 1986. (PB-88235668/CC)

150. Moser, M.A., "The Response of Stick-Slip Systems to Random Seismic Excitation," EERL 86-03, September 1986. (PB-89-194427/AS)

151. Burridge, P.B., "Failure of Slopes," SML 87-01, March 1987. (PB-89-194401/AS)

152. Jayakumar, P., "Modeling and Identification in Structural Dynamics," EERL 87-01, May 1987. (PB-89-194146/AS)

153. Dowling, M.J., "Nonlinear Seismic Analysis of Arch Dams," EERL 87-03, September 1987. (PB-89-194443/AS)

154. Duron, Z.H., "Experimental and Finite Element Studies of a Large Arch Dam," EERL 87-02, September 1987. (PB-89-194435/AS)

155. Whirley, R.G., "Random Response of Nonlinear Continuous Systems," EERL 87-04, September 1987. (PB-89-194153/AS)

156. Peng, C.-Y., "Generalized Model Identification of Linear and Nonlinear Dynamic Systems," EERL 87-05, September 1987. (PB-89-194419/AS)

157. Levine, M.B., J.L. Beck, W.D. Iwan, P.C. Jennings and R. Relles, "Accelerograms Recorded at Caltech During the Whittier Narrows Earthquakes of October 1 and 4, 1987: A Preliminary Report," EERL 88-01, August 1988. PB-

158. Nowak, P.S., "Effect of Nonuniform Seismic Input on Arch Dams," EERL 88-03, September 1988. (PB-89-194450/AS)

159. El-Aidi, B., "Nonlinear Earthquake Response of Concrete Gravity Dam Systems," EERL 88-02, August 1988. (PB-89-193124/AS)

160. Smith, P.W., Jr., "Considerations for the Design of Gas-Lubricated Slider Bearings," DYNL 89-01, January 1988. PB-

161. Donlon, W.P., Jr., "Experimental Investigation of the Nonlinear Seismic Response of Concrete Gravity Dams," EERL 89-01, January 1989. PB-